Universidad
Carlos III de Madrid
www.uc3m.es

TESIS DOCTORAL

Continuum Models for the Dynamic behavior of 1D Nonlinear Structured Solids

Autor:

Javier Vila Morán

Directores:

José Fernández Sáez y Ramón Zaera Polo

DEPARTAMENTO de
MECÁNICA de MEDIOS CONTINUOS y TEORÍA DE ESTRUCTURAS

Leganés, Julio de 2016

Universidad Carlos III de Madrid
www.uc3m.es

TESIS DOCTORAL

Continuum Models for the Dynamic behavior of 1D Nonlinear Structured Solids

Autor: *Javier Vila Morán*

Director/es: José Fernández Sáez y Ramón Zaera Polo

Firma del Tribunal Calificador:

Firma

Presidente: Enrique Barbero Pozuelo

Vocal: Julián J. Rimoli

Secretario: Eugenio Giner Maravilla

Calificación:

Leganés, 12 de Julio de 2016

"Le hizo un trato al colchón, con su espuma se forró el corazón.
Anoche era de piedra, y al alba era de mimbre, que se dobla antes de partirse."

K. Romero

Acknowledgements

I want to thank my thesis advisors for believing in me, sharing so much wisdom and working so hard in this project, always with a smile. All your efforts have shuttle my academic career. Thanks.

I also want to thank the department of Mecánica de Medios Continuos y Teoría de Estructuras from the Universidad Carlos III de Madrid for the great opportunity that they gave me and all the resources I had at my disposal.

The financial support of the Ministerio de Ciencia e Innovación de España (Project DPI/2014-57989-P) is greatly acknowledged. The subject of this Thesis is a core part of the research project.

I am also indebted to the Universidad Carlos III de Madrid for the financial support during my stay at Georgia Institute of Technology. During that stay I was hosted by Massimo Ruzzene, director of the Vibration and Wave propagation Lab. I want to thank him and his co-workers for their will to collaborate and all the things that I learned there.

I want to thank my parents. Of course. Your support permitted me to leave my work in such a hard time and to start this scientific journey. Now I do what I always wanted to, never stop exploring. I love you.

Thanks to my sister, I have you in my mind, and I know you will love me ever.

I should thank my partner María, because she stood me and comprehended my hard times and bad anger. You supported me and I know you will kill me if I do not mention you here. Plus, you deserve this place with maximum honors.

Greetings to all my friends from Santander, the colleagues from Madrid and the people I knew in Atlanta. You made my laugh and feel alive.

Javier Vila Morán
June 2016

A mis padres y hermana.
A María.

Abstract

The main objective of this thesis is to propose and validate generalized continuum models for analyzing and predicting the free vibrations of 1D linear elastic structured solids subjected to finite deformations.

With this aim, two different generalized continuum models that account for geometric nonlinearities have been proposed: a nonlocal nonlinear model and a gradient velocity nonlinear one, here referred to as the inertia gradient nonlinear model. These models contain one or more microstructural parameters.

The formulation of the cited theories has been devised for general 3D solids, but in this thesis they have been applied to the study of nonlinear axial and nonlinear axial-transverse coupled vibrations of a kind of 1D structured solids. The 1D structured solids chosen as reference are such that, under certain conditions, the classical nonlinear continuum model adequately reproduces its main features. However, it is well known that the classical theory is not able to capture the size effect presented in this kind of solids.

Moreover, a non-standard continualization technique has been applied to the discrete system in order to get appropriate continuous equations of motion. Unlike the postulated generalized continuum models, this continualization technique permits to derive, from the characteristics of the solid structure, the additional parameters appearing in the formulation.

The results for the two nonlinear analyzed problems (axial vibrations and axial-transverse coupled vibrations) obtained from the classical, generalized nonlinear continuum, and continualized models have been compared to those derived from the discrete solution taken as reference.

From this critical comparison, the advantages and shortcomings of the different theories have been pointed out clearly showing the ability of the generalized continuum models to adequately address the size effects in structured solids, observed in many practical applications.

Resumen

El objetivo principal de esta tesis es proponer y validar modelos del continuo generalizado para analizar y predecir el comportamiento de vibraciones libres de sólidos estructurados unidimensionales elásticos y lineales sometidos a deformaciones finitas.

Con este objetivo, se han propuesto dos modelos del continuo generalizado diferentes que consideran las no linealidades geométricas: un modelo no lineal no local y otro no lineal de gradiente de la velocidad, aquí referido como modelo con gradiente de inercia. Estos modelos contienen uno o más parámetros microestructurales.

Las formulaciones de dichas teorías se han planteado para sólidos tridimensionales, pero en esta tesis se han aplicado al estudio de las vibraciones no lineales longitudinales y las vibraciones nolineales acopladas axiales-transversales en un tipo de sólidos 1D estructurados. El sólido 1D estructurado elegido como referencia es tal que, bajo ciertas condiciones, el modelo continuo no lineal clásico reproduce adecuadamente sus características principales. Sin embargo, es bien sabido que la teoría clásica no es capaz de capturar los efectos de tamaño que presentan este tipo de sólidos.

Por otra parte, se ha aplicado una técnica de continualización no estándar al sistema discreto con el fin de obtener las ecuaciones continuas del movimiento. A diferencia de los modelos del continuo generalizado postulados, esta técnica de continualización permite derivar, a partir de las características del sólido estructurado, los parámetros adicionales que aparecen en la formulación del problema.

Los resultados para los dos problemas no lineales analizados (vibraciones axiales y axiales-transversales acopladas) obtenidos mediante los modelos continuo clásico, continuos no lineales generalizados, y los continualizados se han comparado con los derivados de la solución discreta que se toma como referencia.

A partir de esta comparación crítica, se han señalado las ventajas y los inconvenientes de las diferentes teorías, mostrando claramente la capacidad de los modelos del continuo generalizado para tratar adecuadamente los efectos de tamaño en los sólidos estructurados, observados éstos en muchas aplicaciones prácticas.

Contents

List of Figures

List of Tables

1 Introduction and objectives

1.1 Introduction

In the last decades, the scientific community has paid attention to microstructured and nanostructured materials. It is well known that matter is essentially discrete. Figure 1.1 shows a STM image of a crystalline material that provides evidence of the discrete and highly organized nature of crystalline solids.

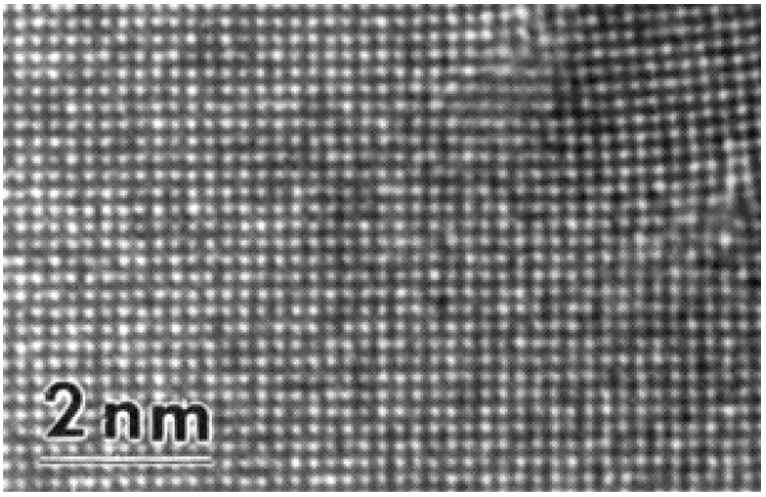

Figure 1.1: STM image of a metallic material. Source: www.gettyimages.es

Therefore, atomistic and molecular dynamic formulations have been used to understand solids behavior. Discrete models and molecular dynamics algorithms constitute a well-known tool to simulate the behavior of microstructured materials and nano-scale elements. The increasing capabilities of computers (number of cores, RAM capacity, fast access solid state memory), together along with parallel computation techniques developed in last decade, took discrete simulation codes

to a next level, making their use feasible for larger computations. However, this calculations consume a lot of time, even for a relatively low number of particles if the interaction between them is complex. This approach may not be recommended for an element that must be tested for a large number of loading cases and different boundary or initial conditions. In addition, these models need the definition of the interaction potentials, their shape and constants. These properties would need to be encountered for the material under study, which adds additional costs to the designing process.

Due to the high computational cost of solving the discrete formulation in such a big systems, continuum approaches are widely used to analyze large scale problems. In particular, classical continuum solid mechanics theories have been considered to solve fundamental problems in civil, mechanical and materials engineering, as well as in various fields of physics and life sciences. The origin of its success lies on the fact that the scale of observation is significantly larger than the characteristic dimensions of the underlying microstructure.

However, there are engineering problems related to composites, functionally graded materials, polycrystalline solids, granular materials, etc., in which the characteristic lengths of the studied phenomena (wavelengths, length of variation of applied external force, etc.) are similar to the size of microstructure.

A kind of systems whose dimensions clearly become comparable to the size of their material microstructures or molecular distances are the nanostructures used in technological applications such as micro- or nano-electromechanical (MEMS or NEMS) devices [10], nanomachines [11 14], as well as in biotechnology and biomedical fields [15]. Two commonly used MEMS sensors are shown in Fig. 1.2. There is, therefore, high technological and scientific interest in the development of a powerful tool for the design of microstructured solids.

In such cases, unrealistic predictions may be reached using classical continuum models and interesting effects inherent to the microstructure may not be captured (dispersive propagation of waves, size-dependent structural behavior, beaming effect, etc.). That is because the classical continuum approach is a scale-free theory and their constitutive equations lack an internal length.

Another possibility consists in the development of stochastic models. These models present the advantage of condensing information about the micro-scale phenomena into probabilistic functions. Thus, the model solves a continuum macro-scale

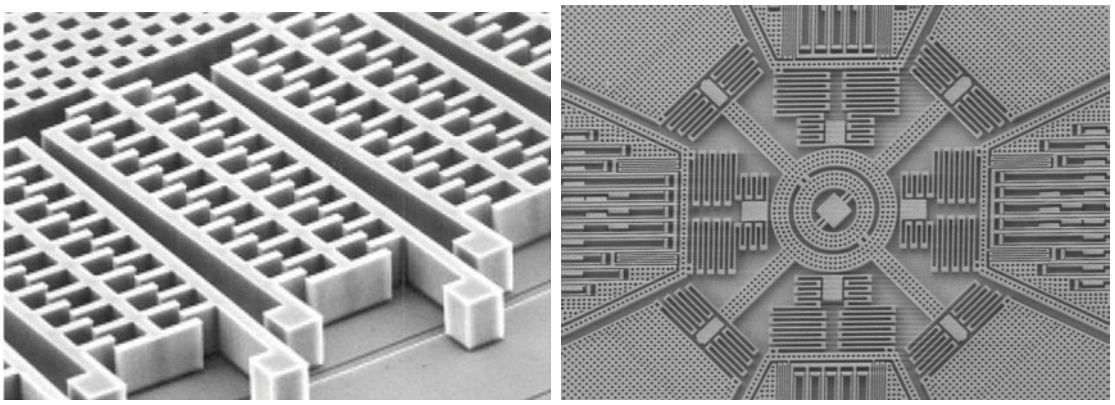

(a) (b)

Figure 1.2: Two MEMS sensors used in smartphones and robotics. (a) MEM accelerometer. Source: www.digikey.com. (b) MEM gyroscope. Source: www.mitpune.com

problem that includes a stochastic part, taking advantage of the computational efficiency of continuum algorithms. There are some works in the field of stochastic MEMS/NEMS analysis, e. g. the studies about chaotic movement in nonlinear resonators of Miandoab et al. [16, 17] or the investigations about mass absorption measurements in MEMS resonators by Djurić et al. [18].

In contrast, some deterministic generalized continuum models have been developed by researchers in this field in order to capture the size effects in the dynamic behavior of microstructured materials. Since the 19^{th} century (works by Cauchy and Voigt), and in the beginning of the 20^{th} century (works by Cosserat brothers) it is possible to find some attempts to capture the effects of microstructure using the continuum equations of elasticity with additional higher-order derivatives. Moreover, the works of Mindlin and Tiersten [19], Kröner [20], Toupin [21, 22], Green and Rivlin [23], Mindlin [24, 25] and Mindlin and Eshel [26], dated in the 1960s suppose a great boost of the topic, although these theories were excessively complex with too many parameters and equations.

On the other hand, Eringen postulated [27, 28] an integral nonlocal constitutive relation for microstructured materials. From this earlier nonlocal theories, he derived a differential version which contains only one additional length scale parameter [29]. This model has been widely used to address different kind of problems, such as wave propagation, dislocation, and crack singularities.

All the above works assume a linear relation between strains and displacements (infinitesimal deformations framework), and only a few attempts have been done

up to date to incorporate large strains and rotations. There exist nonlinear solids with an inherent microstructure such as live tissues, highly deformable rubber lattices and other organic compounds that exhibit significant nonlinearities under elastic deformations. In addition, nanomaterials and nanostructures (grafene, CNTs, etc.) can be manufactured with a very low amount of defects, which prevents their collapse under high loads, allowing high deformations and leading to remarkable nonlinear behavior.

Nonlinear microstructured materials have a large amount of potential applications in tunable devices, since the properties of these microstructured solids may be controlled by the amplitude of the phonons propagating through them. Therefore, they could be used for manufacturing non-conventional filters and wave selectors. In addition, depending on their nonlinear nature, they may allow the existence of solitons.

There is already interest in nonlinear problems. In this respect, Reddy considered [30] the nonlinear von Kármán strains in the analysis of nonlocal formulation of bending of beams and plates under the assumptions of small strains and moderate rotations. Subsequently, this theory has been applied to study the large amplitude free vibration of nanobeams by Şimşek [31]. Nevertheless, in these works a general formulation of the Eringen nonlocal theory of elasticity valid for finite deformations is not given. In addition, these works are based on the application of the differential version formulation, not the original integral one.

In this thesis we study problems in which geometric nonlinearities are present. To find continuous equations capable of reproducing the behavior of structured solids, we postulated, rigorously developed, two generalized continuum models:

- A formal extension of the Eringen non-local elasticity theory to finite deformations.
- A hyperelastic model with gradient enrichment of the kinetic energy.

These formulations are valid to analyze mechanical problems of microstructured solids in which nonlinear effects are relevant.

1.2 Objectives

In the general context previously described, the main objective pursued in this doctoral thesis is **to develop continuum models** able to accurately reproduce the essential features of the **dynamical behavior of 1D structured solids undergoing finite deformations**.

In order to do so, the subsequent secondary objectives are targeted:

- To formulate generalized continuum models applicable to finite deformations. Preexisting linear generalized continuum models for microstructured materials are taken as a base.
- To apply these models to the analysis of nonlinear axial and axial-transverse coupled vibrations of 1D structured solids. To that aim, a nonlinear discrete problem, taken as a reference, will be formulated and solved.
- To investigate the possibilities to identify, from the structural characteristic of the solids, the additional scale parameters present in the generalized continuum models. In this respect, the application of non-standard continualization techniques will be examined.
- To validate the proposed continuum models, critically comparing their prediction with that derived from the direct solution of the discrete system taken as a reference. This contrast will permit highlighting the advantages and shortcomings of the different approaches.
- From the all above analysis, to get new insights on the ability of the generalized continuum models to adequately address the size effects in the dynamics of nonlinear structured solids.

1.3 Contents

The thesis is organized going from the postulation of some nonlinear generalized continuum theories to their application over 1D cases. There are 8 chapters organized as follows:

In the present chapter 1, the context of the challenge was presented. Then, the main goals of the thesis are stated and the relation of contents is summarized.

In chapter 2, relevant technological applications of structured solids are presented. A brief explanation on how the classical continuum model fails in reproducing the behavior of these solids is given.

In chapter 3, the most used existing linear continuum theories are presented. A concise state of the art is developed.

In chapter 4, we postulate two nonlinear generalized continuum theories, in addition to the classical nonlinear continuum theory for hyperelastic materials. These novel models will be used in ulterior chapters for predicting the dynamic behavior of a 1D microstructured solid.

A 1D nonlinear discrete system is formulated in chapter 5. This model is going to be solved by explicit integration algorithms and its behavior taken as a reference for one-dimensional microstructured materials or elements. Postulated nonlinear continuum models are intended to reproduce the dynamic behavior of the discrete element.

The next two chapters, 6 and 7, deal with specific dynamic problems and have a common structure. The nonlinear vibrational behavior of a 1D element is analyzed, under longitudinal oscillations in chapter 6 and axial-transverse coupled oscillations in chapter 7. The movement is modeled using the discrete model of chapter 5. This model is then continualized using two different approaches to get continuous equations of motion. Subsequently, the generalized continuum nonlinear theories proposed in chapter 4 are specialized to this problem.

The predictions of the continuous formulations are contrasted with simulations of the discrete one. An extended discussion about the size effects and nonlinear effects is addressed to decided whether the generalized continuum is applicable or not for modeling microstructured solids.

The main goals achieved in these research are presented in chapter 8. Next, the main conclusions extracted from them are summarized. Some future research topics are outlined, expressing the main ideas for the continuation of the project.

Finally, a detailed list of all the references cited in the thesis is included.

2 Structured solids and Discrete systems

Nowadays, structured solids play a major role in technology. Structured solids are those in which density and stiffness are not equal in all the points, but distributed following a certain periodic pattern. In this chapter, several applications involving this kind of solids are presented. We then explain how the behavior of these solids can be successfully formulated through discrete models. In the last part, we briefly show the scale effects in a one dimensional solid, that is, the influence of the underlying structure in the behavior of this kind of solids when the wavelength is of the order of the structure characteristic length. Classical continuum models fail in capturing the dynamic behavior of structured solids because they do not predict the scale effects.

2.1 Technological applications involving structured solids

Structured solids, periodic structures, lattice systems, nanostructures... are present in a number of different products and systems. Moreover, some of them are of high scientific and technological importance due to their interesting and rare electro-mechanical properties.

In the following sections, four main fields in which the scale effects are relevant will be addressed.

2.1.1 Carbon nanostructures

The keystone of nanostructured materials in the scientific community are graphene and carbon nanostructures, such as fullerenes, carbon nanotubes (CNTs), graphene nano-ribbons, carbon nano-torus etc.

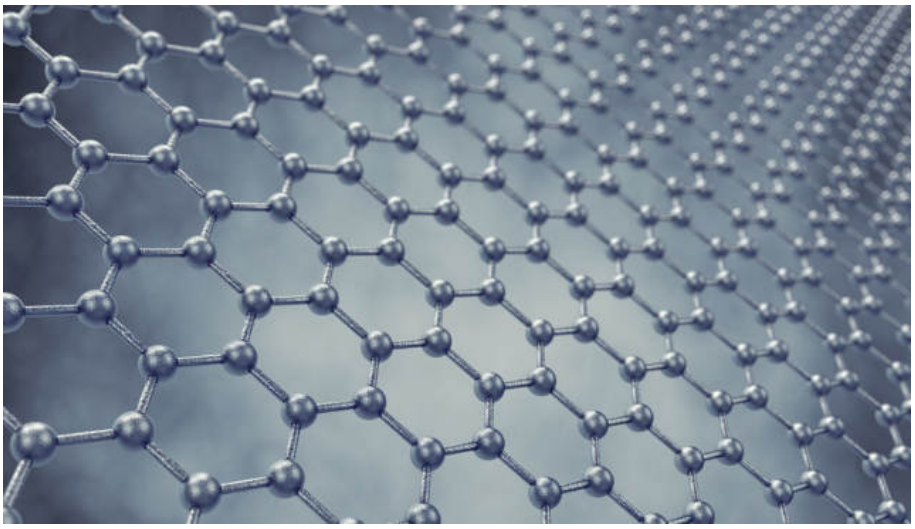

Figure 2.1: Artistic representation of a graphene layer. Source: www.azonano.com

Graphene is a mono-layer material made exclusively of carbon atoms disposed in an hexagonal lattice. Fig. 2.1 shows a scheme of a graphene layer. The energy potentials of atomic interactions have been extensively studied, e.g. [32]. The interaction potentials are commonly used for obtaining the macro-mechanical properties and performing simulations of a wide range of different phenomena, see

[33 36] among others. An interesting review of graphene, its properties, fabrication processes and potential applications can be found in [37].

Regarding the nonlinear effects in graphene, several authors have developed molecular dynamics, lattice and discrete FEM models to characterize its behavior under finite deformations. The study by Georgantzinos et al. [38] uses a discrete approach similar to the one developed in chapter 5. It shows notable change in stiffness under elastic deformations before failure. In addition, a correlation between the size of the graphene ribbon and the nonlinear behavior is found, showing that the smaller the nanoribbon, the higher the admissible finite deformations. This is a clear manifestation of the aforementioned size effects.

Although is not relevant for this thesis, the electro-magnetic properties of graphene are also of high interest for the scientific community. Significant nonlinear behavior has been found also in that aspect, see [39].

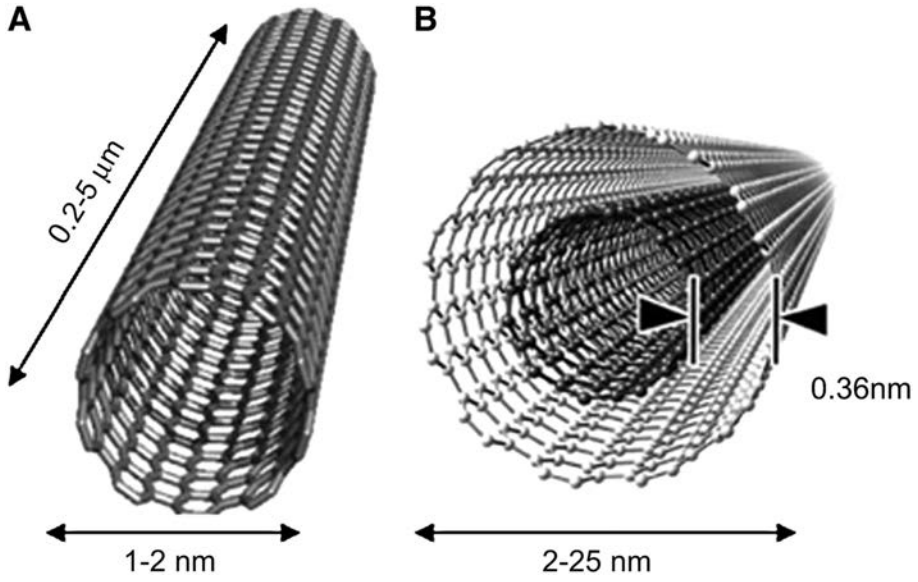

Figure 2.2: Schematics of two CNTs. Source: jnm.snmjournals.org

Besides, one of the most relevant aspect of graphene is its ability to fold an conform regular structures that present completely different electro-mechanical properties. Graphene can be, for example, rolled up to form a cylinder, what is called a carbon nanotube (CNT). Fig. 2.2 shows schematics of both a single-walled and a double-walled CNTs. Fig. 2.3 shows a Scanning Electron Microscope image of a bundle of CNTs.

CNTs are nowadays widely used for composite material reinforcement. Their high stiffness in longitudinal direction with such a low diameter makes them ideal as

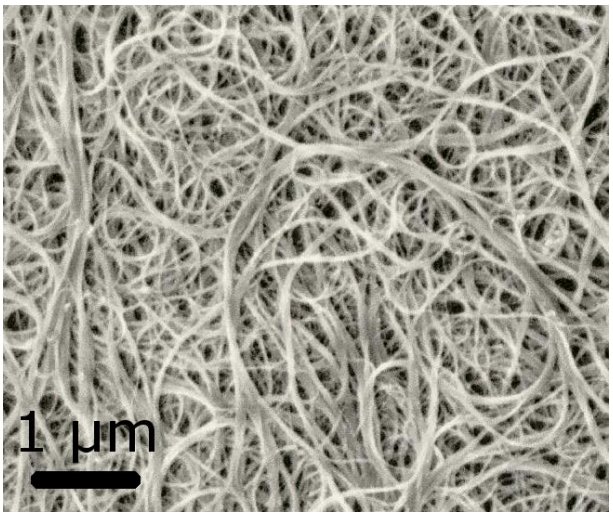

Figure 2.3: SEM image of a bundle of CNTs. Source: en.wikipedia.org

fibers. They are used in ceramics and metals [40], organic resin matrices [41], and other composites reinforcements. In addition, these nanostructures have an incredibly high specific surface area [42], which leads to high Van der Waals forces between them. They could be used for adhesives, crack reparations, fiber cohesion in fabrics, etc. Fig. 2.4 shows a scheme on how to use CNTs for a crack reparation and crack growth prevention.

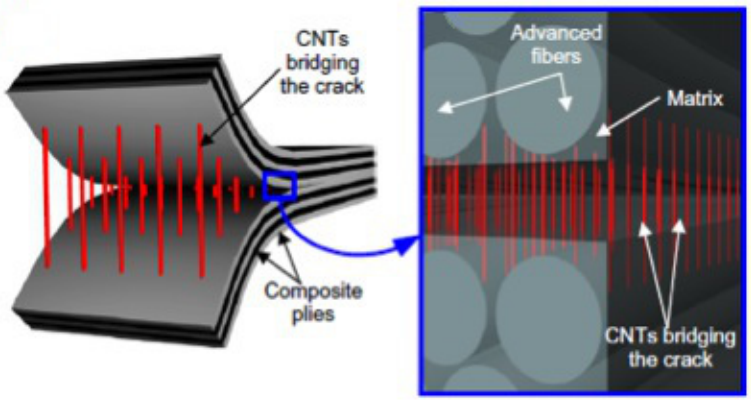

Figure 2.4: Schematics of how to bridge a crack using CNTs. Source: aerospaceengineeringblog.com

For increasing the resistance of CFRP, methods for attaching or dispersing CNTs onto a carbon fiber cloth have been developed. Fig. 2.5 shows two SEM images before and after the process of diffusion. The strength of CNTs reinforced CFRP was encountered significantly higher than normal CFRP. Depending on how the CNTs are distributed, long nonlinear elastic behavior may be found, see [43].

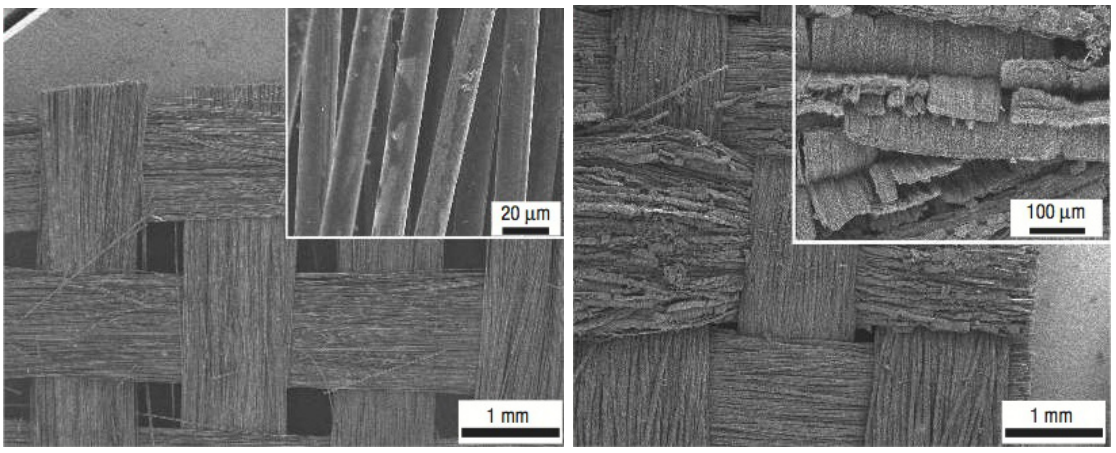

(a) (b)

Figure 2.5: SEM images showing the a carbon fiber cloth. (a) Clean (b) After CNTs diffusion. Source: aerospaceengineeringblog.com

Figure 2.6: Artistic representation of a CNT passing through a carbon nanotorus.

A carbon nanotube is the perfect example of a 1D nanostructured solid that may be subjected to finite deformations. The analysis of CNTs behavior in different linear scenarios has been performed using Eringen elasticity and other linear nonlocal theories [44 46]. There exist few research in the application of the Eringen nonlocal continuum model for large deformation analysis of CNTs.

Linear Mindlin-type strain gradient theories has been also used for reproducing the behavior of CNTs [47 50]. Nonlinear continuum models derived from discrete ones after applying continualization techniques have been also used for CNTs and CNCs (carbon nano-cones) modeling [51, 52].

Nonlinear generalized continuum models constitute a solid alternative to discrete models and continualized ones for analyzing and designing the behavior of

graphene, nano-ribbons, CNTs and other carbon-based nanostructures.

There are more carbon structures with varied and rare properties. Several scientific groups around the world are working on the discovery and manufacturing processes of new carbon nanostructures. For example carbon nano torus (Fig. 2.6).

More possibilities arise with the hybridization of nanostructures. There are several groups working in the hybridization of graphene and CNTs. This nanostructure has a huge specific surface, which makes it ideal for energy storage components. As an example, an optimized growth process was developed in 2014 [1]. Figure 2.7 shows schematics and SEM image of the graphene-CNTs structure.

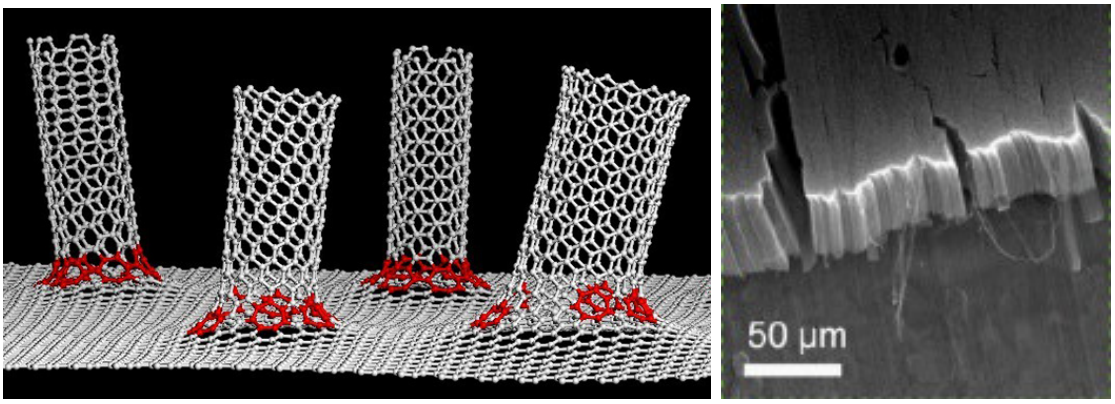

(a) (b)

Figure 2.7: Images of a hybrid graphene-CNT nanostructure. (a) Schematics (b) SEM. Source: Ref. [1]

2.1.2 Nano and micro electro-mechanical systems

Another important group of structures that may be analyzed using generalized continuum models are nano and micro electro-mechanical systems (NEMS and MEMS). The critical physical dimensions of NEMS/MEMS devices can vary from well below one micron on the lower end of the dimensional spectrum, all the way to several millimeters. These systems are commonly used nowadays in machines with relevant weight or size issues.

Starting from the lowest size to the highest, NEMS are commonly designed as sensors. Roukes group is working, at California Institute of Technology, in a variety of very simple nanostructures for acoustic sensors, among other NEMS. In Fig. 2.8 there are two images of nanobeams with different boundary conditions. These structures are used in robotics and biosensors [53], in which the size and the weight of the introduced device play a major role.

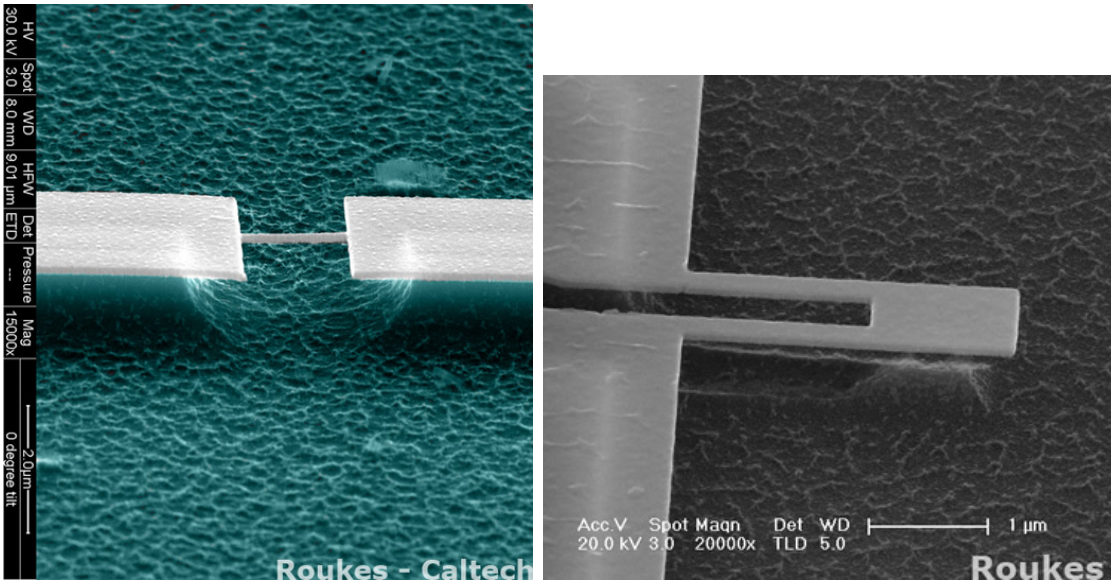

(a) (b)

Figure 2.8: SEM images of a nanobeam. (a) Clamped (b) Cantilever. Source: nano.caltech.edu

Despite of the apparent simplicity of this nanosensors, the design, fabrication process and calibration of them can be extremely complex due to the desired tolerances and measurement errors.

NEMS are used for detecting a wide variety of different phenomena. In a recent paper [2], the group of Lemme demonstrated superior pressure-sensing performance

of graphene NEMS sensors compared to competing technologies. The graphene sensor is constructed by first cutting open a trench in a silicon dioxide substrate and then depositing a graphene sheet over the trench. A SEM image of this device is depicted in Fig. 2.9.

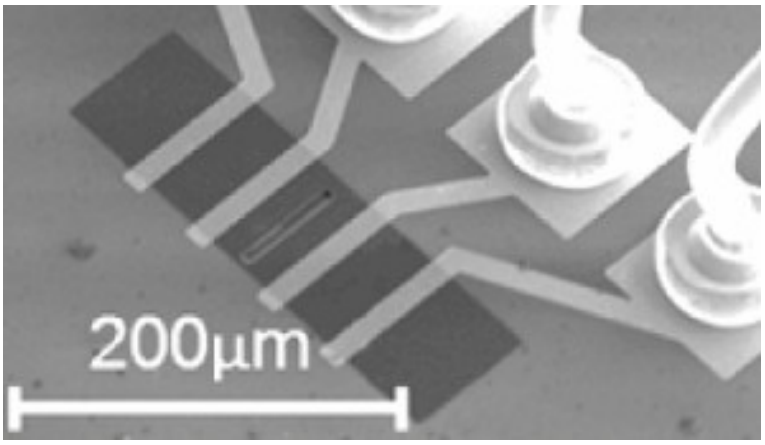

Figure 2.9: Graphene NEMS pressure sensor, consisting of a single graphene layer suspended above a trench in the substrate. Source: Ref. [2]

Likewise, the types of MEMS devices can vary from relatively simple structures having no moving elements, to extremely complex electromechanical systems with multiple moving elements under the control of integrated microelectronics. While the functional elements of MEMS are miniaturized structures, sensors, actuators, and microelectronics, the most notable (and perhaps most interesting) elements are the microsensors and microactuators.

More recently, the MEMS research and development community has demonstrated a number of microactuators including: microvalves for control of gas and liquid flows; optical switches and mirrors to redirect or modulate light beams; independently controlled micromirror arrays for displays, microresonators for a number of different applications, micropumps to develop positive fluid pressures, microflaps to modulate air streams on airfoils, as well as many others. Surprisingly, even though these microactuators are extremely small, they frequently can cause effects at the macro-scale level; that is, these tiny actuators can perform mechanical feats far larger than their size would imply [54]. For example, researchers have placed small microactuators on the leading edge of airfoils of an aircraft and have been able to steer the aircraft using only these microminiaturized devices.

As an example, in Figs. 2.10 and 2.11 two actuators and two micro electromechanical machines are shown.

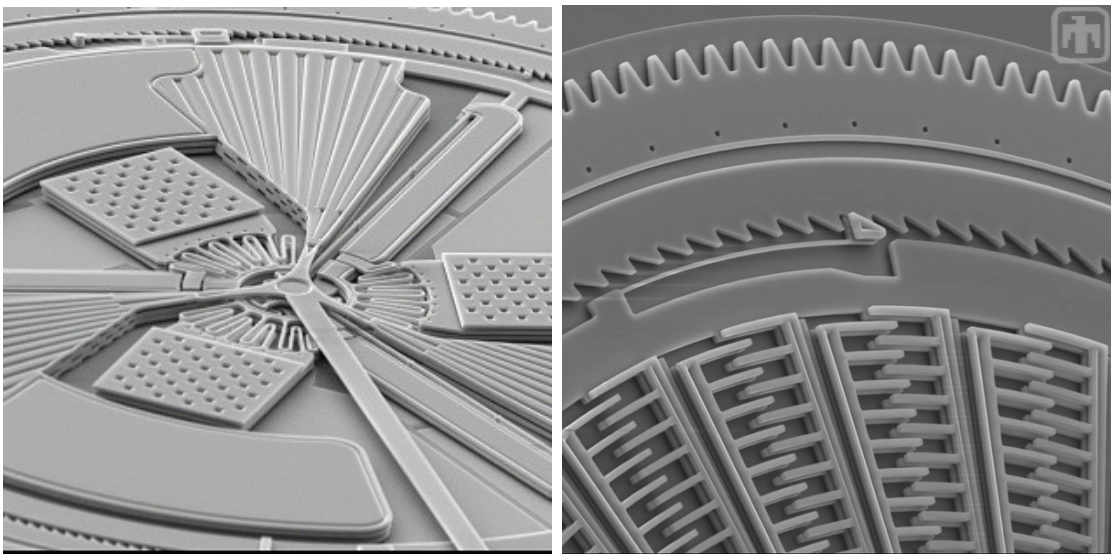

(a) (b)

Figure 2.10: MEMS: (a) thermal actuator (b) torsional actuator. Source: www.memx.com

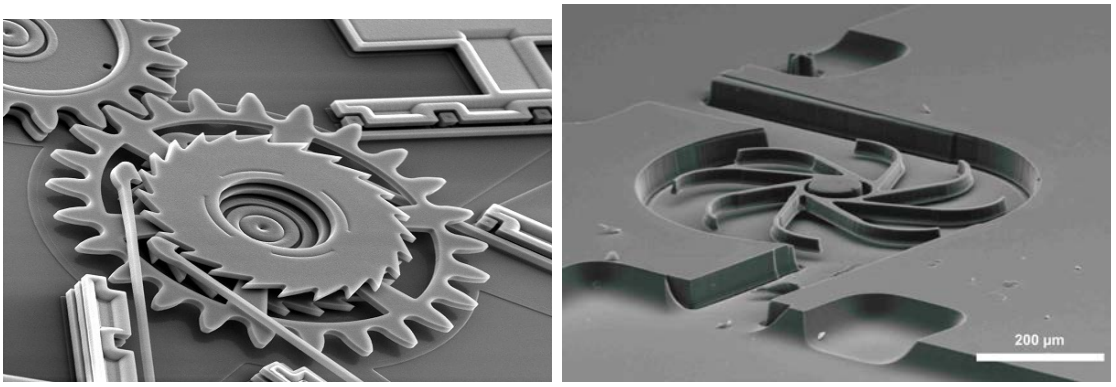

(a) (b)

Figure 2.11: MEMS: (a) micro-ratchet (b) micro-turbine. Source: www.memx.com

The average global size of MEMS is large enough to consider valid the hypotheses of classical continuum theories. However, some parts, usually the most critical, are very small or thin and close to the grain-size scale. Generalize continuum theories could provide an accurate tool for their mechanical design.

2.1.3 Macro-scale structured materials

In addition to all the materials, structures and devices whose size is in the molecular or grain-size scale order, there exists materials and structures in the macro-scale subjected to scale effects. This is the case of some composites, functionally graded materials, polycrystalline solids, granular materials, etc.

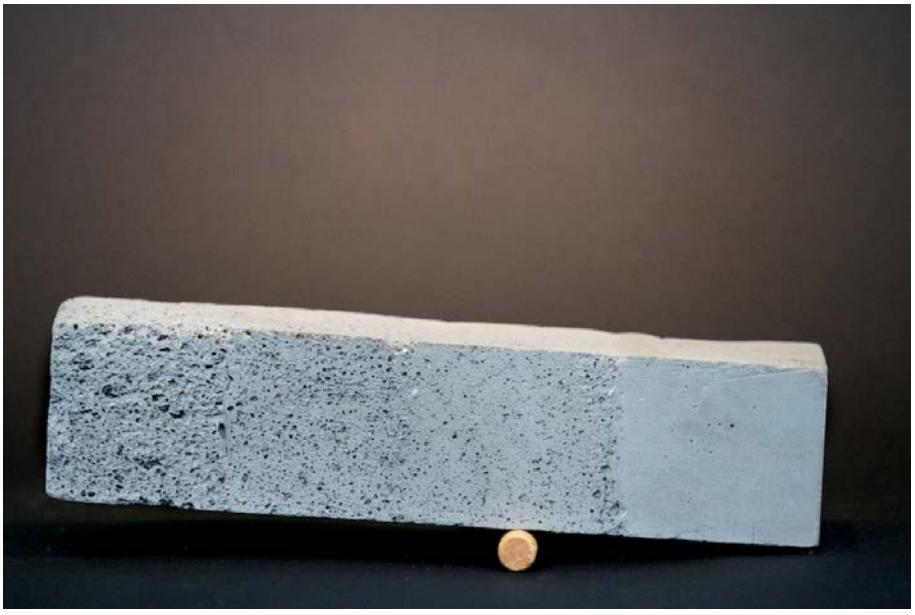

Figure 2.12: A functionally graded beam 3D printed at MIT. Source: matter.media.mit.edu

Figure 2.12 shows a functionally graded beam. Functionally graded materials, materials with spatially varying composition or microstructure, are omnipresent in nature. From palm trees with radial density gradients, to the spongy trabeculae structure of bone, to the hardness gradient found in many types of beaks, graded materials offer material and structural efficiency. In man-made structures such as concrete pillars, materials are typically volumetrically homogeneous. While using homogeneous materials allows for ease of production, improvements in strength, weight, and material usage can be obtained by designing with functionally graded materials. Li et al. [55] used a mixed linear nonlocal and linear strain gradient theory for analyzing the free vibration behavior of Timoshenko beams made of functionally graded material.

There also exists live tissues with an important underlying macro-structure, such as bones. Fig. 2.13 shows a longitudinal cut of a bone hinge union. The internal structure is appreciable at plain sight.

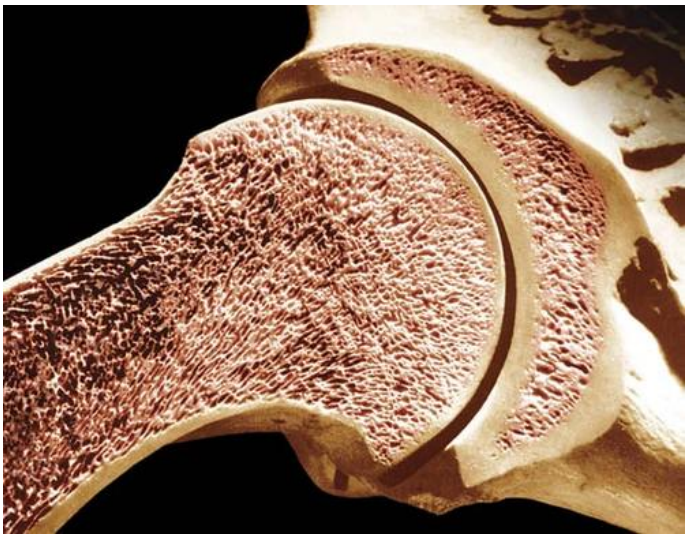

Figure 2.13: Human bone is a structured live tissue. Source: depts.washington.edu

It is difficult to construct a discrete model for the behavior of these materials, since mass is not concentrated in points but distributed following certain patters. Besides, any model coming from a discretization would be extremely complex. It is possible to develop classical continuum models with the specific geometry and mechanical properties of macro-scale structured solids. Fig. 2.14 illustrates the process of FEM modeling a trabecular bone structure followed by Martí et al. [3]. However, this is a long, time-consuming process.

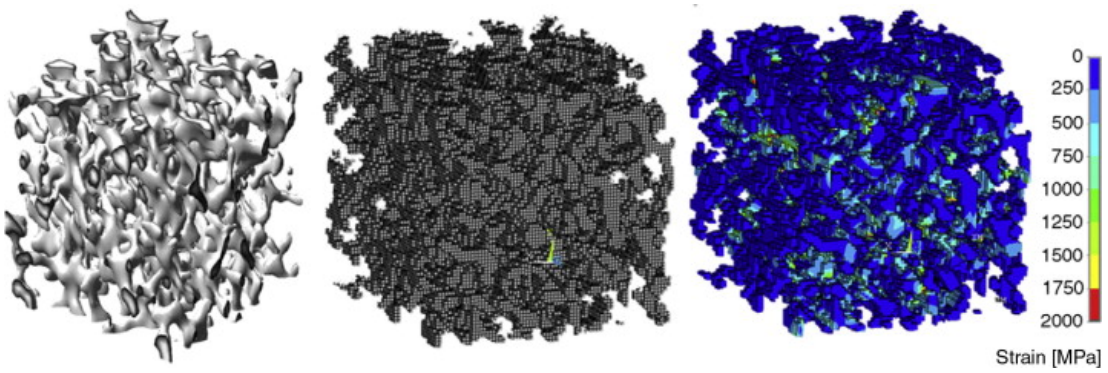

Figure 2.14: Left, 3D reconstruction of trabecular bone extracted from high spatial resolution MR images. Center, conversion of the trabecular bone geometry into a finite element model based on small hexahedron elements. Right, parametric map shows nodal strain caused by simulated compression. Source: Ref. [3]

An alternative is to use generalized continuum models. In this regard, Madeo et al. [56] used a second gradient model to reproduce the micro-inertia effects over the dynamic behavior of healing bones. Gitman [57] and Gitman et al. [58] used

an anisotropic gradient elasticity theory for modelling bone tissue around a crack tip. Hosseini et al. [59] developed a nonlocal gradient-enhanced damage-plastic model for bone plastic deformation analysis.

Moreover, there are other live tissues that remain elastic even under higher deformations. Some micro-structured soft tissues are prone to undergo high stretches. Arteries are a very good example. Gasser, Ogden and Holzapfel developed a generalized continuum hyperelastic theory for arterial layers modeling [4], see Fig. 2.15.

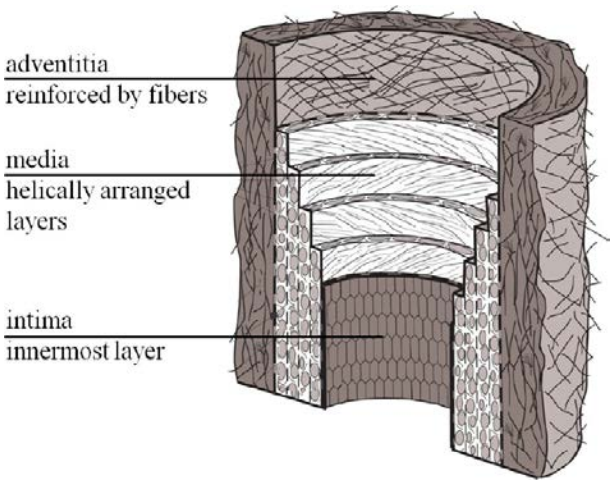

Figure 2.15: Diagrammatic model of a healthy elastic astery composed of three layers. Source: Ref. [4].

2.1.4 Periodic structures: lattices

Apart from naturally structured materials, artificial periodic structures are studied and designed for different scientific and technological purposes. These very regular periodic structures are called lattices. Lattices originally occurred in the context of condensed matter physics, where the atoms of a crystal automatically form a lattice. In mineralogy and crystallography, a crystal structure is a unique arrangement of atoms, ions or molecules in a crystalline liquid or solid. It describes a highly ordered structure, occurring due to the intrinsic nature of its constituents to form symmetric patterns.

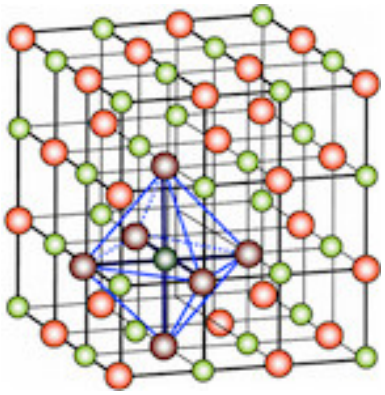

Figure 2.16: Schematics of a cubic crystallographic structure and its unit cell. Source: study.com

The element can be thought of as an array of small boxes or cells infinitely repeating in all three spatial directions. Such a unit cell is the smallest unit of volume that contains all of the structural and symmetry information to build up the macroscopic structure of the lattice by translation. Fig. 2.16 shows schematics of a cubic crystallographic structure. Its unit cell is boxed in blue lines.

The lengths of the edges of a unit cell and the angles between them are called the lattice parameters. The symmetry properties of the crystal are embodied in its space group. Graphene structure is a classical atomic bi-dimensional hexagonal lattice.

Different macro-scale lattices are constructed and investigated nowadays. They provide a full insight into acoustic and thermal propagation phenomena.

They also have rare and interesting mechanical properties. Different dispersion diagrams, and band-gaps are encountered depending on the type of the lattice and given values to lattice parameters. Some lattices have several parameters that

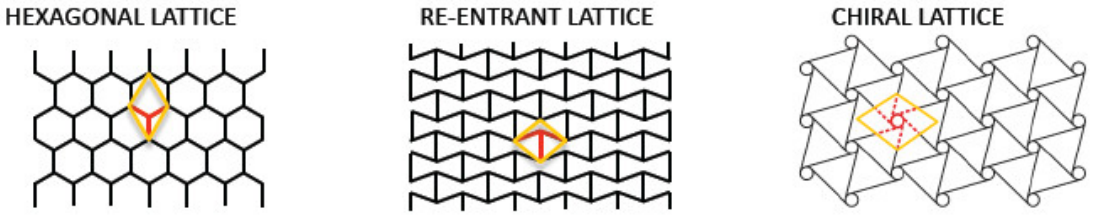

Figure 2.17: Schematics of three different lattices. The unit cell is boxed and their elements are depicted in red. Source: [5, 6]

can be designed to accomplish specific functionality requirements. For example, if a filter is being designed, the desired cutoff frequency and attenuation rate can be satisfied by playing with the lattice parameters. Figure 2.17 shows schematics for three different bi-dimensional lattices and their basic unit cell.

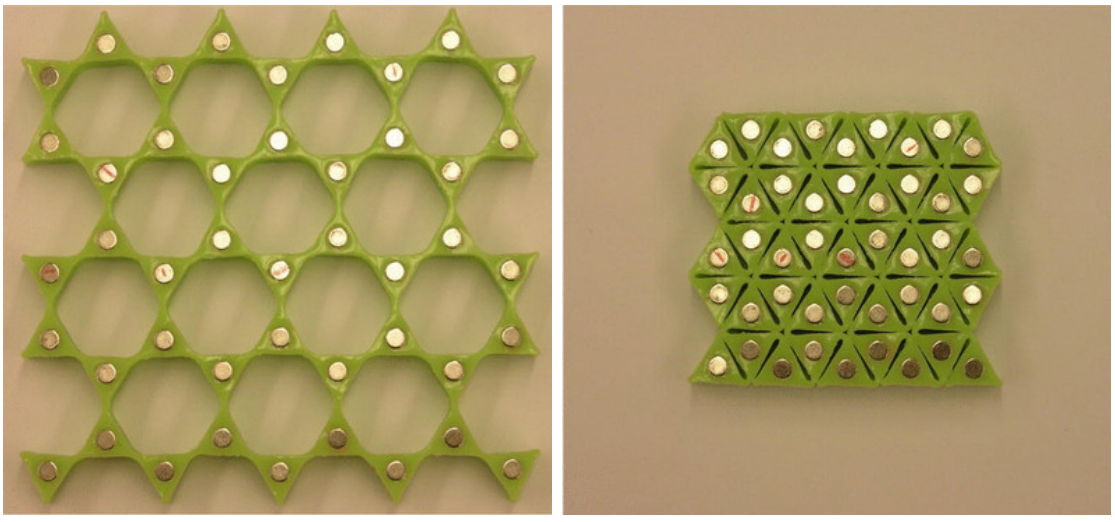

(a) (b)

Figure 2.18: A highly tunable 3D printed Kagome lattice. (a) Expanded. (b) Compressed. Source: Ref. [7]

In addition, some structures are flexible enough to accommodate significant geometrical changes under relatively low external forces. These geometrical changes will imply a change in the dynamic behavior, making the lattice structure highly tunable. This is the case of the Kagome lattice [7], which is show in Fig. 2.18.

At the same time, some scientific groups are working in lattices that display negative macro-scale Poisson ratio, reproducing the behavior of what is called an auxetic solid [60]. Two popular examples are re-entrant lattices and chiral ones. These structured solids show the rare and interesting property of transversally

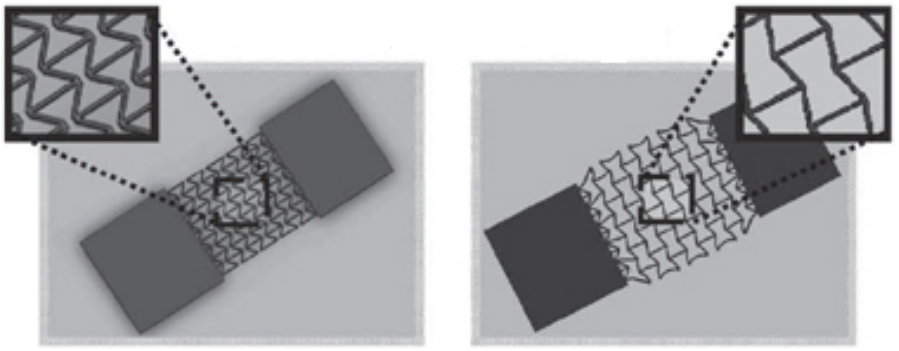

Figure 2.19: An reentrant lattice subjected to finite stretch. The lattice was 3D printed in hyperelastic material. Left, relaxed. Right, stretched. Source: Ref. [8]

deforming in the same direction (shrinking or stretching) in which the main deformation is externally imposed, in contrast with typical solids. Figure 2.19 shows a real fabricated auxetic reentrant lattice before and after being stretched.

A considerable number of structured solids applications has been shown. Although some of them are related to other fields, in this thesis we will stick to the mechanical response of one dimensional structured solids.

2.2 Discrete models for structured solids

Several kinds of discrete models have been used in mechanical and engineering fields to reproduce static and dynamic elastic behavior, plasticity, damage evolution and failure of materials. Despite their computational cost, the discrete models can be used to represent some of the phenomena that take place in the aforementioned solids in this section.

Lattice models are commonly used. They consist in a system of masses interacting through springs of different types, organized in a periodic manner. Although it is not relevant for this thesis, viscous behavior can be also introduced by using dashpots. A variety of phenomena can be reproduced by adjusting the springs and dashpots behavior.

Currently, lattice models are quite popular in theoretical physics, for many reasons. Some models are exactly solvable, and thus offer great insight into the physics of the solid. Lattice models are also ideal for studies carried out by the methods of computational physics, as the discretization of any continuum model automatically turns it into a lattice model [61].

One very interesting feature about lattice models is their capability to capture the scale effects inherent to structured solids. This scale effects are not only visible in experiments, but can be observed in numerical solutions of discrete models. Moreover, they can be analytically proven, see [62].

The well-known Born-Kármán discrete model is now briefly analyzed as an easy but clarifying example of a 1D lattice. This lattice consists in an infinite chain of identical and equally spaced concentrated masses, interacting through linear springs. Since the model is linear, it suffices studying the propagation of a plane wave through the lattice. Any other mechanical perturbation (or phonon) can be decomposed as a sum of plane waves. Then, the temporal frequency ω of a wave can be analytically expressed as a function of its spatial frequency κ, i. e., the dispersion relation can be derived as [62]

$$\omega^2 = \frac{4G}{m} \sin^2 \left(\frac{\kappa d}{2} \right) \tag{2.1}$$

where G is the springs constant, m is the mass and d is the distance between masses. The derivation of this expression is detailed in section 5.2.3. In dimensionless variables $\bar{\kappa} = \kappa d$ and $\bar{\omega} = \frac{d}{c_0}\omega$, the dispersion relation is expressed by

$$\bar{\omega} = 2\sin\left(\frac{\bar{\kappa}}{2}\right), \tag{2.2}$$

where c_0 is the classical speed of sound $c_0 = d\sqrt{\frac{G}{m}}$.

From the dispersion relation, the phase and group velocity of traveling waves are obtained as a function of $\bar{\kappa}$ or $\bar{\omega}$. The phase velocity $\bar{v}_p$ is the rate at which the phase of the wave propagates in space. This is the velocity at which the phase of any one frequency component of the oscillation travels. The group velocity $\bar{v}_g$ is the velocity with which the overall shape of the phonons' amplitudes -known as the modulation or envelope of the oscillation- propagates through space. Fig. 2.20 shows the characteristics of oscillations propagating through the Born-Kármán chain within the first Brillouin zone [62].

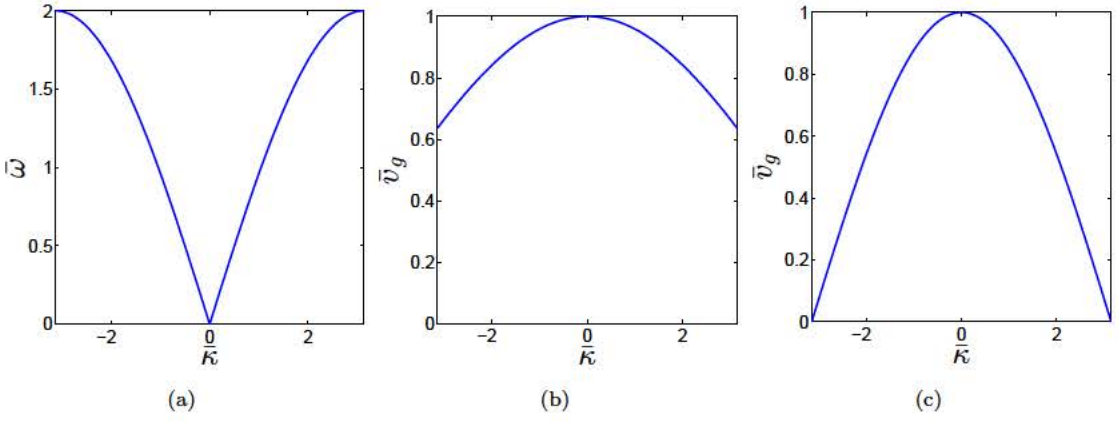

Figure 2.20: Born-Kármán chain dynamic characteristics. (a) Dispersion relation. (b) Phase velocity. (c) Group velocity.

Two important scale effects are revealed by this discrete model:

- Wave dispersion. Oscillations with different spatial frequency propagate at different velocities through the lattice.
- Cut-off frequency. There is a maximum frequency $\bar{\omega} = 2$ allowed to travel through the lattice. Higher frequencies do not propagate.

More complex lattice models show other scale effects such as band-gaps, negative propagation velocity, etc.

2.3 Inability of classical continuum to capture scale effects

Continuum mechanics deals with the analysis of the kinematics and the mechanical behavior of solids modeled as a continuous mass rather than as discrete particles. Modeling an object as a continuum assumes that the substance of the object completely fills the space it occupies. Modeling objects in this way ignores the fact that matter is made of atoms, and so is not continuous; however, when the wavelength of the problem is much greater than inter-atomic distances, such models are highly accurate. Figure 2.21 shows a continuum tube as a continuum representation of a CNT.

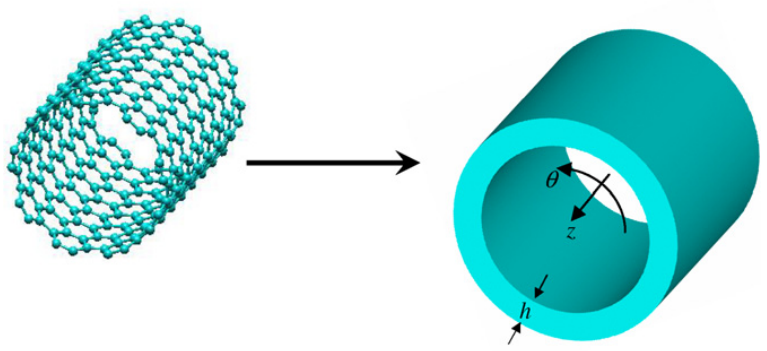

Figure 2.21: A continuous model for a CNT [9].

Continuum mechanics models have a computational advantage over the underlying discrete model. Another advantage of continuum models is the wide range of analytical and numerical methods that are available.

Unfortunately, disregarding the underlying discrete nature has its counterpart. When the scale of observation approaches the scale of the solid structure, the continuum model can predict inaccurate or unreal behavior. In fact, classical continuum mechanics models are unable to capture the aforementioned scale effects.

Following the example of the Born-Kármán chain, a continuum rod model can be formulated as a feasible alternative, see Fig. 2.22. The dimensions, density and other mechanical properties of the continuum rod are related to the properties of the discrete model. Making use of the linear continuum elasticity theory and the conservation of momentum law, the governing equation of the rod is found.

Figure 2.22: A discrete and an equivalent continuum for a rod.

Then, the dispersion relation of the classical continuum linear rod is reached by imposing a plane wave solution to the problem's continuum formulation.

$$\omega = \sqrt{\frac{E}{\rho}}\kappa \tag{2.3}$$

where ρ is the density and E is the Young modulus of the solid.

Given the relation between discrete and continuum models variables (see chapter 6), the dimensionless dispersion relation predicted by the continuum model reads

$$\bar{\omega} = \bar{\kappa} \tag{2.4}$$

Then, the phase and group velocities v_p, v_g of the continuum rod are constant, equal to the unity and independent of the wave length or frequency.

The continuum model:

- Does not predict wave dispersion. Oscillations with different spatial frequency propagate at the same velocity through the lattice.
- Does not show a cutoff frequency. All the frequencies propagate through the lattice.

The mechanical behavior predicted by the continuum model matches the discrete one when $\kappa d \ll 1$, that is, when the structural distance is much smaller than the characteristic length of the perturbations that take place in the considered phenomenon.

3 Brief overview on some generalized continuum linear theories and continualization methods

Microstructured solids present characteristic scale effects, such as the existence of band-gaps or forbidden frequencies, a cutoff frequency and highly dispersive dynamic behavior.

The classical continuum models do not depend on any size nor micro-structure parameter. These models are consequently not able to predict any size effect. Therefore, a broad number of different generalized continuum models have been postulated in order to have a versatile analytic tool for the study and resolution of problems involving structured solids.

There are two kinds of generalized continuum models widely used nowadays:

- Nonlocal continuum models.
- Gradient continuum models.

In the subsequent sections one nonlocal and two gradient preexisting models are presented. These elasticity theories were developed for infinitesimal deformations problems. In chapter 4, we propose original extensions of these generalized continuum models to finite deformations formulation.

3.1 Nonlocal linear Eringen elasticity theory

Eringen derived [27, 28, 63, 64] an integral constitutive formulation which contains only one additional length scale parameter. The Eringen formulation states that the nonlocal stress-tensor $\underline{\underline{\sigma}}(\underline{x}, t)$ at any point x in a body can be expressed as

$$\underline{\underline{\sigma}}(\underline{x}, t) = \int_{\mathbf{B}} \alpha\left(|\underline{x}' - \underline{x}|, k_e\right) \underline{\underline{\widetilde{\sigma}}}(\underline{x}, t) d\mathbf{B}(\underline{x}') \tag{3.1}$$

where $\underline{\underline{\widetilde{\sigma}}}(\underline{x}, t)$ is the classical local stress tensor at point $\underline{x}$, which is related to the infinitesimal strain tensor $\underline{\underline{e}}(\underline{x}, t)$ by the conventional constitutive relations for a Hookean material

$$\underline{\underline{\widetilde{\sigma}}}(\underline{x}, t) = \underline{\underline{\mathbf{C}}} : \underline{\underline{e}}(\underline{x}, t) \tag{3.2}$$

where $\underline{\underline{\mathbf{C}}}$ is the fourth-order elasticity tensor and $\underline{\underline{e}}(\underline{x}, t)$ is given by

$$\underline{\underline{e}}(\underline{x}, t) = \frac{1}{2}\left(\underline{\nabla} \underline{u}(\underline{x}, t) + \underline{u}(\underline{x}, t) \underline{\nabla}\right) \tag{3.3}$$

where $\underline{u}$ is the displacement and $\underline{\nabla}$ is the gradient operator.

According to the nonlocal theory, the stress tensor in a point is function not only of the strain tensor in that point, but of the strains in the whole solid. Eq. (3.1) states the contribution to the stress field at the point $\underline{x}$ of the strain field in all the points of the body, weighted through the nonlocal modulus $\alpha\left(|\underline{x}' - \underline{x}|, k_e\right)$. Here, $|\underline{x}' - \underline{x}|$ is the Euclidean distance and k_e is a material constant given by $k_e = e_0 d$, that depends on the microstructure characteristic length d trough an adjusting constant of the material e_0.

The kernel should meet the following main properties [65 67]:

1. It acquires a maximum at $x' = x$ and has to decay to zero at large distances (i.e., satisfies the Saint-Venant principle).

2. When k tends to zero, it must revert to the Dirac delta and classical elasticity is recovered in the limit of vanishing internal characteristic lengths.

3. It has to satisfy the normalization condition.

4. It is a Green function of a linear differential operator L with constant or variable coefficients of any order, thus $\mathbb{L}k(|x - x'|, k) = \delta(|x - x'|)$.

5. It has dimensions of [length]$^{-n}$, n being the spatial dimensions of the problem at hand.

Both Eqs. (3.1) and (3.2) define the considered nonlocal constitutive behavior of a Hookean solid.

The equation of motion is obtained by applying momentum conservation

$$\nabla_x \cdot \underline{\underline{\sigma}}(\underline{x}, t) + \underline{f}(\underline{x}, t) = \rho(\underline{x}) \frac{\partial^2 \underline{u}(\underline{x}, t)}{\partial t^2} \tag{3.4}$$

$$\underline{\underline{\sigma}}(\underline{x}, t) = \underline{\underline{\sigma}}(\underline{x}, t)^T. \tag{3.5}$$

This model has been hardly used in its original integral formulation, since its application leads to integro-differential equations of motion, whose analytical solution is not straightforward. Therefore, there are some works in which FE based solutions are proposed [68, 69].

In addition, since the kernel is normalized for an infinite domain, there are issues associated to the application of this model to finite domains. To solve them and based on the original theory, Altan [70] and Eringen [64] postulated, separately, a mixed local-nonlocal elasticity theory. This theory defines the stress as a combination of a local part and a nonlocal one. The local and nonlocal stress parts are weighted to obtain the total stress. The mixed local-nonlocal theory has been used by several authors [71 74].

In practice, the integral definition of the Eringen nonlocal constitutive model represents a difficult hurdle to save when solving any real or theoretical problem.

For a class of physically admissible kernel $\alpha\left(|\mathbf{x'} - \mathbf{x}|, k_e\right)$, Eringen showed [75] that the nonlocal constitutive equations given by the integral formulation could be replaced by gradients. So, for the case of the following kernel

$$\alpha\left(|\underline{x}' - \underline{x}|, k_e\right) = \frac{1}{2k_e} e^{-\frac{|\underline{x}' - \underline{x}|}{k_e}}, \tag{3.6}$$

the constitutive equation Eq. (3.1) can be written its equivalent differential form using the Helmholtz operator $\mathbb{H}$

$$\mathbb{H} = \left(1 - k_e^2 \underline{\underline{\nabla_x^2}}\right) \tag{3.7}$$

Then, in some cases,

$$\underline{\underline{\sigma}}(\underline{x}, t) = \int_{\mathbf{B}} \alpha\left(|\underline{x}' - \underline{x}|, k_e\right) \underline{\underline{\widetilde{\sigma}}}(\underline{x}, t) d\mathbf{B}(\underline{x}') \tag{3.8}$$

is equivalent to

$$\mathbb{H}\underline{\underline{\sigma}}(\underline{x}, t) = \underline{\underline{\widetilde{\sigma}}}(\underline{x}, t) \tag{3.9}$$

Where applicable, the Eringen constitutive relation is then equivalent to

$$\underline{\underline{\sigma}}(\underline{x}, t) - k_e^2 \underline{\underline{\nabla_x^2}}\,\underline{\underline{\sigma}}(\underline{x}, t) = \Lambda \mathrm{tr}\underline{\underline{e}}(\underline{x}, t)\mathrm{I} + 2\mu \underline{\underline{e}}(\underline{x}, t) \tag{3.10}$$

The balance of linear momentum results in the following equation of motion

$$\nabla \cdot \underline{\underline{\sigma}}(\underline{x}, t) + \underline{f}(\underline{x}, t) = \rho \underline{\ddot{u}}(\underline{x}, t) \tag{3.11}$$

where $\underline{f}$ represents the external body forces vector. After using Eq. (3.9), the governing equation is obtained as

$$\nabla \cdot \underline{\underline{\widetilde{\sigma}}}(\underline{x}, t) + \left(1 - k_e^2 \underline{\underline{\nabla_x^2}}\right) \underline{f}(\underline{x}, t) = \left(1 - k_e^2 \underline{\underline{\nabla_x^2}}\right) \rho \underline{\ddot{u}}(\underline{x}, t) \tag{3.12}$$

Note that the displacement field of a nonlocal solid subject to an external body force field $\underline{f}(\underline{x}, t)$ and an inertial body force $-\rho\underline{\ddot{u}}(\underline{x}, t)$ is the same as that of a classical solid subject to the external force $\left(1 - k_e^2 \underline{\underline{\nabla_x^2}}\right) \underline{f}(\underline{x}, t)$ and an inertial body force $-\left(1 - k_e^2 \underline{\underline{\nabla_x^2}}\right) \rho \underline{\ddot{u}}(\underline{x}, t)$.

Considering that the material is isotropic, the equations of motion can be obtained in terms of the displacements as

$$\begin{aligned} \left(1 - k_e^2 \underline{\underline{\nabla_x^2}}\right) \rho \underline{\ddot{u}}(\underline{x}, t) = {} & (\Lambda + \mu)\, \underline{\nabla_x} \left(\underline{\nabla_x} \underline{u}(\underline{x}, t)\right) + \mu \underline{\underline{\nabla_x^2}} \underline{u}(\underline{x}, t) \\ & + \left(1 - k_e^2 \underline{\underline{\nabla_x^2}}\right) \underline{f}(\underline{x}, t) \end{aligned} \tag{3.13}$$

Peddieson et al. [76] applied this formulation to illustrate, for the first time, the nonlocal effects in a Euler-Bernouilli nanobeam statically loaded. From this work, the differential formulation of Eringen nonlocal elasticity theory has been used to analyze the mechanical behavior of multiple nanostructures: rods [77 84], beams [85 91], beams under rotation [92 95], plates [96 98], graphene sheets [99], cylindrical shells [100 102], spherical shells [103 105], conical shells [106 108], rings [109, 110] and particles [111], as well as CNTs [112 119].

Several authors have pointed out the inconsistent results obtained from the Eringen differential model regarding both the static [76, 120 123] and dynamic behavior of a cantilever beam when compared to other boundary conditions. For all boundary conditions except the cantilever, the model predicts softening effect as the nonlocal parameter is increased. Moreover, in the dynamic behavior of free cantilever beams, Real values of the eigenvalues are not found when the nonlocal parameter is high [124]. The physical meaning of non-real eigenvalues is temporal attenuation of the movement. This is paradoxical, because the model is conservative.

Almost all the authors that claim to use Eringen theory do not apply the original formulation. In general, they have made the transformation into the differential formulation without taking into account the limits of its applicability. There are many publications that use this formulation and claim to use the nonlocal Eringen elasticity, whether the mathematical equivalence can be proven or not.

Recently, Fernández-Sáez et al. [125] showed that, in general, the results obtained with the differential formulation are not equivalent to those obtained with the integral one for a bounded Bernoulli-Euler beam. This impediment has been highlighted in a bending problem, but it also applies to other solid mechanics problems when dealing with bounded domains.

The transformation of the integral form of the constitutive equation into the differential form is valid only under certain circumstances. The validity of this transformation is, in fact, very reduced, and its requirements are difficult to accomplish in real cases.

In conclusion, the applicability of the differential formulation is reduced and should be avoided in general.

3.2 Mindlin gradient models

The Mindlin model is very interesting for its completeness and physical sense. In his seminal paper in 1964 [126], a general theory of elasticity with microstructure was presented. This theory leads to general continuous equations of motion that include the size effects of the microstructure, conditioning the behavior of the material.

Mindlin postulated a general elasticity theory based in the existence of a micro and a macro-structure, both with different densities, mechanical properties and a mechanical interaction between them. This general theory includes the displacements and rotations of both the micro and the macro-structure, involves six constitutive tensors and contain 1764 coefficients in total (903 independent). For homogeneous, centrosymmetric and isotropic materials, the number of independent constants can be reduced to 18. The equations of motion are obtained by applying the Hamilton's principle for independent variations of the micro and macrostructure displacements. In practice, the original Mindlin model is not implementable for real calculations due to the outrageous amount of parameters in it.

In the same paper [126], three alternative mathematical ways of expressing the constitutive equations in terms of the macro-structure displacement exclusively (and its derivatives) were also presented. These specializations of the general theory were called Forms I, II, and III. The derivation shows that all the three forms conduce to the same governing equations in the microstructured solid. These equations contain only three independent parameters, in addition to the Lamé constants.

In that work, the kinetic energy density was eventually formulated only in terms of the macro-velocities and their gradients

$$T = \frac{1}{2}\rho \dot{u}_j \dot{u}_j + \frac{1}{6} l^2_{pkmn} \rho' \dot{u}_{p,k} \dot{u}_{m,n} \tag{3.14}$$

where ρ and ρ' are the densities of the macro and the micro-structure respectively, and l^2_{pkmn} is a fourth order tensor that contains the scale parameters. The first subscript of the displacements indicates the direction of the considered displacement and the ones following the comma indicate derivation with respect to spatial coordinates.

The linear relation between the micro-velocity and the macro-velocity gradients established by Mindlin is the following

$$\dot{\psi}_{ij} = h_{ijkl}\dot{u}_{l,k} \tag{3.15}$$

where $\underline{\underline{\psi}}$ are the displacements and rotations of the microstructure and h_{ijkl} the relations of them to the macro-displacement velocities $\dot{u}_{l,k}$. The application of kinematic relations leads to an expression of the parameters fourth-order tensor h_{ijkl} as a function of two parameters α and β exclusively (δ_{ij} is the Kronecker delta function)

$$h_{ijkl} = \frac{1}{2}\left(\delta_{ik}\delta_{jl} - \delta_{il}\delta_{jk}\right) + \alpha\delta_{ij}\delta_{kl} + \frac{1}{2}\beta\left(\delta_{ik}\delta_{jl} + \delta_{il}\delta_{jk}\right) \tag{3.16}$$

This leads to the following value of l^2_{pkmn} tensor

$$l^2_{pkmn} = \frac{1}{2}{d_1}^2\left[\delta_{pm}\delta_{kn} - \delta_{pn}\delta_{km} + 2\alpha\left(3\alpha + 2\beta\right)\delta_{pk}\delta_{mn} + \beta^2\left(\delta_{pm}\delta_{kn} + \delta_{pn}\delta_{km}\right)\right] \tag{3.17}$$

Without loss of generality, we denominate ${k_1}^2 = \alpha\left(3\alpha + 2\beta\right)$ and ${k_2}^2 = \beta^2$. The kinetic energy is then expressed in terms of the macro-structure velocity $\underline{\dot{u}}$, the macro-structure velocity gradients $\underline{\dot{u}}'$ and three microstructure parameters d_1, k_1 and k_2.

In a paper released the year after [127], Mindlin postulated a strain and kinetic energy densities only in terms of the macro-displacements and their derivatives, that lead to the same governing equation of his previous work. This was accomplished adding higher-order derivatives of the displacements in the strain energy. The strain energy-density W was assumed to be a function of three polyadics

$$W = W(\underline{\underline{\varepsilon_1}}, \underline{\underline{\varepsilon_2}}, \underline{\underline{\varepsilon_3}}) \tag{3.18}$$

where

$$\underline{\underline{\varepsilon_1}} = \frac{1}{2}\left(\underline{\nabla}\,\underline{u} + \underline{u}\,\underline{\nabla}\right), \quad \underline{\underline{\varepsilon_2}} = \underline{\nabla}\,\underline{\nabla}\,\underline{u}, \quad \underline{\underline{\varepsilon_3}} = \underline{\nabla}\,\underline{\nabla}\,\underline{\nabla}\,\underline{u} \tag{3.19}$$

The symmetric dyadic $\underline{\underline{\varepsilon_1}}$ is the classical infinitesimal strain tensor, which contains six independent components. The triadic $\underline{\underline{\varepsilon_2}}$, symmetric in the first two positions, has eighteen independent components which could be replaced by the strain-gradient $\underline{\nabla}\underline{\underline{\varepsilon_1}}$ [126], with eighteen independent components. Similarly, $\underline{\underline{\varepsilon_3}}$,

symmetric in the first three positions, has thirty independent components which could be replaced by the second gradient of strain $\underline{\underline{\varepsilon_2}}$ or by a variety of combinations of other polyadics. Thus, the energy-density could be expressed as any one of a large number of functions of fifty-four independent variables. For homogeneous, centrosymmetric, isotropic materials, only 18 parameters remain independent (consistent with the previous theory in [126]). The strain energy density of this case was postulated as

$$\begin{aligned} W =& \frac{1}{2}\Lambda\varepsilon_{ii}\varepsilon_{jj} + \mu\varepsilon_{ij}\varepsilon_{ij} + a_1\varepsilon_{ijj}\varepsilon_{ikk} + a_2\varepsilon_{iik}\varepsilon_{kjj} + a_3\varepsilon_{iik}\varepsilon_{jjk} + a_4\varepsilon_{ijk}\varepsilon_{ijk} + a_5\varepsilon_{ijk}\varepsilon_{kji} \\ &+ b_1\varepsilon_{iijj}\varepsilon_{kkll} + b_2\varepsilon_{ijkk}\varepsilon_{ijll} + b_3\varepsilon_{iijk}\varepsilon_{jkll} + b_4\varepsilon_{iijk}\varepsilon_{llkj} + b_5\varepsilon_{iijk}\varepsilon_{lljk} + b_6\varepsilon_{ijkl}\varepsilon_{ijkl} \\ &+ b_7\varepsilon_{ijkl}\varepsilon_{jkli} + c_1\varepsilon_{ii}\varepsilon_{jjkk} + c_2\varepsilon_{ij}\varepsilon_{ijkk} + c_3\varepsilon_{ij}\varepsilon_{kkij} + b_0\varepsilon_{iijj}. \end{aligned} \tag{3.20}$$

where Λ and μ are the usual Lamé constants, and $a_1 - a_5$, $b_0 - b_7$ and $c_1 - c_3$ are the additional scale parameters. A considerable amount of independent parameters is present. Making the simplifications and hypotheses of Forms I, II or III, the number of microstructure parameters can be drastically reduced to three, leading to a more tractable model.

Once the kinetic and strain energies are defined, the Lagrangian $\mathbb{L}$ of the solid, in absence of external forces, reads

$$\mathbb{L} = \int_{\mathbf{B}} T d\mathbf{B} - \int_{\mathbf{B}} W d\mathbf{B}. \tag{3.21}$$

Applying the Hamilton's principle

$$\delta \int_{t1}^{t2} \mathbb{L} dt = 0, \tag{3.22}$$

where δ is the first variation of the functional $\mathbb{I} = \int_{t1}^{t2} \mathbb{L} dt$.

By the fundamental lemma of variational calculus, the following equation of motion is obtained

$$(\Lambda + \mu)\left(1 - l_2^2 \frac{\partial^2}{\partial x_k^2}\right) u_{j,ij} + \mu\left(1 - l_3^2 \frac{\partial^2}{\partial x_k^2}\right) u_{i,jj} = \rho_0 \left(1 - l_1^2 \frac{\partial^2}{\partial x_j^2}\right) \ddot{u}_i \tag{3.23}$$

As it is mentioned above, this equation contain the two classical Lamé constants, Λ and μ, and three additional scale parameters l_1, l_2, l_3 which have the dimension of length. The first two, l_1 and l_2, are included in the strain energy density definition, while the third one, l_3, affects the kinetic energy and takes into account the micro-inertia effect. For a complete derivation of these equations, the interested reader is referred to the original paper of Mindlin [127] and the review of Askes and Aifantis [128].

Several studies have been developed in recent years by making use of strain gradient models, applying its formulation to solve the behavior of nano-shells [129, 130], micro and nanoplates [131 134], CNT reinforced elements [49, 135], CNTs [136], nano and micro-beams [137 140], micro-structured beams [141 144], multi-cracked beams [145] and fracture mechanics [146] among others.

Moreover, Polyzos and Fotiadis [147]recovered the one-dimensional form of the Mindlin model from a continuous model with micro and macro-structure (similar to the Mindlin's derivation in 1965) and also from the continualization of a 1D discrete lattice.

3.3 Continualization techniques

Continuous models are inherently efficient since all the information about the system's behavior is condensed in only one or few equations. On the contrary, to solve the discrete model, a (large) system of equations needs to be addressed. Therefore, developments that consist in reaching a continualization of the discrete equations are common in the literature.

In this section, two different continualization techniques are presented:

- A Taylor series based method.
- A shift operator expansion method.

Both procedures lead to equations that are comparable to the classical continuum model, but, as it will be shown in subsequent chapters, the one made by using the shift operators method will include an additional term that takes into account the effect of the discreteness, that is, the size effects, through the appropriate scale parameters.

The continuous equations that arise from continualizing the discrete model are going to be compared with those obtained by applying the axiomatic generalized continuum models to the 1D problems addressed in Chapters 6 and 7. The comparison will establish a bridge between the discrete and the continuum models, enabling to relate their constants.

3.3.1 Taylor series method

One possible manner to continualize discrete equations consists in developing Taylor series expansion of the displacements of the particles $n+1$ and $n-1$ as a function of the displacement of particle n and its derivatives. In the case in which the displacement u depends only on one spatial variable

$$u_{n\pm1} = u_n \pm \frac{u'_n d}{1} + \frac{u''_n d^2}{2!} \pm \frac{u'''_n d^3}{3!} + ... \tag{3.24}$$

where d is the distance between particles in the considered lattice. The series is truncated at the desired order, compromising an equilibrium between the complexity of the obtained equation and the loss of information in the truncation.

3.3.2 Shift operator method

Another way to continualize the lattice model equations is following a non-standard approach based in pseudo-differential operators. This method was used before by Rosenau [148, 149] to continualize linear lattices. The main idea is to obtain a continuous expression for the Lagrangian of the model, and then apply the Hamilton's principle to get continuous equation(s) of motion.

The following shift operator

$$e^{d\partial_x} = 1 + d\ \partial_x + \frac{d^2}{2}\partial_x^2 + \frac{d^3}{6}\partial_x^3 + \cdots \tag{3.25}$$

permits to relate displacements between neighbor particles as

$$u_{n+1} = e^{d\partial_x} u_n. \tag{3.26}$$

Defining a continuum displacement variable u via

$$\frac{\partial u}{\partial x} = \frac{u_{n+1} - u_n}{d}, \tag{3.27}$$

and considering the pseudo-operator $\mathbb{Q}$

$$\mathbb{Q} = \frac{d\partial_x}{e^{d\partial_x} - 1} \tag{3.28}$$

u_n is described in terms of u as

$$u_n = \mathbb{Q}\ u = \left(1 - \frac{d\partial_x}{2} + \frac{d^2\partial_x^2}{12} + O(d^4)\right) u. \tag{3.29}$$

Therefore, the kinetic energy term $\dot{u}_n$ in terms of u is given by [149]

$$\dot{u}_n^2 = (\mathbb{Q}\dot{u}, \mathbb{Q}\dot{u}) = \dot{u}^2 + \frac{d^2}{12}\left(\dot{u}'\right)^2 + O(d^4) \tag{3.30}$$

Using these relations in the definition of strain and kinetic energies of the model, the Lagrangian of the system is formulated in continuous variables.

4 Formulation of two nonlinear generalized continuum models

In the last chapter, we presented a brief review of the most used linear generalized continuum models. Those models have been widely used to predict the static and dynamic behavior of structured solids under the assumptions of linearity, that is, whenever the deformations are infinitesimal.

As stated before, there are a considerable amount of problems of technological interest and applications in which structured solids are subjected to nonlinear elastic deformations.

With the aim of deriving continuum models which capture scale effects in nonlinear structured solids, we propose two axiomatic generalized continuum models, based in the aforementioned linear theories. These novel models constitute an alternative to nonlinear discrete models and address the deficiencies of the classical continuum ones.

The models are used afterwards for the analysis and resolution of two nonlinear mechanical problems in chapters 6 and 7, which represent two nonlinear discrete solids described in chapter 5.

4.1 Classical nonlinear model

First, we explain a well-known classical nonlinear continuum model and its particularization for infinitesimal deformations. This model will constitute a special case of the nonlinear generalized continuum ones, as it is are recovered if the microstructure is disregarded and therefore will be only valid for non structured solids.

4.1.1 Nonlinear St. Venant-Kirchhoff model

The classical St. Venant-Kirchhoff continuum model is briefly presented in this section. In the following formulations, capital letter variables are referred to initial configuration (Lagrangian formulation) and lower case indicate the actual deformed one.

The displacement vector of a material (Lagrangian) point P is given by

$$\underline{u}(X,t) = \underline{x} - \underline{X}, \tag{4.1}$$

where $\underline{X}$ are the coordinates of the point P in the initial undeformed configuration and $\underline{x}$ the coordinates in the current configuration.

The movement of a body with initial or undeformed configuration given by $\mathbf{B}_0 \subset \mathbb{R}^3$ is described by the function $\underline{\chi} : \mathbf{B}_0 \rightarrow \mathbf{B}_t \subset \mathbb{R}^3$. The displacement function $\underline{\chi}$ maps the material point $\underline{X}$ into the spatial (Eulerian) point $\underline{x} = \underline{\chi}(\underline{X}, t)$. The deformation gradient tensor $\underline{\underline{F}}(\underline{X}, t)$ is defined by

$$\underline{\underline{F}}(\underline{X}, t) = \underline{\nabla_X}\, \underline{\chi}(\underline{X}, t) \tag{4.2}$$

A solid is defined as hyperelastic if a stored energy density function $W(\underline{\underline{F}}(\underline{X}, t), \underline{X})$ exists, so that the First Piola-Kirchhoff Stress Tensor $\underline{\underline{\tilde{P}}}(\underline{X}, t)$ can be derived as [150]

$$\underline{\underline{\tilde{P}}}(\underline{X}, t) = \frac{\partial W(\underline{\underline{F}}(\underline{X}, t), \underline{X})}{\partial \underline{\underline{F}}(\underline{X}, t)} \tag{4.3}$$

Due to objectivity reasons, the general constitutive Equation (4.3) can be expressed in terms of the second Piola-Kirchhoff stress tensor, $\underline{\underline{\widetilde{S}}}(\underline{X},t)$, as [151]

$$\underline{\underline{\widetilde{S}}}(\underline{X},t)=\frac{\partial W(\underline{\underline{\varepsilon}}^{GL}(\underline{X},t),\underline{X})}{\partial \underline{\underline{\varepsilon}}^{GL}(\underline{X},t)} \tag{4.4}$$

where $\underline{\underline{\varepsilon}}^{GL}(\underline{X},t)$ is the Green-Lagrange strain tensor, defined as [152]

$$\underline{\underline{\varepsilon}}^{GL}(\underline{X},t)=\frac{1}{2}\left(\underline{\underline{F}}^{T}(\underline{X},t)\underline{\underline{F}}(\underline{X},t)-\mathrm{I}\right) \tag{4.5}$$

where I is the identity tensor.

For the case of the classical Saint Venant-Kirchhoff model (SVK), the energy stored in the solid is expressed as

$$W=\frac{1}{2}\Lambda\left(\mathrm{tr}\underline{\underline{\varepsilon}}^{GL}(\underline{X},t)\right)^{2}\mathrm{I}+\mu\underline{\underline{\varepsilon}}^{GL}(\underline{X},t):\underline{\underline{\varepsilon}}^{GL}(\underline{X},t), \tag{4.6}$$

Therefore the following relation holds [151] between the second Piola-Kirchhoff stress tensor $\underline{\underline{\widetilde{S}}}(\underline{X},t)$ and its energetically conjugated pair, $\underline{\underline{\varepsilon}}^{GL}(\underline{X},t)$

$$\underline{\underline{\widetilde{S}}}(\underline{X},t)=\Lambda\mathrm{tr}\underline{\underline{\varepsilon}}^{GL}(\underline{X},t)\mathrm{I}+2\mu\underline{\underline{\varepsilon}}^{GL}(\underline{X},t) \tag{4.7}$$

The second Piola-Kirchhoff stress tensor $\underline{\underline{\widetilde{S}}}(\underline{X},t)$ and the first Piola-Kirchhoff stress tensor $\underline{\underline{\widetilde{P}}}(\underline{X},t)$ are related by [151]

$$\underline{\underline{\widetilde{P}}}(\underline{X},t)=\underline{\underline{F}}(\underline{X},t)\underline{\underline{\widetilde{S}}}(\underline{X},t). \tag{4.8}$$

To formulate the equation of motion of the nonlinear elastic problem, it is necessary to add, to the above constitutive equations, the corresponding balance laws (linear and angular momentum), i.e. [150]

$$\underline{\nabla_X}\cdot\underline{\underline{\widetilde{P}}}(\underline{X},t)+\underline{f}(\underline{X},t)=\rho_0(\underline{X})\frac{\partial^2\underline{u}(\underline{X},t)}{\partial t^2} \tag{4.9}$$

$$\underline{\underline{\widetilde{P}}}(\underline{X},t)\underline{\underline{F}}(\underline{X},t)^{T}=\underline{\underline{F}}(\underline{X},t)\underline{\underline{\widetilde{P}}}^{T}(\underline{X},t) \tag{4.10}$$

where $\underline{f}(\underline{X},t)$ are the body forces, $\rho_0(\underline{X})$ is the mass density referred to the initial (Lagrangian) configuration and $\frac{\partial(\bullet)}{\partial(t)}$ is the material time derivative.

The problem formulation should be completed with the appropriate initial and boundary conditions.

4.1.1.1 Recovery of the linear elasticity continuum model

For the case of infinitesimal deformations, the following relations hold

$$\underline{\underline{\varepsilon}}^{GL}(\underline{X},t) \approx \underline{\underline{e}}(\underline{x},t), \qquad \underline{\underline{\widetilde{S}}}(\underline{X},t) \approx \underline{\underline{\widetilde{P}}}(\underline{X},t) \approx \underline{\underline{\widetilde{\sigma}}}(\underline{x},t) \tag{4.11}$$

where $\underline{\underline{\widetilde{\sigma}}}(\underline{x},t)$ is the Cauchy stress tensor. Thus, the classical linear equations for the elasticity theory in infinitesimal deformations are recovered

$$\underline{\underline{\widetilde{\sigma}}}(\underline{x},t) = \Lambda \mathrm{tr}\underline{\underline{e}}(\underline{x},t)\mathrm{I} + 2\mu\underline{\underline{e}}(\underline{x},t) \tag{4.12}$$

$$\underline{\underline{e}}(\underline{x},t) = \frac{1}{2}\left(\nabla\underline{u}(\underline{x},t) + \nabla\underline{u}(\underline{x},t)^T\right) \tag{4.13}$$

where $\underline{\underline{e}}(\underline{x},t)$ is the infinitesimal strain tensor. The linear and angular momentum balance equations of the classical linear model read

$$\underline{\nabla_x} \cdot \underline{\underline{\widetilde{\sigma}}}(\underline{x},t) + \underline{f}(\underline{x},t) = \rho(\underline{x})\frac{\partial^2\underline{u}(\underline{x},t)}{\partial t^2} \tag{4.14}$$

$$\underline{\underline{\widetilde{\sigma}}}(\underline{x},t) = \underline{\underline{\widetilde{\sigma}}}(\underline{x},t)^T \tag{4.15}$$

4.2 Nonlinear nonlocal model

The Eringen nonlocal elasticity theory is widely used in infinitesimal deformation problems, and only a few attempts have been done up to date to incorporate large strains and rotations. However, those works used the differential formulation of the Eringen elasticity. In this respect, Reddy [30] considered the nonlinear von Kármán strains in the analysis of nonlocal formulation of bending of beams and plates under the assumptions of small strains and moderate rotations. Subsequently, this theory has been applied to study the large amplitude free vibration of nanobeams by Şimşek [31]. In addition, the work of Li [153] studies the buckling of nonlinear beams based on a nonlocal continuum theory. Nevertheless, in these works a general formulation of the Eringen nonlocal theory of elasticity valid for finite deformations is not given. In this section we postulate a general extension of this theory to finite deformations in integral form, and we call it nonlinear nonlocal model (NNL).

We consider a nonlocal hyperelastic material as follows

$$\underline{\underline{P}}(\underline{X},t)=\int_{\mathbf{B}_0}\alpha\left(|\underline{X}'-\underline{X}|,k_e\right)\frac{\partial W(\underline{\underline{F}}(\underline{X}',t),\underline{X}')}{\partial\underline{\underline{F}}(\underline{X}',t)}d\mathbf{B}_0(\underline{X}') \tag{4.16}$$

From the previous definition, we stated that $\underline{\underline{P}}(\underline{X},t)$, the nonlocal first Piola-Kirchhoff stress tensor in a point, is defined as the integral of local first Piola-Kirchhoff stress tensor, $\underline{\underline{\widetilde{P}}}(\underline{X})$, weighted by a kernel function α

$$\underline{\underline{P}}(\underline{X},t)=\int_{\mathbf{B}_0}\alpha\left(|\underline{X}'-\underline{X}|,k_e\right)\underline{\underline{\widetilde{P}}}(\underline{X}',t)d\mathbf{B}_0(\underline{X}') \tag{4.17}$$

The kernel function $\alpha\left(|\underline{X}'-\underline{X}|,k_e\right)$ in Eqs. (4.16) and (4.17) characterizes the nonlocal modulus. Euclidean Lagrangian distance is expressed by $|\underline{X}'-\underline{X}|$ and the constant $k_e=e_0d$ is a scale factor that takes into account scale effects in microstructured solid modelling.

Using the definition of local first Piola-Kirchhoff stress tensor $\underline{\underline{\widetilde{P}}}(\underline{X})$ from Eqs. (4.7) and (4.8), the constitutive equation corresponding to nonlocal elasticity valid for

finite deformations can be written in integral form as

$$\underline{\underline{P}}(\underline{X},t) = \int_{\mathbf{B}_0} \alpha\left(|\underline{X}' - \underline{X}|, k_e\right) \underline{\underline{F}}(\underline{X}',t) \left(\Lambda \mathrm{tr}\ \underline{\underline{\varepsilon}}^{GL}(\underline{X}',t)\mathrm{I} + 2\mu \underline{\underline{\varepsilon}}^{GL}(\underline{X}',t)\right) d\mathbf{B}_0(\underline{X}') \tag{4.18}$$

Thus, an elastic nonlocal problem is formulated using constitutive Eq. (4.18) and momentum conservation Eqs. (4.9) and (4.10), which do not change in the nonlocal formulation

$$\underline{\nabla_X} \cdot \underline{\underline{P}}(\underline{X},t) + \underline{f}(\underline{X},t) = \rho_0(\underline{X}) \frac{\partial^2 \underline{u}(\underline{X},t)}{\partial t^2} \tag{4.19}$$

$$\underline{\underline{P}}(\underline{X},t)\underline{\underline{F}}(\underline{X},t)^T = \underline{\underline{F}}(\underline{X},t)\underline{\underline{P}}^T(\underline{X},t) \tag{4.20}$$

The integro-differential problem should be completed with appropriate boundary and initial conditions. Due to the definition of the stresses in the model, the essential boundary conditions may differ from those of the classical model formulation.

For the case of infinitesimal deformations, the following relations hold

$$\underline{\underline{\varepsilon}}^{GL}(\underline{X},t) \approx \underline{\underline{e}}(\underline{x},t), \qquad \underline{\underline{\widetilde{S}}}(\underline{X},t) \approx \underline{\underline{\widetilde{P}}}(\underline{X},t) \approx \underline{\underline{\widetilde{\sigma}}}(\underline{x},t) \tag{4.21}$$

where $\underline{\underline{\sigma}}(\underline{x},t)$ is the nonlocal Cauchy stress tensor. Thus, the original equations for the linear nonlocal elasticity theory are recovered

$$\underline{\underline{\sigma}}(\underline{x},t) = \int_{\mathbf{B}} \alpha\left(|\underline{x}' - \underline{x}|, k_e\right) \underline{\underline{\widetilde{\sigma}}}(\underline{x}',t) d\mathbf{B}(\underline{x}') \tag{4.22}$$

$$\underline{\underline{\widetilde{\sigma}}}(\underline{x},t) = \Lambda \mathrm{tr}\underline{\underline{e}}(\underline{x},t)\mathrm{I} + 2\mu \underline{\underline{e}}(\underline{x},t) \tag{4.23}$$

$$\underline{\underline{e}}(\underline{x},t) = \frac{1}{2}\left(\nabla \underline{u}(\underline{x},t) + \nabla \underline{u}(\underline{x},t)^T\right) \tag{4.24}$$

The proposed formulation constitutes a generalization of the Eringen nonlocal elasticity theory that is applicable in finite deformation problems.

4.3 Inertia gradient nonlinear models

Part of the scientific community focused its research in nonlinear microstructured elements, studying their behavior with strain gradient based models. Thus, Vatankhah et al. [154] presented a study of nonlinear vibrations in micro-beams. Lazopoulos et al. [155] formulated the nonlinear bending and buckling of beams by using a model with higher-order derivatives of the displacements.

Other authors are more interested in wave propagation in nonlinear microstructured media. In this sense, several works have been done regarding the existence, interaction and nature of solitons within nonlinear microstructured longitudinal elements [156 159]. These works consider the existence of a micro and a macrostructure and, analogously to Mindlin's treatment, end up with a equation of motion that includes higher-order derivative terms.

4.3.0.2 The IGN model

In this thesis, we propose to use the formulation of the kinetic energy by Mindlin stated in Eq. (3.14) to account for the size-effects present in micro-structured elements. In order to capture the nonlinear behavior of the material, we use the strain energy density associated to classical hyperelastic materials. Specifically, we use the St. Venant-Kirchhoff constitutive equation, but any other hyperelastic model may be used to represent the proper nonlinear behavior of the considered material.

Therefore, in the proposed gradient nonlinear model, the following energy densities are considered

$$Strain: \qquad W = \frac{1}{2}\Lambda\left(\mathrm{tr}\underline{\underline{\varepsilon}}^{GL}(\underline{X},t)\right)^2 \mathrm{I} + \mu\underline{\underline{\varepsilon}}^{GL}(\underline{X},t) : \underline{\underline{\varepsilon}}^{GL}(\underline{X},t), \tag{4.25}$$

$$Kinetic: \qquad T = \frac{1}{2}\rho_0\left(\dot{u}_j\dot{u}_j + \frac{1}{3}l^2_{pkmn}\dot{u}_{p,k}\dot{u}_{m,n}\right), \tag{4.26}$$

where we took the densities of the micro and macro-structures to be identical.

Following the relation between the micro-velocity and the macro-velocity gradients established by Mindlin [126], the scale parameters tensor l^2_{pkmn} is expressed as

$$l^2_{pkmn} = \frac{1}{2} {d_1}^2 \left[\delta_{pm}\delta_{kn} - \delta_{pn}\delta_{km} + 2{k_1}^2\delta_{pk}\delta_{mn} + {k_2}^2\left(\delta_{pm}\delta_{kn} + \delta_{pn}\delta_{km}\right)\right] \tag{4.27}$$

The kinetic energy is then expressed in terms of the macro-structure velocity $\underline{\dot{u}}$, the macro-structure velocity gradients $\underline{\dot{u}}'$ and three scale parameters d_1, k_1 and k_2. As the kinetic energy has to be positive definite and polyconvex to accomplish thermodynamic principle's requirements, we found that the following relations must be satisfied by the model constants

$$\begin{aligned} {d_1}^2 &> 0 \\ {k_2}^2 &> 0 \\ 3{k_1}^2 + 2{k_2}^2 &> 0 \end{aligned} \tag{4.28}$$

From now on, this model is referred as the "inertia gradient nonlinear model" or IGN.

4.3.0.3 The IGN1 model

Moreover, a simpler model can be defined by reducing the number of constants or microstructure parameters. From Mindlin's strain gradient theory in 1965 [25], the kinetic energy may be postulated with only one additional scale parameter accounting for the microstructure. In that case, the scale parameters tensor l^2_{pkmn} is equal to a parameter $3k^2$ times the fourth order identity matrix with major symmetry ($l^2_{pkmn} = 3k^2\delta_{pm}\delta_{kn}$). Recall that this simplification leads to the Form I, II or III of the original theory in the linear case, Eq. (3.23), see [128].

The simplified kinetic energy density is then formulated as follows

$$T(\underline{X}, t) = \frac{1}{2}\rho_0 \left[\frac{\partial \underline{u}(\underline{X}, t)}{\partial t}\frac{\partial \underline{u}(\underline{X}, t)}{\partial t} + k^2 \frac{\partial \left(\nabla \underline{u}(\underline{X}, t)\right)}{\partial t} : \frac{\partial \left(\nabla \underline{u}(\underline{X}, t)\right)}{\partial t}\right]. \tag{4.29}$$

Then, this model has only 3 independent constitutive parameters, the two classical Lamé constants Λ and μ, and the additional microstructure parameter k. As it has only 1 additional parameter, we call this model the "One parameter inertia gradient nonlinear model" or IGN1.

Once the kinetic and strain energies are defined, the Lagrangian of the solids reads

$$\mathbb{L} = T - W. \tag{4.30}$$

By applying the Hamilton's principle

$$\delta \int_{t1}^{t2} \mathbb{L} dt = 0. \tag{4.31}$$

and the fundamental lemma of variational calculus the governing equation and the BCs are obtained.

In infinitesimal deformation problems, the Green-Lagrange strain tensor is identical to the infinitesimal deformation tensor and the original form (linear) of the Mindlin theory is recovered.

5 Discrete modelization of a kind of 1D structured solids

In this chapter, a discrete model of a one dimensional chain (a monodimensional lattice) is presented. This model is used for analyzing the nonlinear oscillations of a structured 1D solid in axial and coupled bending-axial oscillations respectively. To that extent, we particularize this 1D discrete model into two simpler formulations of the problems under study in Sections 5.2 and 5.3. The mechanical behavior of this model when the 1D element is subjected to infinitesimal deformations (linear behavior) is well know, but its analysis in Sections 5.2.3 and 5.3.3 will be very useful to understand the behavior of structured solids.

In the subsequent two chapters, 6 and 7, the performance of generalized continuum models in predicting the dynamic behavior of a structured 1D nonlinear solid is analyzed. This discrete model is taken as a reference to compare the predictions of the continuous formulations. Specific solutions obtained by both discrete and continuum models are shown and compared.

5.1 The 1D nonlinear discrete model

The model of a chain of N particles equally spaced at distance d with two degrees of freedom (horizontal and vertical displacements) is formulated. Every particle has the same mass m. Particles are joined to first neighbors by two longitudinal nonlinear elastic springs. These longitudinal springs are joined by linear elastic torsional springs between them. A sketch of the chain is shown in Fig. 5.1. Horizontal and vertical displacements of the n^{th} particle from the free equilibrium position are named u_n and v_n, meanwhile θ_n is the angle of longitudinal the n^{th} spring.

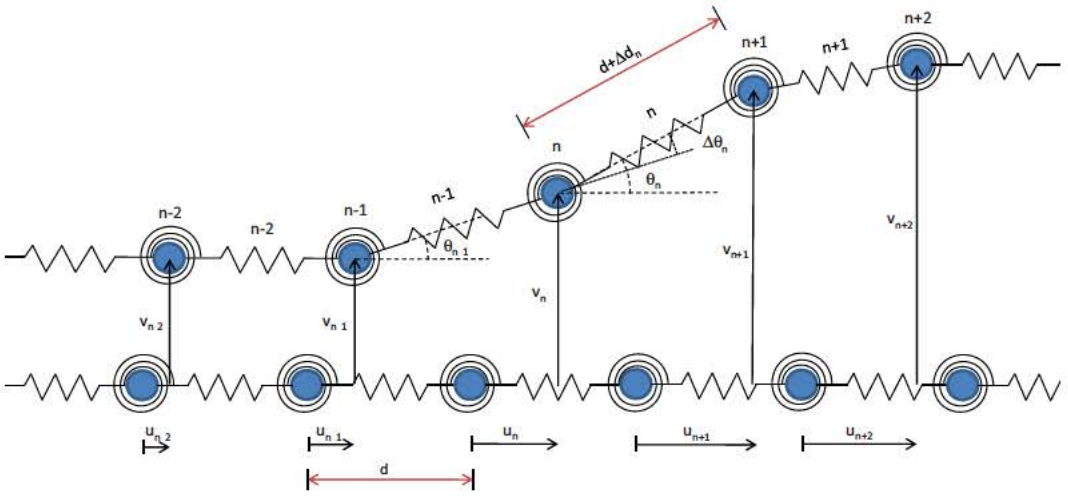

Figure 5.1: Sketch of discrete model

The constitutive equation of the nonlinear longitudinal springs is stated as

$$N_n = G\,\Delta d_n + A\,\Delta d_n^2 + B\,\Delta d_n^3 \tag{5.1}$$

where Δd_n is the variation of distance between particles from their free equilibrium distance d. The free equilibrium distance d may be referred as the characteristic length of the structured solid or the microstructure characteristic length in the future. N_n are the longitudinal forces that the springs exert over the contiguous masses, G being the linear constant of the longitudinal springs. A and B are the constants of quadratic and cubic terms of the force respectively.

The constitutive equation of the linear torsional springs is

$$M_n = C\,\Delta\Theta_n \tag{5.2}$$

where $\Delta\Theta_n$ is the variation of angle between consecutive longitudinal springs and M are the couples that the torsional springs exert over them; C is the linear constant of the torsional springs.

According to Fig. 5.1, the following kinematic relations are derived

$$\sin\Theta_n = \frac{v_{n+1} - v_n}{d + \Delta d_n} \tag{5.3}$$

$$(d + \Delta d_n)^2 = (u_{n+1} - u_n + d)^2 + (v_{n+1} - v_n)^2 \tag{5.4}$$

Then, given a set of displacements $(\{u_1, u_2, ..., u_N\}, \{v_1, ..., v_N\})$, the longitudinal force and the couple may be obtained for any spring of the chain.

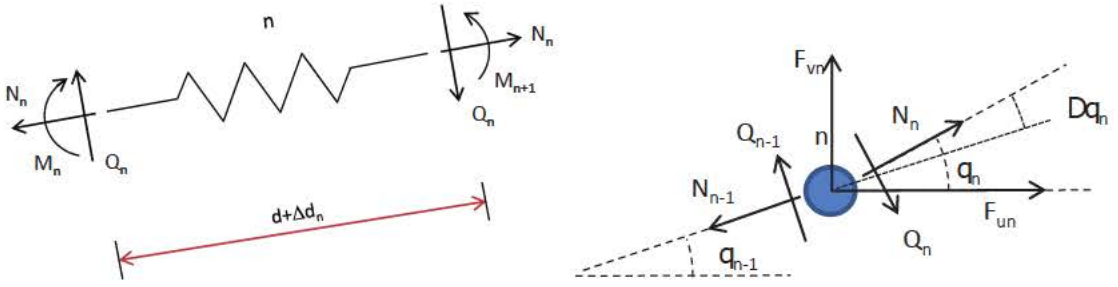

Figure 5.2: Longitudinal, normal forces and couple over: (a) n^{th} linear spring, (b) n^{th} particle.

Angular momentum balance is applied over a longitudinal spring in order to relate couples with normal forces, see Fig. 5.2(a). As the springs are massless, their inertia is zero and normal force has the same value at both ends.

$$Q_n = \frac{M_{n+1} - M_n}{d + \Delta d_n} \tag{5.5}$$

Applying linear momentum balance to each particle, two systems of equations are obtained. The first one is linked to the horizontal direction

$$N_n \cos\Theta_n - N_{n-1}\cos\Theta_{n-1} + Q_n \sin\Theta_n - Q_{n-1}\sin\Theta_{n-1} + F_{ui} = m\frac{d^2u_n}{dt^2} \tag{5.6}$$

where F_{ui} is the horizontal component of the external force over n^{th} particle.

The second is linked to the vertical direction

$$N_n \sin\Theta_n - N_{n-1}\sin\Theta_{n-1} - Q_n\cos\Theta_n + Q_{n-1}\cos\Theta_{n-1} + F_{vi} = m\frac{d^2v_n}{dt^2} \quad (5.7)$$

where F_{vi} is vertical component of external force.

These two differential system of equations, (5.6) and (5.7), govern the mechanical behavior of the 1D lattice. The reader should notice their high nonlinear character. Adding some assumptions on the nature of displacements (u, v) and generalized elongations (Δd, $\Delta\Theta$), the equations shall be simplified and eventually linearized. In this chapter, the general lattice model will be specialized to axial behavior and to coupled bending-axial behavior under small deformations and moderate rotations.

5.2 Specialization of the discrete model for longitudinal vibrations

In this section we specialize the model to address the longitudinal oscillations problem exclusively.

5.2.1 Discrete formulation of the problem

The model considers oscillations exclusively in longitudinal direction. Therefore, the transverse movement is disregarded and the torsional springs will play no role. The chain behaves identically to the one showed in Fig. 5.3.

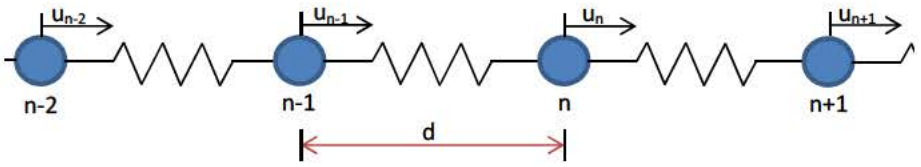

Figure 5.3: Specialized discrete model for exclusive axial oscillations

The governing equation of the problem then reads

$$\begin{aligned} m\ddot{u}_n =& G(u_{n+1} - 2u_n + u_{n-1}) + \\ & A\left[(u_{n+1} - u_n)^2 - (u_n - u_{n-1})^2\right] + \\ & B\left[(u_{n+1} - u_n)^3 - (u_n - u_{n-1})^3\right] \end{aligned} \tag{5.8}$$

The previous system of equations for $n = 1$ to N, with initial and boundary conditions, permits to analyze the dynamic behavior of the nonlinear lattice.

5.2.2 Numerical solution of the discrete problem

Evaluating existing internal forces at each time interval and applying Newton's second law , it is possible to compute the acceleration of each particle any particular configuration.

Given initial and boundary conditions it is possible to calculate the evolution of a finite chain using an integration algorithm. To do so, the Verlet algorithm [160] is proposed, which consists in expressing Δu_n as a Taylor series of $u_n^t(t)$

$$u_n^{t+1} = u_n^t + \frac{du_n^t}{dt}\Delta t + \frac{1}{2}\frac{d^2u_n^t}{dt^2}\Delta t^2 + O(\Delta t^3) \tag{5.9}$$

Higher order terms are dismissed and a uniformly accelerated motion is assumed in each time step. The first derivative is the actual velocity and the second one is the calculated acceleration. Using finite difference formula for the velocity, $\frac{du_n^t}{dt} = \frac{u_n^t - u_n^{t-1}}{\Delta t} + O(\Delta t^2)$, the explicit algorithm to calculate the next position knowing the previous two positions and acceleration is the following

$$u_n^{t+1} = 2u_n^t - u_n^{t-1} + \frac{1}{2}\frac{F_n^t}{m}\Delta t^2 + O(\Delta t^3) \tag{5.10}$$

where F_n^t is the total force over n particle at instant t, m is the mass particle, Δt is the time increment of numerical integration and the truncation error is of the order of $(\Delta t)^3$.

Forces are evaluated from particle distances using Eq. (5.1)

$$\begin{aligned} F_n =& G(u_{n+1} - 2u_n + u_{n-1}) \\ &+ A\left[(u_{n+1} - u_n)^2 - (u_n - u_{n-1})^2\right] \\ &+ B\left[(u_{n+1} - u_n)^3 - (u_n - u_{n-1})^3\right] \end{aligned} \tag{5.11}$$

If boundary conditions are free ends, the two particles in left and right boundaries are only subjected to their right and left spring respectively. On the contrary, if BC is fixed end, the displacement of the first or/and the last particle is prevented.

If the chain is initially at rest, this means that the initial condition is nil velocity for every particle. The initial condition is needed to calculate the second step position of particles. For the calculation of the second time position it is not

possible to use Verlet algorithm as it needs the two previous positions. Then, Eq. (5.9) is used directly instead, taking the velocity to be the first derivative of the displacement respect to time $\dot{u}_n^{t=1} = v^{t=1}$.

$$u_n^{t=2} = u_n^{Initial} + v^{Initial} \cdot \Delta t + \frac{1}{2}\frac{F_n^{Initial}}{m}\Delta t^2 + O(\Delta t^3) \tag{5.12}$$

Given initial and boundary conditions, the dynamic behavior of the chain is calculated step by step. A simple program has been developed and used to obtain numerical solutions from the discrete model.

Although we will study the free motion problem, it is possible to obtain the solution to a forced motion one. By introducing the external actions $F_{n,Ext}^t(n,t)$ in the sum of forces over each particle,

$$F_n^t = \sum F_{n,int}^t(u_{n-1}^t, u_n^t, u_{n+1}^t) + F_{n,Ext}^t(n,t), \tag{5.13}$$

the solution to a forced motion problem will be encountered.

Once the simulation is performed, the FFT algorithm is applied over any particle horizontal displacement -except the ones at the boundaries in no free-ends problems- to reveal normal frequencies of vibration for any specific excited normal mode.

5.2.3 Linearized longitudinal vibration problem

From Eq. (5.8), let us consider a problem in which the deformations are small, $\Delta d \ll d$, $u_{n+1} - u_n \ll 1$. The nonlinear terms will be neglected because $(u_{n+1} - u_n)^2 \ll (u_{n+1} - u_n)$. The following linear equation for free vibrations is reached.

$$m\ddot{u}_n = G\left(u_{n+1} + u_{n-1} - 2u_n\right). \tag{5.14}$$

As the governing equation of the problem is linear, the principle of superposition holds. Then, any solution can be decompose in a sum of plane waves.

Introducing the general problem solution of a longitudinal wave

$$u_n(X,t) = \hat{U}e^{i(\omega t - \kappa X)} \qquad X = nd \tag{5.15}$$

The dispersion equation is obtained as

$$\begin{aligned} u_{n\pm1} &= \hat{U}e^{i(\omega t - \kappa(n\pm1)d)} = u_n \cdot e^{\mp i\kappa d} \\ -m\omega^2 &= G\left(\cdot e^{-i\kappa d} + \cdot e^{i\kappa d} - 2\right) \end{aligned} \tag{5.16}$$

Euler sine formula is then used

$$\begin{aligned} \sin\kappa d &= \frac{e^{i\kappa d} - e^{-i\kappa d}}{2i} \\ \sin^2\kappa d &= \frac{2 - e^{2i\kappa d} - e^{-2i\kappa d}}{4} \end{aligned} \tag{5.17}$$

The dispersion relation of a discrete linear unidimensional chain vibrating in the axial direction is obtained

$$\omega^2 = \frac{4G}{m}\sin^2\left(\frac{\kappa d}{2}\right) \tag{5.18}$$

This is the dispersion relation of Born-Kármán model [62] where, using the wave velocity definition of classical continuum model $c_0 = d\sqrt{\frac{G}{m}}$, we get

$$\omega^2 = \frac{4}{d^2}c_0^2\sin^2\left(\frac{\kappa d}{2}\right) \tag{5.19}$$

In non-dimensional variables, the dispersion relation is expressed by

$$\bar{\omega} = 2\sin\left(\frac{\bar{\kappa}}{2}\right), \tag{5.20}$$

where $\bar{\kappa} = \kappa d$ and $\bar{\omega} = \frac{d}{c_0}\omega$. Figure 5.4 compares this dispersion relation to the classical continuum rod model.

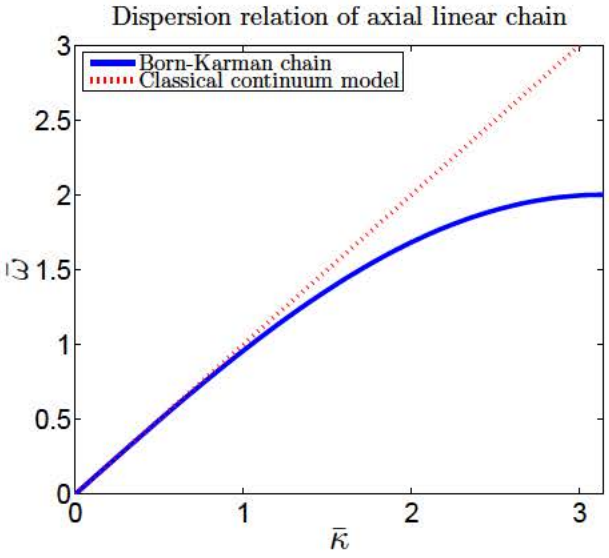

Figure 5.4: Dispersion relation of the Born-Kármán linear chain.

Once the dispersion relation is obtained, all the possible solutions of an infinite system are achieved. Moreover, the solution of a finite chain is a sum of standing waves with specific wavenumbers κ that accomplish with the BCs. These standing waves will have the frequency ω corresponding to its wavenumber κ in the dispersion relation. Therefore, the solutions of a finite chain are points of the dispersion curve. By finding the dispersion relation, all the possible solutions of a finite or infinite linear lattice are obtained.

For long waves in which the characteristic length of the lattice is much smaller than the wavelength $d \ll \lambda$, the classical linear solution shall be recovered. Therefore, in the long wave regime, $\kappa = \frac{2\pi}{\lambda} \ll \frac{2\pi}{d}$, $\kappa d \ll 2\pi$; the sine is approximated by the angle.

$$\lim_{\frac{\kappa d}{2}\to 0} \omega^2 = c_0^2\kappa^2 \tag{5.21}$$

It is important to notice that longitudinal waves are dispersive in this model, as real structured materials are. Classical continuum models are not able to capture this scale effect.

5.3 Specialization of the discrete model for the axial-transverse coupled vibrations under small deformations and moderate rotations

It is recalled that the full discrete model behavior is described by Eqs. (5.1) to (5.7), repeated here for convenience.

$$N_n = G\,\Delta d_n + A\,\Delta d_n^2 + B\,\Delta d_n^3 \tag{5.22}$$

$$M_n = C\,\Delta\Theta_n \tag{5.23}$$

$$\sin\Theta_n = \frac{v_{n+1} - v_n}{d + \Delta d_n} \tag{5.24}$$

$$(d + \Delta d_n)^2 = (u_{n+1} - u_n + d)^2 + (v_{n+1} - v_n)^2 \tag{5.25}$$

$$Q_n = \frac{M_{n+1} - M_n}{d + \Delta d_n} \tag{5.26}$$

$$N_n \cos\Theta_n - N_{n-1}\cos\Theta_{n-1} + Q_n \sin\Theta_n - Q_{n-1}\sin\Theta_{n-1} + F_{ui} = m\frac{d^2 u_n}{dt^2} \tag{5.27}$$

$$N_n \sin\Theta_n - N_{n-1}\sin\Theta_{n-1} - Q_n \cos\Theta_n + Q_{n-1}\cos\Theta_{n-1} + F_{vi} = m\frac{d^2 v_n}{dt^2} \tag{5.28}$$

This formulation is going to be specialized for small deformations ($\Delta d \ll 1$) and moderate rotations ($\Delta\Theta < 1$).

5.3.1 Discrete formulation of the problem

Considering that the displacements are small and rotations are moderate, Eqs. (5.24) and (5.25) can be approximated by

$$\sin\Theta_n = \Theta_n + O\left[{\Theta_n}^3\right] \tag{5.29}$$

$$\left(1 + \frac{\Delta d_n}{d}\right)^2 = 1 + 2\frac{\Delta d_n}{d} + \left(\frac{\Delta d_n}{d}\right)^2 = 1 + 2\frac{\Delta d_n}{d} + O\left[\left(\frac{\Delta d_n}{d}\right)^2\right] \tag{5.30}$$

Considering these approximations and the fact that $\Delta d \ll d$, Eqs. (5.24) and (5.25) lead to

$$\Theta_n = \frac{v_{n+1} - v_n}{d} \tag{5.31}$$

$$\Delta d_n = u_{n+1} - u_n + \frac{1}{2}\left(\frac{v_{n+1} - v_n}{d}\right)^2 d \tag{5.32}$$

Then, making $\cos\Theta_n \approx 1$ and $\sin\Theta_n \approx \Theta_n$, and considering that the axial stiffness is significantly higher than the flexural one in slender beams, $Q_n \sin\Theta_n \ll N_n$, the governing equations read

$$N_n - N_{n-1} + F_{ui} = m\frac{d^2 u_n}{dt^2} \tag{5.33}$$

$$N_n\Theta_n - N_{n-1}\Theta_{n-1} - Q_n + Q_{n-1} + F_{vi} = m\frac{d^2 v_n}{dt^2} \tag{5.34}$$

This equation shall be expressed in terms of springs forces (longitudinal force and couple)

$$N_n\Theta_n - N_{n-1}\Theta_{n-1} - \left(\frac{M_{n+1} - 2M_n + M_{n-1}}{d}\right) + F_{vi} = m\frac{d^2 v_n}{dt^2} \tag{5.35}$$

with

$$N_n = G\left(u_{n+1} - u_n + \frac{1}{2}\left(\frac{v_{n+1} - v_n}{d}\right)^2 d\right) \tag{5.36}$$

$$M_n = C\left(\frac{v_{n+1} - 2v_n + v_{n-1}}{d}\right) \tag{5.37}$$

where $\Delta d^2 \ll \Delta d$ has been assumed. Eqs. (5.33) and (5.35), together with the springs forces definitions in terms of displacements -Eqs. (5.36) and (5.37)-, constitute the governing equations of motion in this case.

5.3.2 Numerical solution of the discrete problem

The Verlet algorithm [160] has also been used to solve this problem numerically. The reader may recall that the algorithm integrates explicitly the governing equations step by step at each particle, based on time series expansion of the displacement vector $\underline{\delta}_n(u_n, v_n)$

$$ {}^{t+\Delta t}\underline{\delta}_n = 2\ {}^{t}\underline{\delta}_n - {}^{t-\Delta t}\underline{\delta}_n + \frac{1}{2}\frac{{}^{t}\underline{F}_n}{m}\Delta t^2 + O(\Delta t^3) \tag{5.38} $$

where ${}^{t}\underline{F}_n$ is total force over n^{th} particle at instant t, Δt is the time increment of numerical integration where the truncation error is of order $(\Delta t)^3$. The forces are evaluated from particles location using Eqs. (5.22) and (5.23). Given initial and boundary conditions, the dynamic behavior of the chain is calculated iteratively.

5.3.3 Linearized bending vibration problem

On the other hand, we may consider the case in which the horizontal displacement is zero ($u = 0$). In this case, if the vertical displacements are small, a linear system of equations govern the movement of the chain. From Eq. (5.4), and considering $v \ll d$,

$$(v_{n+1} - v_n) \ll d, \quad \tan\Theta_n = \frac{v_{n+1} - v_n}{d} \ll 1, \quad \Theta_n \simeq \frac{v_{n+1} - v_n}{d}, \quad \Delta d = \frac{\Theta^2}{2} d. \tag{5.39}$$

The elongation of the chain is, therefore, negligible. Then, from Eqs. (5.1) and (5.5) we have the following values of forces over particles

$$\begin{aligned} N_n &= 0, \\ Q_n &= C\frac{v_{n+2} - 3v_{n+1} + 3v_n - v_{n-1}}{d^2}. \end{aligned} \tag{5.40}$$

From Eq. (5.35) and taking into account that $\sin\Theta_n \approx 0$, we get

$$-Q_n + Q_{n-1} + F_{vi} = m\frac{d^2 v_n}{dt^2}. \tag{5.41}$$

For the case of free vibrations, the subsequent linear system of equations predicts the behavior of the chain.

$$C\frac{-v_{n+2} + 4v_{n+1} - 6v_n + 4v_{n-1} - v_{n-2}}{d^2} = m\frac{d^2 v_n}{dt^2}. \tag{5.42}$$

Analogously to the previous section, a wave solution is imposed

$$v_n(X,t) = \hat{V} e^{i(\omega t - \kappa X)} \qquad X = nd \tag{5.43}$$

$$-m\omega^2 = \frac{C}{d^2}\left(-e^{2i\kappa d} + 4e^{i\kappa d} - 6 + 4e^{-i\kappa d} - e^{-2i\kappa d}\right) \tag{5.44}$$

Applying Euler formula the dispersion relation of pure bending is obtained as

$$\omega^2 = \frac{16C}{md^2}\sin^4\left(\frac{\kappa d}{2}\right) \tag{5.45}$$

Taking into account that the axial and bending stiffness are related through the radius of gyration, $\frac{C}{G} = r^2$, the dispersion may be expressed as

$$\omega = 4\frac{c_0 r}{d^2}\sin^2\left(\frac{\kappa d}{2}\right) \tag{5.46}$$

In non-dimensional variables, the dispersion relation is expressed as

$$\bar{\omega} = 4\gamma^* \sin^2\left(\frac{\bar{\kappa}}{2}\right) \tag{5.47}$$

where γ^* is the non-dimensional radius of gyration $\gamma^* = \dfrac{r}{d}$.

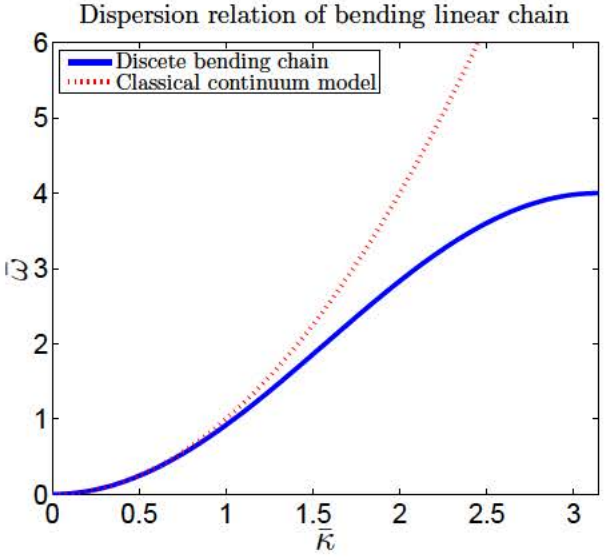

Figure 5.5: Dispersion relation of the pure bending linear chain for non-dimensional radius of gyration $\gamma^* = \frac{r}{d} = 1$.

In Fig. 5.5 the comparison between the discrete model and the Euler-Bernoulli continuum model dispersion relation is shown.

When considering long waves, the dispersion relation of the classical continuum beam model is recovered.

$$\lim_{\frac{\kappa d}{2}\to 0} \omega^2 = c_0^2 \gamma^* \kappa^4 \tag{5.48}$$

This is coherent, since in long waves the characteristic length of the structured solid is negligible compared to the wavelength of the problem. Thus, the material behaves as homogeneous to all intents.

6 Generalized continuum models for nonlinear longitudinal vibrations of the 1D structured solid

In this chapter, we analyze the free longitudinal vibrations of a finite structured 1D element subjected to large deformations. This solid may be formulated as a discrete 1D lattice of length L, particles of mass m and distance d between particles. However, the problem can be also formulated from the continuum point of view as a uniform elastic finite rod with length L, density ρ_0, and microstructure parameter k or k_e, vibrating longitudinally undergoing large deformations. The discrete system has been continualized following two different techniques, enabling to establish relations between both models parameters.

For the validation of the generalized continuum formulations, solutions will be obtained by making use of both discrete and continuum models in a problem with specific initial and boundary conditions. The objective is to compare, under different conditions, the predicted behavior of the generalized continuum microstructured rod model to what is observed in the discrete model simulations.

6.1 Axiomatic continuum models

Continuum models are inherently efficient since all the degrees of freedom are condensed into one or few through continuous spatial variables. Then, only one or few equations are needed to express the behavior of the solid under study.

In this section, three axiomatic continuum models are considered. First, the classical St. Venant-Kirchhoff (SVK) nonlinear continuum model (Section 4.1) is applied to the problem under study. Then, the NNL (Section 4.2) and IGN (Section 4.3) generalized continuum models are also applied. Subsequently, all the formulations are compared between them and with the non-standard continualization of the discrete model.

We later evince the analogies and discrepancies between the governing equation of the rod using either the NNL model, the IGN one and the non-standard continualization of the discrete model.

6.1.1 Nonlinear St. Venant-Kirchhoff model

In this subsection, the problem of a continuous finite nonlinear rod is formulated, from an axiomatic point of view, using a classical nonlinear model.

For linear homogeneous hyperelastic materials, the following relation between the second Piola-Kirchhoff stress tensor $\underline{\underline{S}}(\underline{X},t)$ and its energetically conjugated pair, the Green-Lagrange strain tensor $\underline{\underline{\varepsilon}}^{GL}(\underline{X},t)$, is established for a St. Venant-Kirchhoff solid [151]

$$\underline{\underline{S}}(\underline{X},t) = \Lambda\ \mathrm{tr}\underline{\underline{\varepsilon}}^{GL}(\underline{X},t)\mathrm{I} + 2\mu\ \underline{\underline{\varepsilon}}^{GL}(\underline{X},t) \tag{6.1}$$

where Λ and μ are the Lamé constants. This definition of the linear hyperelastic material comes from the following value of the strain energy density function

$$W(\underline{X},t) = \frac{1}{2}\Lambda\left(\mathrm{tr}\underline{\underline{\varepsilon}}^{GL}(\underline{X},t)\right)^2 + \mu\ \underline{\underline{\varepsilon}}^{GL}(\underline{X},t) : \underline{\underline{\varepsilon}}^{GL}(\underline{X},t) \tag{6.2}$$

The kinetic energy density is classically stated as

$$T(\underline{X},t) = \frac{1}{2}\rho_0 \frac{\partial \underline{u}(\underline{X},t)}{\partial t}\frac{\partial \underline{u}(\underline{X},t)}{\partial t} \tag{6.3}$$

where $\underline{u}(\underline{X},t) = \underline{x}(\underline{X},t) - \underline{X}$ is the displacement vector and $\frac{\partial(\bullet)}{\partial(t)}$ represents the material time derivative. The application of Eqs. (6.2) and (6.3) to a one-dimensional element axially vibrating reduces to

$$W = \frac{1}{2}E\left(u' + \frac{1}{2}\left(u'\right)^2\right)^2 \tag{6.4}$$

$$T = \frac{1}{2}\rho_0\left(\dot{u}\right)^2 \tag{6.5}$$

In behalf of notation simplicity, from now on spatial derivatives $\frac{\partial(\bullet)}{\partial X}$ will be expressed by $(\bullet)'$ and material time derivatives $\frac{\partial(\bullet)}{\partial t}$ will be expressed by $(\dot{\bullet})$. Also, temporal and spatial functional dependence of problem variables is no longer specified.

In absence of external loads, the Lagrangian $\mathbb{L}$ of the solid is formulated as

$$\mathbb{L} = T - W. \tag{6.6}$$

Applying the Hamilton's principle

$$\delta \int_{t1}^{t2} \mathbb{L} dt = 0. \tag{6.7}$$

From the fundamental lemma of variational calculus [161], the following expression in terms of the Lagrangian is reached [162]

$$-\left(\frac{\partial \mathbb{L}}{\partial u'}\right)' - \frac{\partial}{\partial t}\left(\frac{\partial \mathbb{L}}{\partial \dot{u}}\right) = 0 \tag{6.8}$$

and either one of the following boundary conditions (at $X = 0$ and $X = L$) must be satisfied [162]

$$u = 0 \tag{6.9}$$

$$\frac{\partial \mathbb{L}}{\partial u'} = 0 \tag{6.10}$$

The governing equation (Euler-Lagrange) is then expressed by

$$\ddot{u} = c_0^2\left[\frac{3}{2}\left(u'\right)^2 + \frac{1}{2}\left(u'\right)^3\right]' + c_0^2 u'' \tag{6.11}$$

and boundary conditions are obtained as

$$u = 0 \qquad \text{or} \qquad \frac{c_0^2}{2}\left(2u' + 3\left(u'\right)^2 + \left(u'\right)^3\right) = 0 \tag{6.12}$$

where $c_0 = \sqrt{\frac{E}{\rho_0}}$.

This relation constitutes the movement equation for St. Venant-Kirchhoff one-dimensional solids subjected to finite deformations, which must be solved for appropriate initial and boundary conditions.

The SVK axiomatic constitutive relation is known to have a non-polyconvex energy density function, which may lead to instability problems [163]. The loss of convexity occurs for the value of $u' \leq \frac{\sqrt{3}}{3} - 1 \simeq -0.4226$.

To avoid instabilities in the solution, the results exhibited in section 6.5 are for oscillations under finite but moderate deformations, which ensures that no section of the rod goes beyond the stability region. Despite the inherent instability of the SVK continuum model, we chose it to illustrate the performance of the nonlinear generalized continuum one due to its formal value and well knowingness. Figure

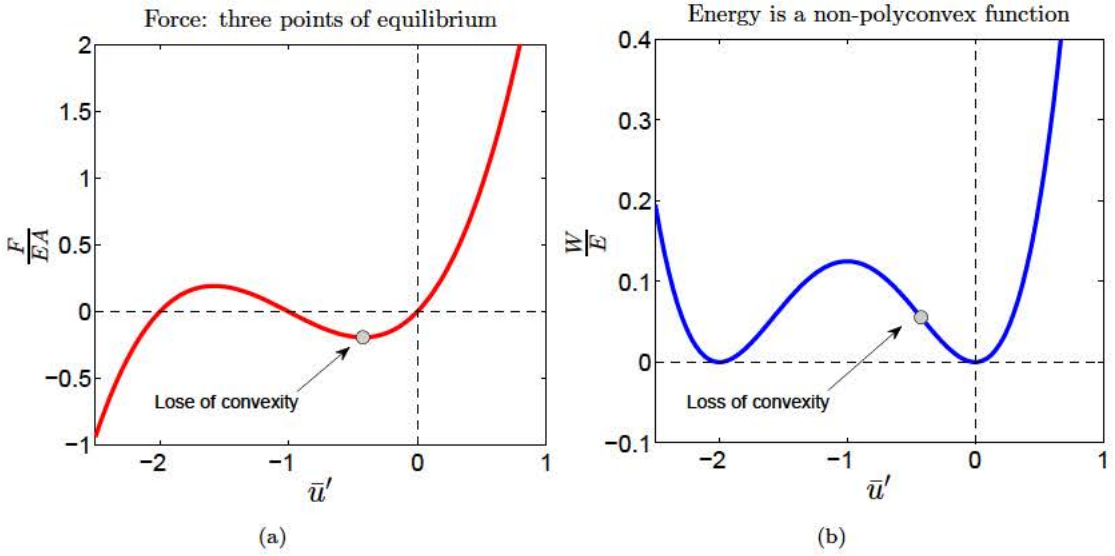

Figure 6.1: Dimensionless (a) axial force and (b) strain energy density in any section of a St. Venant-Kirchhoff rod as a function of its elongation.

6.1 shows the shape of the dimensionless strain energy density and axial force in a section of a SVK rod as a function of its dimensionless elongation u'. The loss of convexity of the energy density function W can be observed for the dimensionless elongation $u' \simeq -0.4226$.

6.1.2 Nonlinear nonlocal model (NNL)

In this section, we derive the equation of motion following the postulated NNL model.

The specialization to one dimension of Eqs. (4.7), (4.8), (4.5), (4.9) and (4.16) is stated by

$$\widetilde{S}(X,t) = E\varepsilon^{GL}(X,t) \tag{6.13}$$

$$\widetilde{P}(X,t) = \left(1 + \frac{\partial u(X,t)}{\partial X}\right)\widetilde{S}(X,t) \tag{6.14}$$

$$\varepsilon^{GL}(X,t) = \frac{\partial u(X,t)}{\partial X} + \frac{1}{2}\left(\frac{\partial u(X,t)}{\partial X}\right)^2 \tag{6.15}$$

$$\frac{\partial P(X,t)}{\partial X} + f(X,t) = \rho_0 \frac{\partial^2 u(X,t)}{\partial t^2} \tag{6.16}$$

$$P(X,t) = \int_L \alpha\left(|X' - X|, k_e\right)\widetilde{P}(X',t)dX' \tag{6.17}$$

where $\widetilde{S}(X,t)$ is the (1,1) component of local second Piola-Kirchhoff stress tensor, $\varepsilon^{GL}(X,t)$ is the (1,1) component of $\underline{\underline{\varepsilon}}^{GL}(X,t)$ and $f(X,t)$ are the external forces. For the nonlocal kernel $\alpha\left(|X' - X|, k_e\right)$, the Helmholtz kernel function

$$\alpha\left(|X' - X|, k_e\right) = \frac{1}{2k_e} e^{-\frac{|X'-X|}{k_e}} \tag{6.18}$$

is chosen.

By combination of Eqs. (6.16) to (6.18), the following is obtained

$$\rho_0 \frac{\partial^2 u(X,t)}{\partial t^2} = \frac{\partial}{\partial X}\int_L \frac{1}{2k_e} e^{-\frac{|X'-X|}{k_e}}\widetilde{P}(X,t)dX' + f(X,t) \tag{6.19}$$

In absence of external loads, the governing equation is then expressed by

$$\ddot{u} = c_0^2 \left(\int_L \frac{e^{-\frac{|X'-X|}{k_e}}}{2k_e}\left(u' + \frac{u'^2}{2}\right)(1+u')\,dX'\right)' \tag{6.20}$$

where $c_0 = \sqrt{\frac{E}{\rho_0}}$ is the classical sound velocity.

This relation constitutes the movement equation for nonlinear nonlocal one-dimensional solids subjected to finite deformations, which must be solved with appropriate initial and boundary conditions. The boundary conditions are, at $X = 0$ and $X = L$,

either prevented motion

$$u = 0 \tag{6.21}$$

or free ends

$$P = 0 \tag{6.22}$$

where the nonlocal stress P is related to displacement u by

$$P = \int_L \frac{e^{-\frac{|X'-X|}{k_e}}}{2k_e} E\left(u' + \frac{u'^2}{2}\right)(1+u')\,dX' \tag{6.23}$$

6.1.3 Inertia gradient nonlinear model

The dynamic problem of a uniform linear elastic finite rod with length L and density ρ_0, as undergoing large deformations, is now formulated by making use of the IGN model, presented in section 4.3.

The application of Eqs. (4.25) and (4.26) to a one-dimensional solid reduces to

$$W = \frac{1}{2}E\left(u' + \frac{1}{2}\left(u'\right)^2\right)^2 \tag{6.24}$$

$$T = \frac{1}{2}\rho_0\left(\left(\dot{u}\right)^2 + \frac{1}{3}l_{1111}^2\left(\dot{u}'\right)^2\right) \tag{6.25}$$

From the simplification of parameters in Eq. (3.17), $l_{1111}^2 = {d_1}^2\left({k_1}^2 + \frac{{k_2}^2}{2}\right)$. However, we can express the coefficient of $\ddot{u}'$ with only one parameter k without loss of generality

$$\frac{1}{3}l_{1111}^2 = \frac{{d_1}^2}{3}\left({k_1}^2 + \frac{{k_2}^2}{2}\right) = k^2 \tag{6.26}$$

Note that, from all the values of the scale parameters tensor l_{pkmn}^2, only l_{1111} plays a role in this problem. We recall that in the IGN1 model, the microstructure parameters are $l_{pkmn}^2 = 3k^2\delta_{pm}\delta_{kn}$. Therefore, the IGN1 model and the IGN one lead to the same equation of motion in this case.

In absence of external loads, applying the Hamilton's principle and the fundamental principle of variational calculus as above

$$-\left(\frac{\partial \mathbb{L}}{\partial u'}\right)' - \frac{\partial}{\partial t}\left(\frac{\partial \mathbb{L}}{\partial \dot{u}}\right) + \frac{\partial}{\partial t}\left(\frac{\partial \mathbb{L}}{\partial \dot{u}'}\right)' = 0 \tag{6.27}$$

and either one of the following boundary conditions (at $X = 0$ and $X = L$) must be satisfied

$$u = 0 \tag{6.28}$$

$$\frac{\partial \mathbb{L}}{\partial u'} - \frac{\partial}{\partial t}\left(\frac{\partial \mathbb{L}}{\partial \dot{u}'}\right) = 0 \tag{6.29}$$

The governing equation is then expressed by

$$\ddot{u} = c_0^2\left[\frac{3}{2}\left(u'\right)^2 + \frac{1}{2}\left(u'\right)^3\right]' + c_0^2 u'' + k^2\left(\ddot{u}\right)'' \tag{6.30}$$

where $c_0 = \sqrt{\frac{E}{\rho_0}}$ is the classical sound velocity.

This relation constitutes the movement equation for this Mindlin-type one-dimensional solids subjected to finite deformations, which must be solved for appropriate initial and boundary conditions.

From Eqs. (6.28) and (6.29), either one of the subsequent boundary conditions must be satisfied at each end

$$u = 0 \tag{6.31}$$

$$\frac{c_0^2}{2}\left(2u' + 3\left(u'\right)^2 + \left(u'\right)^3\right) + k^2\ddot{u}' = 0 \tag{6.32}$$

Comparing the equation of motion of the classical SVK model with the IGN and the IGN1 ones, it is seen that the latter has one more term, $k^2\ddot{u}''$. We will show the influence of this term in the dynamic behavior and how it accounts for the microstructured nature of the solid.

6.2 Continuous equations formulation from continualization techniques

There are different procedures to get a continuous equation from the discrete model formulated above. Here we apply the two continualization procedures that were presented in section 3.3, the Taylor series and the shift operators method.

6.2.1 Taylor series method

A possible way to continualize discrete equations consists in developing Taylor series expansion of displacements of particles $n+1$ and $n-1$ as a function of n particle displacement and its derivatives. From Eq. (3.24),

$$u_{n\pm1} = u_n \pm \frac{\partial u}{\partial X} d + \frac{1}{2}\frac{\partial^2 u}{\partial X^2} d^2 \pm O(d^3) \tag{6.33}$$

where X is the Lagrangian coordinate all along the chain, implying that particle n is placed at position $X = nd$. The series is truncated at the desired order, compromising an equilibrium between the complexity of the obtained equation and the loss of information in the truncation.

Then, the series expansion is introduced in Eq. (5.8) and terms of higher order than $O(d^3)$ are assumed to be negligible

$$\begin{aligned} m\frac{\partial^2 u}{\partial t^2} =& G\left(\frac{\partial^2 u}{\partial X^2} d^2 + \frac{1}{12}\frac{\partial^4 u}{\partial X^4} d^4\right) \\ &+ A\left[\left(\frac{\partial u}{\partial X} d + \frac{1}{2}\frac{\partial^2 u}{\partial X^2} d^2\right)^2 - \left(\frac{\partial u}{\partial X} d - \frac{1}{2}\frac{\partial^2 u}{\partial X^2} d^2\right)^2\right] \\ &+ B\left[\left(\frac{\partial u}{\partial X} d + \frac{1}{2}\frac{\partial^2 u}{\partial X^2} d^2\right)^3 - \left(\frac{\partial u}{\partial X} d - \frac{1}{2}\frac{\partial^2 u}{\partial X^2} d^2\right)^3\right] \end{aligned} \tag{6.34}$$

The powers are evaluated using Newton's binomial theorem. Only odd terms change sign, becoming the ones remaining in the summatory

$$\begin{aligned} m\frac{\partial^2 u}{\partial t^2} =& G\left(\frac{\partial^2 u}{\partial X^2}d^2\right) + A\left(2\frac{\partial u}{\partial X}\frac{\partial^2 u}{\partial X^2}d^3\right) \\ &+B\left(3\left(\frac{\partial u}{\partial X}\right)^2\frac{\partial^2 u}{\partial X^2}d^4 + \frac{1}{4}\left(\frac{\partial^2 u}{\partial X^2}\right)^3 d^6\right) \end{aligned} \tag{6.35}$$

Keeping terms up to 4^{th} order in the continualization (Eq. (6.35)) and discarding those with d^s in which $s > 4$, the following continuous equation is reached

$$\ddot{u} = \frac{d^2 G}{m}u'' + \frac{2d^3 A}{m}u'u'' + \frac{3d^4 B}{m}\left(u'\right)^2 u'' \tag{6.36}$$

The boundary conditions of the lattice model are applicable to the first and last particles of the chain ($n = 1$ and $n = N$). Two possibilities exist, the movement of these particles being either free or constrained. In the case of no motion, the boundary conditions of the continualized model can be stated as

$$u(X_{u_1}, t) = 0, \quad u(X_{u_N}, t) = 0 \tag{6.37}$$

On the contrary, the free BC on the first or last particle may be expressed using an additional ghost particle (u_0 or u_{N+1}). To achieve nil forces, the ghost particles movements shall be equal to the real ones

$$u_0 = u_1, \quad u_{N+1} = u_N \tag{6.38}$$

Fig. 6.2 illustrates how the BC is applied.

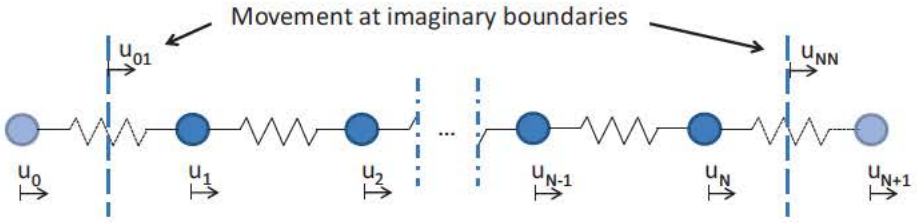

Figure 6.2: Sketch of the artificial construction to apply free ends BCs.

Applying the Taylor series to a point in the middle between real and ghost particles, the following equation is obtained (only left boundary is formulated, right is

analogous)

$$u_1 - u_0 = 2u'_{01}\frac{d}{2} + O\left(d^3\right) \tag{6.39}$$

Considering the same truncation order, the free end boundary condition is stated in the continualized model by

$$u'_{01} = 0, \quad u'_{NN} = 0 \tag{6.40}$$

6.2.2 Shift operator method

The continualization of the lattice model will be now developed following a non-standard approach based in pseudo-differential operators. This method was used before by Rosenau [148, 149] to continualize linear lattices. In this case, the key point is encountering a continuous expression of the kinetic energy density that takes into account the discreteness of the lattice.

The Lagrangian of the discrete model can be written as

$$\mathbb{L}_D = \sum_n \frac{1}{2} m \ \dot{u}_n^2 - \sum_n \left[\frac{1}{2} G \left(u_{n+1} - u_n \right)^2 + \frac{1}{3} A \left(u_{n+1} - u_n \right)^3 + \frac{1}{4} B \left(u_{n+1} - u_n \right)^4 \right] \tag{6.41}$$

The shift operator expressed in Eq. (3.25)

$$e^{d\partial_X} = 1 + d \ \partial_X + \frac{d^2}{2} \partial_X^2 + \frac{d^3}{6} \partial_X^3 + \cdots \tag{6.42}$$

permits to relate displacements between neighbor particles as $u_{n+1} = e^{d\partial_X} u_n$. Now, recalling the definition a continuum displacement variable u in Eq. (3.27)

$$\frac{\partial u}{\partial X} = \frac{u_{n+1} - u_n}{d}, \tag{6.43}$$

and considering pseudo-operator $\mathbb{Q} = \frac{d\partial_X}{e^{d\partial_X} - 1}$, u_n is described in terms of u

$$u_n = \mathbb{Q} \ u = \left(1 - \frac{d\partial_X}{2} + \frac{d^2 \partial_X^2}{12} + O(d^4) \right) u. \tag{6.44}$$

Therefore, the kinetic energy in terms of u is now given by [149]

$$\dot{u}_n^2 = (\mathbb{Q}\dot{u}, \mathbb{Q}\dot{u}) = \dot{u}^2 + \frac{d^2}{12} \left(\dot{u}' \right)^2 + O(d^4) \tag{6.45}$$

In absence of body forces nor external loads, the Lagrangian is expressed as

$$\mathbb{L}(t) = \int_{\mathbf{B}_0} \left(W(\underline{X}, t) - T(\underline{X}, t) \right) d\underline{X} \tag{6.46}$$

Taking advantage of Eq. (6.43) and of Eq. (6.45) up to $O(d^4)$ we obtain the approximate continuum Lagrangian

$$\mathbb{L}_C = \int_L \frac{1}{2}\frac{m}{d}\left[\dot{u}^2 + \frac{d^2}{12}\left(\dot{u}'\right)^2\right]\,\mathrm{d}x - \int_L \left[\frac{1}{2}Gd\left(u'\right)^2 + \frac{1}{3}Ad^2\left(u'\right)^3 + \frac{1}{4}Bd^3\left(u'\right)^4\right]\mathrm{d}x \tag{6.47}$$

Applying the Hamilton's principle,

$$\delta\int_{t_0}^{t_1}\mathbb{L}(t)dt = 0 \tag{6.48}$$

where δ is the first variation of the Lagrangian functional $\mathbb{L}(t)$.

Then, applying the fundamental Lemma of Variational Calculus [162], we get the subsequent Euler-Lagrange equation of motion

$$\ddot{u} = \frac{d^2G}{m}u'' + \frac{2d^3A}{m}u'u'' + \frac{3d^4B}{m}\left(u'\right)^2u'' + \frac{d^2}{12}\ddot{u}'', \tag{6.49}$$

and boundary conditions as

$$u = 0 \tag{6.50}$$

or

$$Gu' + Ad\left(u'\right)^2 + Bd^2\left(u'\right)^3 + \frac{m}{12}\ddot{u}' = 0. \tag{6.51}$$

Once a continuous equation of the problem and its corresponding BCs are available either via Taylor series (6.36) or shift operators (6.49), differential calculus tools can be applied to get the solution. The advantage of much computationally efficient numerical methods arise, but the accuracy of the results shall be proven.

The continualization process itself will distort the behavior of the model due to chopping at $O(d^4)$. Adding higher order terms leads to a continuum model with higher fidelity respect to the discrete one, but also more complex, which would result in a loss of computational advantage.

The comparison between both the discrete and continuum models is addressed in Section 6.5.

6.3 Comparison between models and brief discussion

In this section we summarize and discuss the different strategies, models and equations for the structured rod motion formulation.

We used two assumptions in the different formulations: considering the solid as a discrete system or as a continuous one. Then, we achieved six formulations by addressing the problem with three particular strategies:

1. Formulating the reference discrete model.
2. Formulating the problem using axiomatic continuum models.
   (a) With the classical SVK continuum theory.
   (b) With the postulated nonlinear nonlocal model (NNL).
   (c) With the postulated inertia gradient nonlinear model (IGN).
3. Continualizing the discrete model formulation.
   (a) With a Taylor series approach.
   (b) With shift operators.

Table (6.1) summarizes all the formulations and their characteristics.

Model Name	Approach	Governing equation	Eq. number	Scale effects?
Reference Discrete	Discrete	$m\ddot{u}_n = G(u_{n+1} - 2u_n + u_{n-1}) + A\left[(u_{n+1} - u_n)^2 - (u_n - u_{n-1})^2\right] + B\left[(u_{n+1} - u_n)^3 - (u_n - u_{n-1})^3\right]$	(5.8)	Yes
SVK	Classical continuum	$\ddot{u} = c_0^2 u'' + 3c_0^2 u' u'' + \frac{3}{2} c_0^2 \left(u'\right)^2 u''$	(6.11)	No
NNL	Generalized continuum	$\ddot{u} = c_0^2 \left(\int_L \frac{e^{-\frac{\lvert X' - X \rvert}{k_e}}}{2k_e} \left(u' + \frac{u'^2}{2} \right) (1 + u')\, dX' \right)'$	(6.20)	Yes
IGN	Generalized continuum	$\ddot{u} = c_0^2 u'' + 3c_0^2 u' u'' + \frac{3}{2} c_0^2 \left(u'\right)^2 u'' + k^2 \left(\ddot{u}\right)''$	(6.30)	Yes
Taylor	Taylor continualization	$\ddot{u} = \frac{d^2 G}{m} u'' + \frac{2d^3 A}{m} u' u'' + \frac{3d^4 B}{m} \left(u'\right)^2 u''$	(6.36)	No
Shift operators	Non-standard continualization	$\ddot{u} = \frac{d^2 G}{m} u'' + \frac{2d^3 A}{m} u' u'' + \frac{3d^4 B}{m} \left(u'\right)^2 u'' + \frac{d^2}{12} \ddot{u}''$	(6.49)	Yes

Table 6.1: Summary of the six formulations used for the longitudinal oscillations problem.

We ended up with a system of second order ODEs for the discrete formulation, 4 different continuous formulations expressed by a nonlinear PDE and the nonlinear Eringen formulation, which is expressed by a nonlinear integro-differential equation.

Let us compare the 4 PDE formulations. First, it is seen that the equation derived from Taylor continualization (6.36) is formally equivalent to that obtained with the axiomatic nonlinear SVK classical continuum model, Eq. (6.11). In particular, they match term by term if the continuous and discrete material properties are related adequately

$$A = \frac{3}{2}\frac{c_0^2 m}{d^3} = \frac{3}{2}\frac{G}{d}; \qquad B = \frac{c_0^2 m}{2d^4} = \frac{G}{2d^2} \tag{6.52}$$

Compatible values of the continuum model constants E and ρ_0 with the last relation are

$$E = \frac{G}{d}; \qquad \rho_0 = \frac{m}{d^3} \tag{6.53}$$

These relations enable to establish the conditions to compare continuum models with the equivalent discrete one, taken as reference.

Now, we take a further step by comparing the equation from the non-standard continualization based on shift operators (6.49) with the equation of the microstructured continuous rod formulated by the generalized continuum IGN model (6.30). Both equations have an additional term that takes into account the size effects. These equations are shown below for a better comparison

$$\begin{aligned} \ddot{u} &= \frac{d^2 G}{m}u'' + \frac{2d^3 A}{m}u'u'' + \frac{3d^4 B}{m}\left(u'\right)^2 u'' + \frac{d^2}{12}\ddot{u}'' \\ \ddot{u} &= \quad c_0^2 u'' \quad + 3c_0^2 u'u'' \quad + \frac{3}{2}c_0^2\left(u'\right)^2 u'' \quad + k^2\ddot{u}'' \end{aligned} \tag{6.54}$$

We conclude that they will be totally equivalent if, in addition to the fitting of the nonlinear potential constants at Eq. (6.52), the microstructure parameter k is set to $k = \frac{d}{\sqrt{12}}$.

On the other hand, we also obtained the governing equation (6.20) following the nonlinear nonlocal model, which is difficult to compare to the other continuous formulations due to its integro-differential nature. This model takes into account scale effects through the additional microstructure parameter k_e.

To have a better understanding of the governing equations of motion, Eqs. (6.20) and (6.30) shall be non-dimensionalized in space and time variables using

$$\bar{u} = \frac{u}{L}; \qquad s = \frac{X}{L}; \qquad \tau = t\omega_0; \qquad \omega_0 = \frac{c_0}{L}; \qquad h = \frac{k}{L}; \qquad h_e = \frac{k_e}{L}; \quad (6.55)$$

where ω_0 is the characteristic frequency of the problem under study.

Please note that, in non-dimensional equations, partial derivatives are done respect to dimensionless spatial variable s and dimensionless time τ: $\bar{u}' = \frac{\partial \bar{u}}{\partial s}$ and $\dot{\bar{u}} = \frac{\partial \bar{u}}{\partial \tau}$, meanwhile in dimensional equations derivatives are still done respect to X and t: $u' = \frac{\partial u}{\partial X}$ and $\dot{u} = \frac{\partial u}{\partial t}$.

The reader may notice that in those problems in which the total length is much greater than the microstructural one, the length-scale parameters h_e and h become negligible ($k_e \ll L$, $k \ll L \Rightarrow h_e, h \to 0$). Thus, the classical nonlinear formulation is recovered [164, 165]

$$\ddot{\bar{u}} = \left[\frac{3}{2}\left(\bar{u}'\right)^2 + \frac{1}{2}\left(\bar{u}'\right)^3\right]' + \bar{u}'' \quad (6.56)$$

On the other hand, when deformations are infinitesimal ($u' \ll 1$), quadratic and cubic terms are assumed to be negligible, and Eqs. (**??**) to (**??**) lead to known linear classical, linear Eringen and linearized IGN formulations respectively. Table 6.2 shows a resume of the continuous governing equations for the different hypotheses.

	Linearized problem	Nonlinear problem
SVK model	$\ddot{\bar{u}} = \bar{u}''$	$\ddot{\bar{u}} = \left[\frac{3}{2}\left(\bar{u}'\right)^2 + \frac{1}{2}\left(\bar{u}'\right)^3\right]' + \bar{u}''$
NNL model	$\ddot{\bar{u}} = \left(\int_0^1 \frac{e^{-\frac{\lvert s'-s\rvert}{h_e}}}{2h_e}\bar{u}'ds'\right)'$	$\ddot{\bar{u}} = \left(\int_0^1 \frac{e^{-\frac{\lvert s'-s\rvert}{h_e}}}{2h_e}\left(\bar{u}' + \frac{\bar{u}'^2}{2}\right)(1+\bar{u}')\,ds'\right)'$
IGN model	$\ddot{\bar{u}} = \bar{u}'' + h^2\left(\ddot{\bar{u}}\right)''$	$\ddot{\bar{u}} = \left[\frac{3}{2}\left(\bar{u}'\right)^2 + \frac{1}{2}\left(\bar{u}'\right)^3\right]' + \bar{u}'' + h^2\left(\ddot{\bar{u}}\right)''$

Table 6.2: Momentum balance equation for different formulations

For a deeper understanding of the influence of the scale parameters, let us compare the dispersion relation of an infinite discrete chain oscillating longitudinally in

linear regime with the dispersion of an infinite rod formulated with the linear Eringen nonlocal elasticity theory and with the linearized IGN theory. Imposing a plane wave solution to the equation of motion, the dispersion relation is obtained.

For the discrete chain, the dispersion relation, stated in Eq. (5.19), reads

$$\omega^2 = \frac{4G}{m}\sin^2\left(\frac{\kappa d}{2}\right)$$

The dispersion relation of the linearized IGN rod obtained by imposing a wave solution reads

$$\omega^2 = c_0^2\frac{\kappa^2}{1+k^2\kappa^2} \tag{6.57}$$

In addition, obtaining the dispersion relation of the linear Eringen nonlocal rod is feasible. It follows that the mathematical transformation of the Eringen constitutive relation into a differential equation through the Helmholtz operator (see Section 3.1) is applicable for infinite solids. Applying the transformation and imposing a plane wave solution, the following dispersion relation is obtained

$$\omega^2 = c_0^2\frac{\kappa^2}{1+{k_e}^2\kappa^2} \tag{6.58}$$

Interestingly, they are identical.

We develop a Maclaurin series expansion of both dispersion equations (discrete and continuum based) and make the first two terms coincide. A surprisingly optimal value for the microstructure parameter is found, $h_e = h = \frac{d}{\sqrt{12}L}$. This value of h^2 is in full agreement with the non-standard continualization approach and so we use it when comparing specific solutions of discrete and generalized continuum models.

It is interesting how the natural value of the microstructure parameter in the gradient theory can be obtained from a non-standard continualization of the discrete model, superseding the need of calibration. This value, not only coincides with the adjustment of the parameter to the linear dispersion diagram, but also has been proposed and used by other authors in several publications [29, 166 168]. Note that in those publications this value of the microstructure parameter is found by calibrating in a phenomenological manner, in contrast with our theoretical development.

6.4 Solution of the continuous equations

The problem of the microstructured rod was formulated as a uniform linear elastic one dimensional element with finite length L, density ρ_0 and microstructure parameter k, vibrating longitudinally undergoing large deformations.

To solve the nonlinear PDEs of the continuous governing equations in Table 6.2, the Galerkin method is used. According to the method, an approximate solution $\bar{U}$ is assumed as

$$\bar{u}(s,\tau) \approx \bar{U}(s,\tau) = \Phi(s)q(\tau) \tag{6.59}$$

where $\Phi(s)$ is the shape function that must satisfy at least the essential boundary conditions and $q(\tau)$ is the unknown time-dependent function to be determined.

The continuous formulation is expressed in a differential or an integro-differential equation, which can be conceptually symbolized as $\pounds(\bar{u}) = 0$, where $\pounds$ is a differential or integro-differential operator. See Table 6.2 to recall the different formulations.

When the solution function $\bar{U}$ is introduced in last equation, we get

$$\pounds(\bar{U}) = r(s,\tau) \neq 0 \tag{6.60}$$

where $r(s,\tau)$ is the residual term.

Applying the Galerkin method

$$\int_0^1 \Phi \pounds(\bar{U}) ds = 0 \tag{6.61}$$

Then, $q(\tau)$ and its derivatives are extracted to get

$$\ddot{q}(\tau) + D_1 q(\tau) + D_2 q^2(\tau) + D_3 q^3(\tau) = 0 \tag{6.62}$$

Let us condense last Eq. (6.62) in

$$\ddot{q}(\tau) = -g(q(\tau)) \tag{6.63}$$

with

$$g(q(\tau)) = D_1 q(\tau) + D_2 q^2(\tau) + D_3 q^3(\tau) \tag{6.64}$$

Applying the following identity,

$$\frac{1}{2}\frac{\partial\left(\dot{q}^2\right)}{\partial q} = \ddot{q}(\tau) = -g(q(\tau)) \tag{6.65}$$

Eq. (6.63) can be solved by quadrature

$$\dot{q}^2 - \dot{q_0}^2 = -2\int_{q_0}^{q} g(\xi)d\xi \tag{6.66}$$

where q_0 and $\dot{q}_0$ are known initial conditions.

Then, $\dot{q}(\tau)$ and $q(\tau)$ can be obtained as follows

$$\dot{q} = \pm\sqrt{-2\int_{q_0}^{q} g(\xi)d\xi + \dot{q_0}^2} \tag{6.67}$$

$$\tau = \pm\int_{q_0}^{q} \frac{d\eta}{\sqrt{-2\int_{q_0}^{\eta} g(\xi)d\xi + \dot{q_0}^2}}. \tag{6.68}$$

6.5 Results and Discussion

Taking the discrete description of the solid as a reference, the results of the developed generalized continuum models will be contrasted paying attention to the specific features resulting from the nonlinear behavior.

Since the parameters E and ρ_0 of the continuum model have been related to the parameters G, A, B and m of the discrete counterpart through Eqs. (6.52) and (6.53), by stating the equivalence between the governing equations of NNL, IGN and continualized discrete models, the comparison of results is feasible. Regarding the third parameter present in the continuum models, k and k_e, we will discuss if their value determined from the continualization of the discrete model permits the continuum models to properly capture the size effects in both linear and nonlinear regimes.

In the subsequent sections, the features of the nonlinear behavior and the size effects are both discussed.

6.5.1 Definition of a baseline problem

In the study of this problem, free ends are considered as boundary conditions. As initial condition, the rod is at rest and deformed following a sinusoidal shape. In the discrete system this means

$$^{\tau=0}\bar{u}_n = \bar{A}_0 \cos\left(\pi\left(n-\frac{1}{2}\right)\frac{d}{L}\right); \quad ^{\tau=0}\dot{\bar{u}}_n = 0 \tag{6.69}$$

as the position of particles in equilibrium is

$$X(n) = \left(n-\frac{1}{2}\right)d \tag{6.70}$$

where $\bar{A}_0 = \frac{A_0}{L}$ is a free parameter of the problem that will be used to modulate the amplitude of deformations in the rod, thus enabling to study the induced vibrations under different regimes. Note that this initial condition impose a deformation with a wavelength of $\lambda = 2L$.

Initial conditions in the continuum model are expressed by

$$\bar{u}(X,0) = \bar{A}_0 \cos\left(\frac{\pi X}{L}\right); \quad \dot{\bar{u}}(X,0) = 0 \tag{6.71}$$

6.5.2 Results from the nonlinear discrete model

A first insight into the influence of nonlinear effects in the vibrational behavior of the solid can be provided by comparing the deformation shapes and frequencies corresponding to two different initial amplitudes, one of them of small value $\bar{A}_0 = 0.01$ and the other $\bar{A}_0 = 0.1$, one order of magnitude greater. The variables are presented in non-dimensional form, following the same procedure used for the continuum models, see Eq. (6.55). Notice that the discrete model behavior is highly dependent on the spring constants values G, A and B. These constants have been adjusted to reproduce St. Venant-Kirchhoff constitutive law. As this model present instabilities, the lattice may have unstable points as well. Nevertheless, the deformations reached in the performed simulations never go beyond the stability limit.

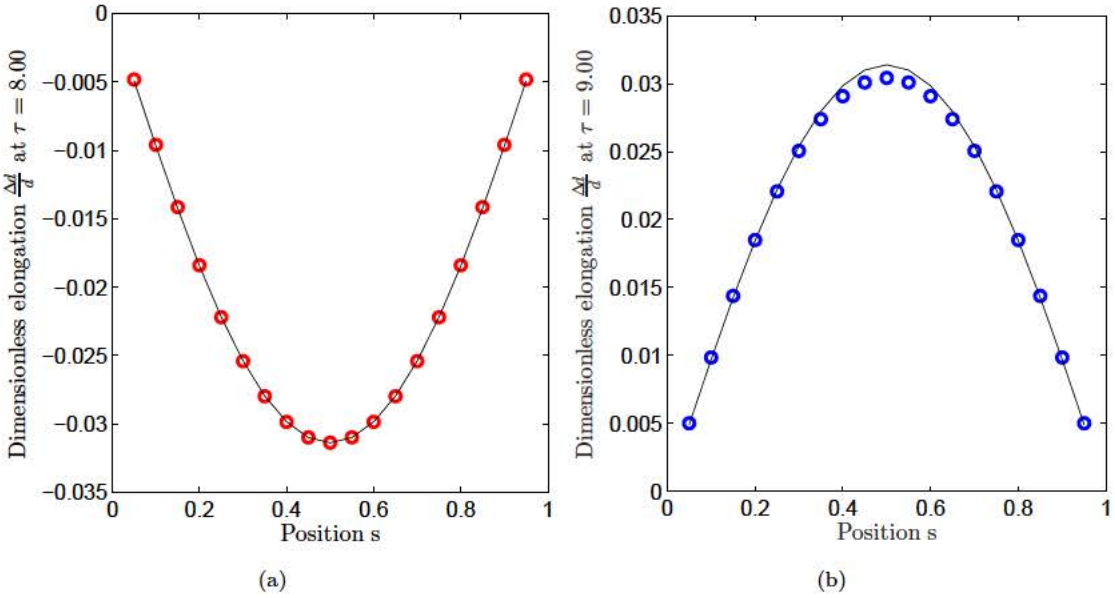

Figure 6.3: Discrete model. Results from oscillations of a 20 particle simulation with $\bar{A}_0 = 0.01$, quasi-linear regime. (a) Dimensionless elongation at a maximum compression instant. (b) Dimensionless elongation at a maximum tension instant. The black lines indicate harmonic dimensionless elongation.

Fig. 6.3 shows the deformation profiles of a lattice with $N = 20$, for the case of small vibration amplitude $\bar{A}_0 = 0.01$. It is noteworthy that the dimensionless

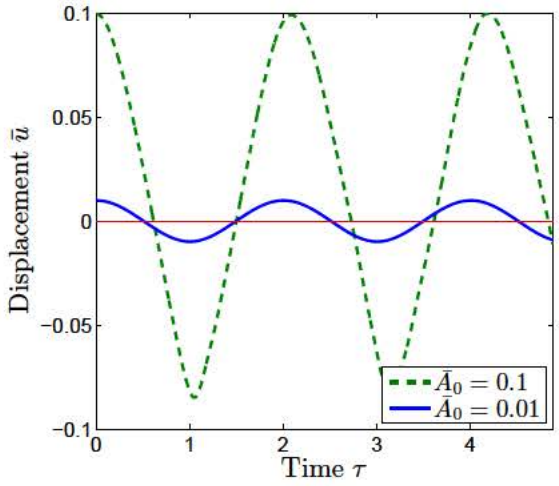

Figure 6.4: Discrete model. Displacement of particle $n = 1$ over time for different values of initial amplitude: $\bar{A}_0 = 0.01$ and $\bar{A}_0 = 0.1$.

elongation is calculated from the positions at two adjacent particles as $\frac{\Delta d}{d}$. It can be seen that the deformed shape follows the sine function, both in tension and in compression phases. Likewise, the trajectory of the particles is harmonic as shown in Fig. 6.4, implying equal amplitudes and semiperiods in tension and compression phases.

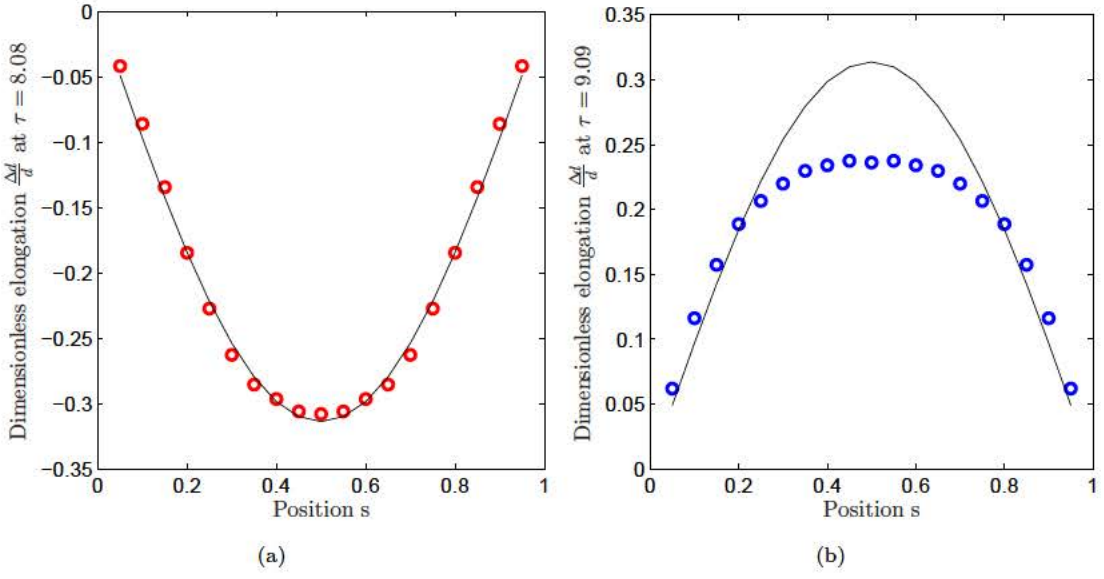

Figure 6.5: Discrete model. Results from oscillations of a 20 particle simulation with $\bar{A}_0 = 0.1$, nonlinear regime. (a) Dimensionless elongation at an instant of time in compression semi-period. (b) Dimensionless elongation at an instant of time in tension semi-period. Black lines indicate harmonic dimensionless elongation.

However, the nonlinear effect emerges as the amplitude increases. For $\bar{A}_0 = 0.1$, the deformed shape diverges from the initial sine function as time increases, as

can be seen in Fig. 6.5. Contrary to the features observed in the small amplitude regime, the trajectory of the particles is no longer harmonic and the compression semi-period becomes longer than the tensile one (see Fig. 6.4). Likewise, the amplitudes corresponding to each regime reach different values. Due to the nonlinear constitutive relation, the material softens under compression and hardens under tension. Peak values of deformation are therefore lower when the rod is elongated. Both effects are related to the constitutive function of the spring $F(\Delta d)$, that can be deduced from Eqs. (5.11) and (6.52).

With the aim to extend the previous analysis, the relation between amplitude and frequency has been determined in greater detail. This relation will subsequently be used to validate the suitability of the developed generalized continuum models in the nonlinear regime, and also to assess the potential advantage of the generalized continuum approaches to capture the size effects found in the discrete approach.

The Fast Fourier Transform of the time-domain results permitted to identify the excited frequencies of oscillation $\bar{\omega}$ and their amplitudes. As the initial shape is not exactly the shape of the normal mode of oscillation, some other normal modes are also excited.

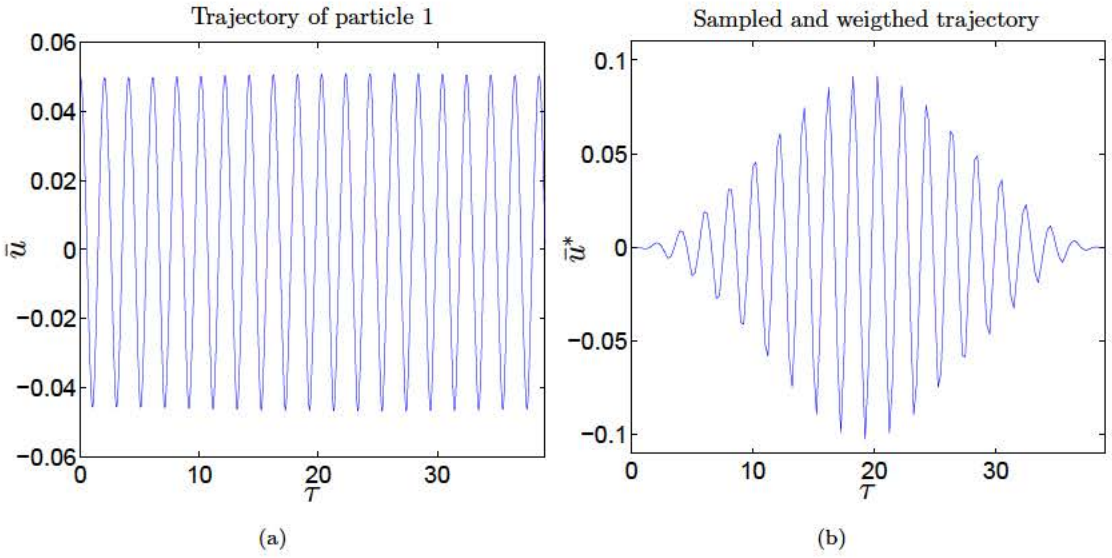

Figure 6.6: Trajectory of particle 1 in a simulation with $\bar{A}_0 = 0.05$ and $\frac{L}{d} = 20$. (a) Raw (b) Sampled and Hanning windowed.

The trajectory of any particle is sampled upon an interval Δt_s, enabling to detect frequencies up to $\omega = \frac{\pi}{\Delta t_s}$. Fig. 6.6 shows how the sampled values are then weighted with a Hanning window to smooth any discontinuities at the two ends

of the simulation interval, leading to the discrete weighted dimensionless displacement $\bar{u}^*$.

The FFT algorithm is therefore applied. Fig. 6.7 shows the frequency domain of the trajectory of a particle in a simulation as an example. In it, the frequency-domain function exhibits a clear peak corresponding to the frequency $\bar{\omega}$ of the mainly excited mode and some much smaller peaks for the additional modes. This main frequency of oscillation $\bar{\omega}$ is independent of the particle selected to sample the time-displacement function.

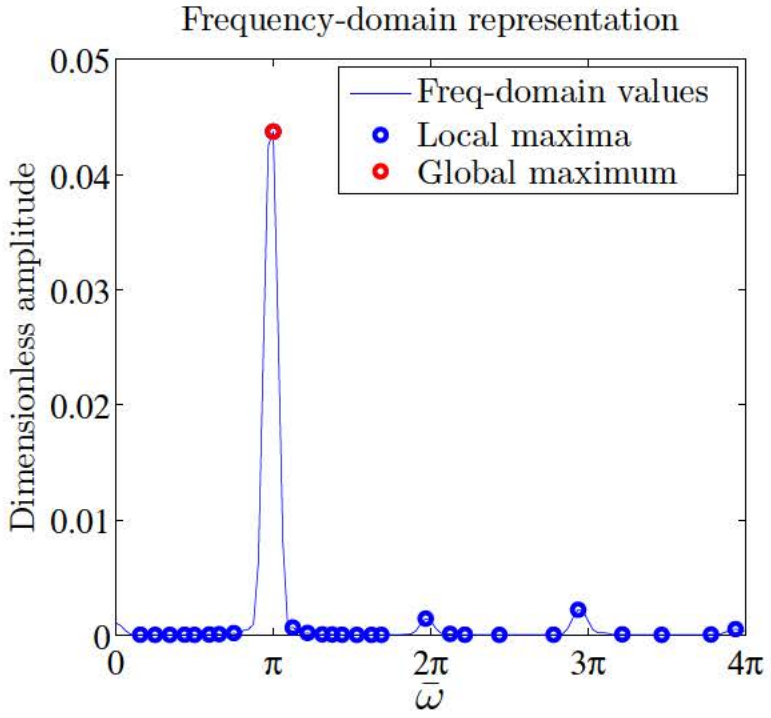

Figure 6.7: Frequency-domain of the particle motion achieved by application of FFT algorithm. Red marker indicates the main frequency of oscillation $\bar{\omega}$.

Fig. 6.8 shows the influence of the initial amplitude $\bar{A}_0$ in $\bar{\omega}$ for several ratios of $\frac{d}{L}$: the frequency decreases with increasing amplitude independently of the $\frac{d}{L}$ ratio. The reason for such a behavior is linked to the fact that the compression semi-period notably increases with $\bar{A}_0$, whereas tension semi-period decreases moderately. Fig. 6.8 also shows how the frequency decreases with increasing microstructural ratio $\frac{d}{L}$. This outcome clearly illustrates the size effect characteristic of a discrete representation of the matter.

Several comments arise from the results derived from the discrete model which, for the sake of clarity, are summarized as follows:

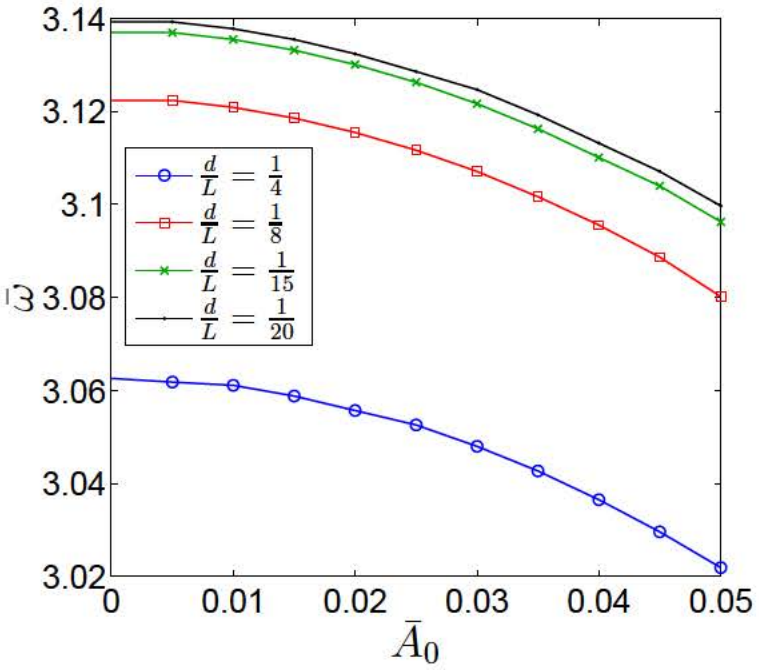

Figure 6.8: Discrete model. Non-dimensional frequency of oscillation $\bar{\omega}$ for different $\frac{d}{L}$ ratios and different initial amplitudes $\bar{A}_0$.

- If the displacement amplitude is small enough, the vibratory behavior approaches that of a linear system, both shape and displacement time-history described by harmonic functions.

- As the displacement amplitude increases, the vibratory behavior starts to show nonlinear features and the trajectory of the particles is no longer harmonic. Furthermore, the specific characteristics of the interaction force selected in this work causes a shorter semiperiod and a smaller amplitude in tension.

- The size effect emerges as the distance between particles changes, leading to smaller frequencies when d is increased, becoming comparable to the wavelength.

6.5.3 Predictions of the nonlinear generalized continuum models

The solution of the nonlinear continualized models is given by Eq. (6.59), where $\Phi(s)$ has to be chosen in accordance with boundary conditions and $q(\tau)$ is solved by Eq. (6.68). The shape function $\Phi = \cos(\pi s)$ is chosen.

In order to meet the initial conditions stated in Eq. (6.71), following values of time-dependent function have been set: $\dot{q}(0) = 0$ and $q(0) = \bar{A}_0$.

Then, from the application of Eqs. (6.66) to (6.68), $\dot{q}(\tau)$ and $q(\tau)$ can be obtained as follows

$$\dot{q}^2 = -2\int_{\bar{A}_0}^{q} g(\xi)d\xi \tag{6.72}$$

$$\dot{q} = \pm\sqrt{-2\int_{\bar{A}_0}^{q} g(\xi)d\xi} \tag{6.73}$$

$$\tau = \pm\frac{1}{\sqrt{2}}\int_{\bar{A}_0}^{q} \frac{d\eta}{\sqrt{-\int_{\bar{A}_0}^{\eta} g(\xi)d\xi}}. \tag{6.74}$$

where

$$g(q(\tau)) = D_1 q(\tau) + D_2 q^2(\tau) + D_3 q^3(\tau) \tag{6.75}$$

The coefficients D_1, D_2 and D_3, obtained by the Galerkin method, are expressed in Table 6.3.

Coefficients	Model	
	NNL	IGN
D_1	$\frac{\pi^2 e^{-1/h_e}\left(e^{1/h_e}\left(\pi^2 {h_e}^2-2h_e+1\right)-2h_e\right)}{\left(\pi^2 {h_e}^2+1\right)^2}$	$\frac{\pi^2}{1+h^2\pi^2}$
D_2	$-2\frac{\pi^2 e^{-1/h_e}\left(3\pi^2 {h_e}^2+e^{1/h_e}\left(5\pi^2 {h_e}^2+2\right)\right)}{4\pi^4 {h_e}^4+5\pi^2 {h_e}^2+1}$	$-4\frac{\pi^2}{1+h^2\pi^2}$
D_3	$\frac{3\pi^4 e^{-1/h_e}\left(e^{1/h_e}\left(9\pi^4 {h_e}^4-16\pi^2 {h_e}^3+10\pi^2 {h_e}^2+1\right)-16\pi^2 {h_e}^3\right)}{8\left(\pi^2 {h_e}^2+1\right)^2\left(9\pi^2 {h_e}^2+1\right)}$	$\frac{3}{8}\frac{\pi^4}{1+h^2\pi^2}$

Table 6.3: Coefficients D_1, D_2 and D_3 for the NNL and the IGN models, obtained by the Galerkin method.

6.5.3.1 Results of the NNL model

Due to the integral definition of the constitutive equation, it results impossible to meet the boundary conditions stated in Eq. (6.21) in this non-linear problem with free boundaries when the separation of variables is applied. Then, to achieve at least the initial condition, the shape function $\Phi = \cos(\pi s)$ is chosen, which imposes a longitudinal deformation with wavelength $\lambda = 2L$. It should be noted that, according to the strain profile imposed by the shape function Φ, a positive value of the time dependent function q corresponds to a compressive state.

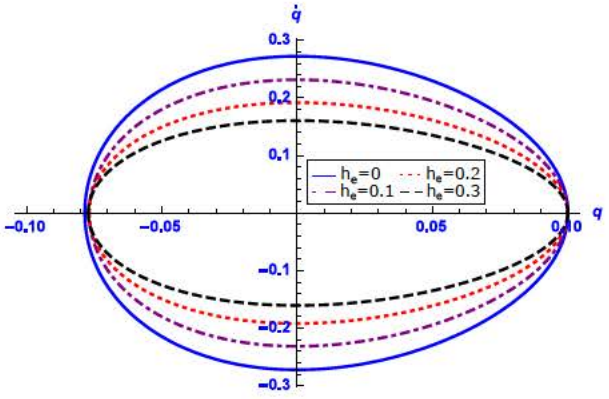

Figure 6.9: NNL continuum model. Phase diagram of the nonlinear oscillation with $\bar{A}_0 = 0.1$ and different values of length scale parameter h_e.

Fig. 6.9 depicts the phase diagram, $\dot{q}$ versus q, for an initial amplitude $\bar{A}_0 = 0.1$ and different values of the length scale parameter h_e, where closed trajectories indicate periodic movement. Fig. 6.10 shows the function q versus time τ for different values of $\bar{A}_0$. Although these values of h_e do not correspond to the $\frac{d}{L}$ ratios used in the analysis of the discrete model, they are useful to carry out a parametric analysis of the continuum model.

6.5.3.2 IGN model results

To meet the boundary conditions stated in Eq. (6.12), the same shape function $\Phi = \cos(\pi s)$ is chosen. As stated above, a positive value of the time dependent function q corresponds to a compressive state.

Fig. 6.11 depicts the phase diagram, $\dot{q}$ versus q, for an initial amplitude $\bar{A}_0 = 0.1$ and different values of the length scale parameter h, where closed trajectories indicate again periodic movement. Fig. 6.12 shows the function q versus time τ for different values of $\bar{A}_0$.

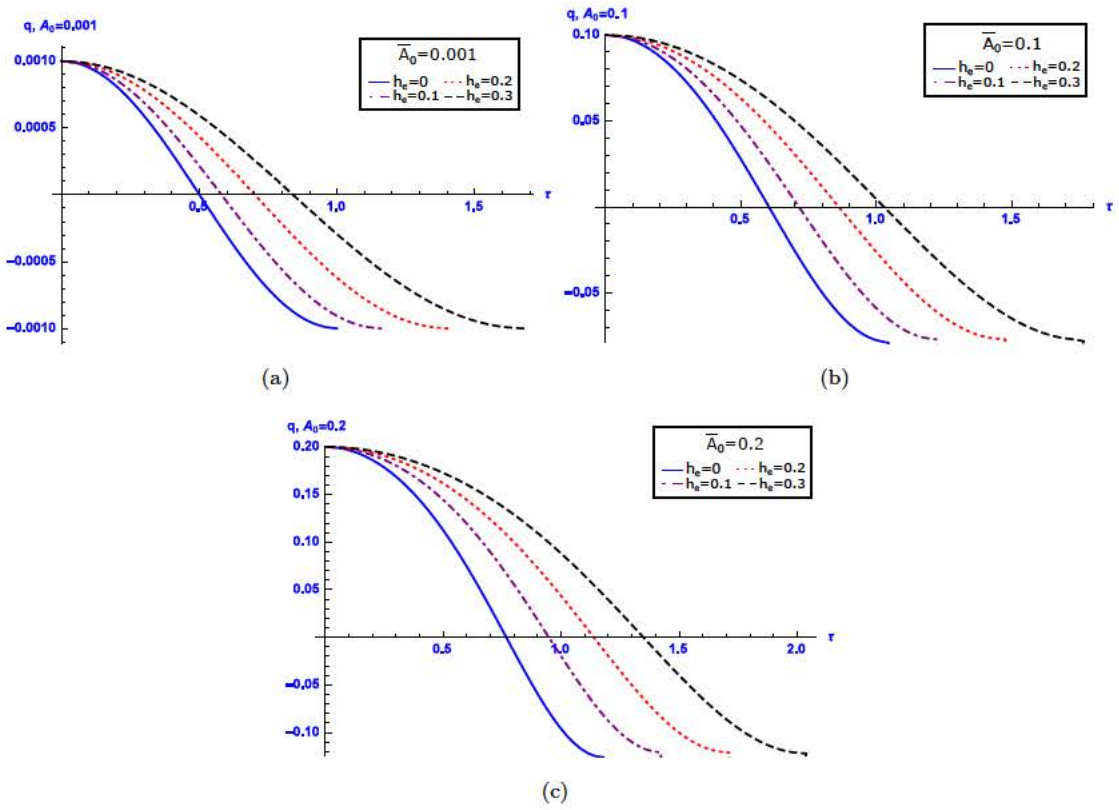

Figure 6.10: NNL continuum model. Time-dependent function q versus non-dimensional time τ for different values of length scale parameter h and initial amplitude (a) $\bar{A}_0 = 0.001$ (b) $\bar{A}_0 = 0.1$ (c) $\bar{A}_0 = 0.2$.

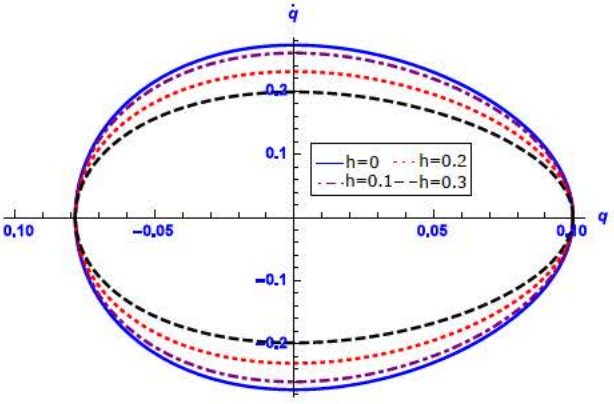

Figure 6.11: IGN continuum model. Phase diagram of the nonlinear oscillation with $\bar{A}_0 = 0.1$ and different values of length scale parameter h.

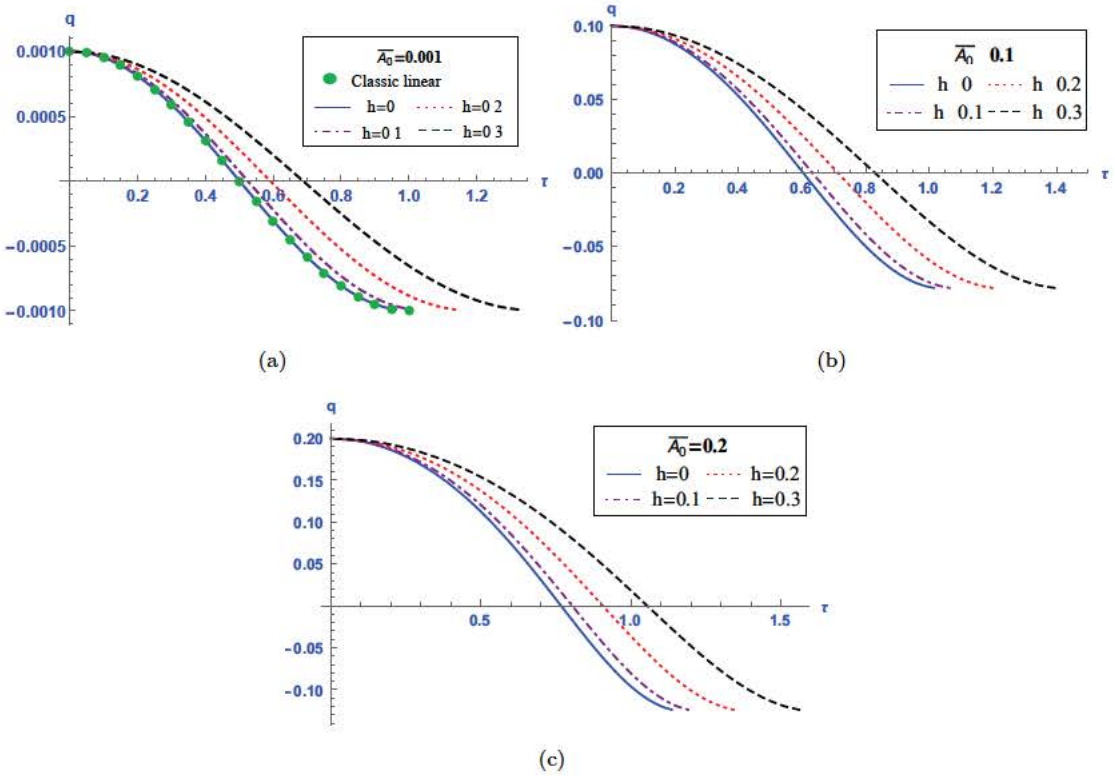

Figure 6.12: IGN continuum model. Time-dependent function q versus non-dimensional time τ for different values of length scale parameter h and initial amplitude (a) $\bar{A}_0 = 0.001$ (b) $\bar{A}_0 = 0.1$ (c) $\bar{A}_0 = 0.2$.

6.5.3.3 Main remarks from the predictions of the generalized continuum nonlinear models

It is seen that the results of the continuum models are qualitatively pretty similar. They predict the same dynamic behavior and the same response to the variables of the problem h_e, h and $\bar{A}_0$. From the analysis of the results, we reached two different conclusions, both of them fully consistent with the outcomes of the discrete model listed above.

First, the amplitude of the compression semi-period is larger. This results from the relation between stress and elongation in St. Venant-Kirchhoff materials subjected to large deformations. Second, the velocity of the oscillation, $\dot{q}$, decreases for increasing values of the length scale parameters h_e, h. Figs. 6.10 and 6.12 also show larger periods as the length scale parameter h_e and h, related to the microstructural effect, increase. This confirms the ability of the generalized continuum models to capture the size effect observed in the discrete model.

It is relevant to point out that the solution predicted by the classical nonlinear model is recovered [164, 165] for $h_e = 0$, $h = 0$, as the influence of the micro-inertia is neglected. That model is, however, unable to capture the size effects.

The continuum models are also able to capture the transient from linear to nonlinear behavior of the solid as the amplitude of the oscillation increases. When the initial amplitude is small ($\bar{A}_0 = 0.01$), the continuum models recover the harmonic trajectory of the particles, see Figs. 6.10 and 6.12. However, at higher amplitudes ($\bar{A}_0 = 0.1$, $\bar{A}_0 = 0.2$) the oscillations become nonlinear with shorter semiperiod and smaller amplitude in tension, in full accordance with the results of the discrete model.

So far, the comparison between discrete and continuum models has been strictly qualitative. The trends predicted by both models are all consistent, but a quantitative validation is still required. To that aim, the relation between amplitude and frequency has been further developed, as it was done with the discrete model. The non-dimensional angular frequency has been determined with the aid of Eq. (6.68), where the period T has been calculated as twice the difference between the times corresponding to two consecutive extrema of the function q

$$T = \frac{1}{\omega_0} 2|\tau_{q,min} - \tau_{q,max}| \tag{6.76}$$

thus leading to

$$\bar{\omega} = \frac{\pi}{|\tau_{q,min} - \tau_{q,max}|} \tag{6.77}$$

The main outcomes of the quantitative comparative analysis are discussed below.

6.5.4 Quantitative comparison. Accuracy of the generalized continuum models

The results of the discrete model highlighted the nonlinear and scale effects present in the axil vibratory behavior of the 1D media. The first is triggered by increasing values in the first derivative of the displacements, which are proportional to $\bar{A}_0$, while the second is related to changes in the microstructural ratio $\frac{d}{L}$.

On the other side, the nonlinear generalized continuum models presented herein are able to capture both effects. The trends observed with the discrete model in the angular frequencies $\bar{\omega}$, as well as the features related with the distinctive behavior in tension and compression, are properly captured by the continuum models.

Fig. 6.13 shows the dimensionless angular frequency $\bar{\omega}$ for different values of the initial amplitude $\bar{A}_0$. The length scale parameters h_e, h were suitably adjusted to $\frac{1}{\sqrt{12}}\frac{d}{L}$. The curves are replicated in each of these sub-figures in order to compare them with the results of the discrete model for $N = \{20, 15, 8, 4\}$ particles, corresponding to $\frac{d}{L} = \{\frac{1}{20}, \frac{1}{15}, \frac{1}{8}, \frac{1}{4}\}$. Fig. 6.14 shows the predictions of NNL model for the dimensionless angular frequency $\bar{\omega}$. Note that Eringen model predictions are not shown in subfigures (c) and (d) because they are out of the scale.

The curve corresponding to $h = 0$, which represents the classical case, is obviously the same for all sub-figures. As shown in Fig. 6.13(a), the results obtained with the classical nonlinear model are close to those of the discrete model if the number of particles is large, i. e. $d \ll L$. In such a case, the wave number is small compared to the limit of first Brillouin zone, and the hypotheses of the classical continuum are still valid.

On the contrary, as L and d become comparable in a discrete media with a lower $\frac{d}{L}$ ratio, the oscillation frequencies predicted by the classical continuum differ significantly from those predicted by the discrete model. Since the classical continuum is independent of the ratio $\frac{d}{L}$, it is unable to properly capture size effects.

It is seen that the predictions of the IGN continuum model are much more accurate than the classical model ones. In addition, calibration of micro-inertia parameter was not needed, but the value of h was naturally determined by a non-standard analysis of the discrete model formulation.

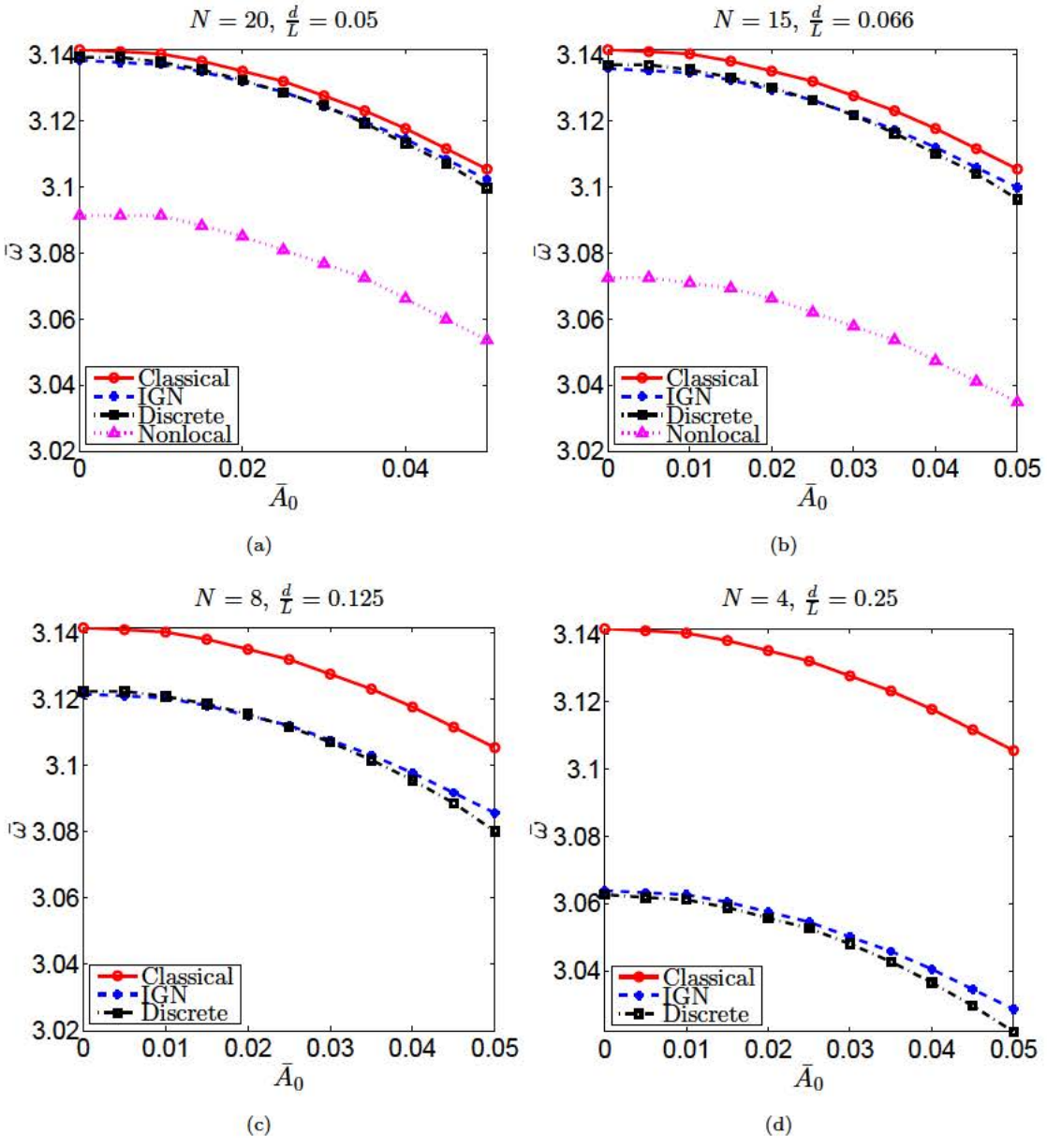

Figure 6.13: Results comparison of NNL, IGN and classical continuum models to the discrete model in a lattice with different number of particles. (a) $N = 20$. (b) $N = 15$. (c) $N = 8$. (d) $N = 4$.

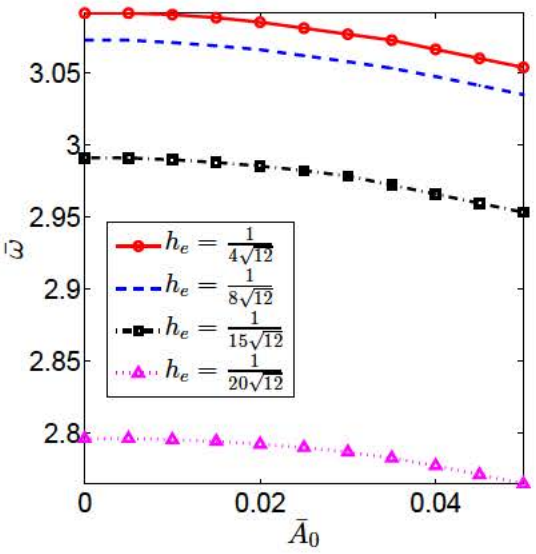

Figure 6.14: Results from NNL continuum model.

On the contrary, the predictions of the nonlinear nonlocal model are not so similar to the discrete model results. We thought of three possible causes for this bad performance of the model.

One of them is that the approximate solution from Galerkin method is not good enough. We are using only one shape function to approximate it, better approximations could be found by using two or more shape functions. Therefore, we got solutions using more shape functions, but the results did not virtually vary. In addition, the shape function(s) does not fulfill natural BCs. Regarding the free BC formulation from Eqs. 6.21 and 6.23, the BC is stated by a nonlinear integro-differential equation in which the stress at the free end depends on the deformation along the whole rod in a nonlinear way. From this fact, it is very difficult to accomplish the free end BCs.

Another possibility is related to the adjustment of the scale parameter h_e. Although we adjusted it by comparing the dispersion relation to the Born-Kármán one, other procedures may lead to a more suitable adjustment.

The other possible explanation is related to the applicability of nonlocal integral model in finite solids, see Section 3.1. Eringen himself was awarded of the problems in the applications of his original elasticity theory in finite domain problems [64]. It is also seen that its integro-differential formulation is certainly intricate. For all these reasons, we do not use this model in the following Chapter (7).

The comparison shows that the proposed IGN model provides a continuum tool for the study of nonlinear 1D structured solids. This generalized continuum model is able to predict scale effects that occur in microstructured solids and nanostructures undergoing finite deformations.

6.6 Remarks

From the previous results and their discussion, the following remarks are summarized:

- Both the NNL and the IGN continuum models lead to different governing equations for a structured rod which contains one microstructure parameter.
- The non-standard continualization of the discrete model leads to the same equation of motion as the IGN model. In this case, the scale parameter is directly related to the microstructure characteristics.
- The classical continuum model for large deformations reproduce adequately the nonlinear effects but it is unable to capture the scale effects.
- For validation purposes, the behavior of the lattice model is taken as reference. The predictions of the generalized continuum IGN model match the behavior observed in the discrete one for a value of $h = \frac{d}{\sqrt{12}L}$. On the contrary, nonlinear nonlocal model predictions are not so close to discrete model results.
- Therefore, the IGN continuum model adequately captures nonlinear and scale effects.

7 Generalized continuum models for nonlinear transverse vibrations of the 1D structured solid

In this chapter, the coupled axial-transverse oscillations of the 1D lattice formulated in chapter 5 (full model) are calculated considering the hypotheses of small displacements and moderate rotations. These hypotheses may lead to the so-called von Kármán beam in the classical continuous models. Several works considered this simplification of the full nonlinear coupled axial and bending motion as a first approximation. Among others, the paper of J. G. Eisley [169] gives a full insight into the classical continuum model that results from making von Kármán geometric nonlinearity assumptions.

The discrete counterpart of the von Kármán bending model was also studied in previous works, e.g. the paper by K. Manktelow et al. [170]. Nevertheless, these two papers considered an additional hypotheses of constant axial force along the beam/chain to avoid solving the complete coupled problem in vertical and horizontal displacements.

Here we formulate the complete dynamic problem of the 1D lattice model oscillating under small displacements and moderate rotations, as well as its standard and non-standard continualization. Then, we also derive the problem equations of a continuous Euler-Bernoulli beam under moderate rotations following the axiomatic classical and generalized continuum models formulated in chapter 4.

7.1 Axiomatic continuum models

The problem of the nonlinear axial-transverse coupled vibrations in a uniform finite beam of length L, cross-sectional area Ω, inertia I and density ρ_0 is now addressed with the aforementioned classical and generalized continuum models for microstructured solids.

7.1.1 Kinematic assumptions of the von Kármán beam

Firstly, the kinematic hypotheses and relations are derived. Then, the different continuum hyperelastic models are used to obtain the governing equation of motion.

Let us call (X, Y, Z) to the Lagrangian coordinates of the material point vector $\underline{X}$, (x, y, z) to the Eulerian coordinates of the position vector $\underline{x}(t)$, (x_0, y_0, z_0) to the components of medium line position vector $\underline{x}_0(t)$, and (u, v, w) to the components of displacement $\underline{u}(\underline{x}(t), t) = \underline{x}(t) - \underline{X}$.

According to the Euler-Bernoulli beam theory, perpendicular planes to the medium line of the undeformed beam remain plane and perpendicular in the deformed shape. Therefore, the position of any point $\underline{x}$ can be related to the position of the medium line points $\underline{x}_0$

$$x(X, Y, t) = x_0(X, t) - Y \sin \varphi(X, t) \tag{7.1}$$

$$y(X, Y, t) = y_0(X, t) + Y \cos \varphi(X, t) \tag{7.2}$$

$$z(X, Y, t) = 0 \tag{7.3}$$

where $\varphi(X, t)$ is the rotation of the considered section X at time t.

The rotation $\varphi(X, t)$ is related to the slope of the neutral axis as

$$\tan \varphi(X, t) = \frac{\partial y_0}{\partial x_0} = \frac{\partial y_0}{\partial X}\frac{\partial X}{\partial x_0} = \frac{\partial y_0}{\partial X}\left(1 + \frac{\partial u_0}{\partial X}\right)^{-1} = \frac{\partial v_0}{\partial X}\left(1 + \frac{\partial u_0}{\partial X}\right)^{-1} \tag{7.4}$$

As small displacements are considered ($|\underline{u}| \ll 1$), subsequent approximations are commonly applied

$$\begin{aligned} \cos\varphi(X,t) &\approx 1 \\ \tan\varphi(X,t) \approx \sin\varphi(X,t) &\approx \varphi(X,t) \end{aligned} \tag{7.5}$$

Small strain in the horizontal direction $\frac{\partial u_0}{\partial X} \ll 1$ is also considered

$$\left(1 + \frac{\partial u_0}{\partial X}\right)^{-1} \approx 1 \tag{7.6}$$

thus leading to the following displacement field in the beam

$$u(X,Y,t) = u_0(X,t) - Y\frac{\partial v_0}{\partial X} \tag{7.7}$$

$$v(X,Y,t) = v_0(X,t) \tag{7.8}$$

$$w(X,Y,t) = w_0(X,t) = 0 \tag{7.9}$$

The general expression for the component $(1,1)$ of the Green-Lagrange strain tensor is

$$\varepsilon_{XX}^{GL}(\underline{X},t) = \frac{\partial u}{\partial X} + \frac{1}{2}\left(\left(\frac{\partial u}{\partial X}\right)^2 + \left(\frac{\partial v}{\partial X}\right)^2 + \left(\frac{\partial w}{\partial X}\right)^2\right) \tag{7.10}$$

The nonlinear strain-displacement relationship based on assumptions of finite transverse displacements is then given by

$$\varepsilon_{XX}^{GL}(\underline{X},t) = \frac{\partial u}{\partial X} + \frac{1}{2}\left(\frac{\partial u}{\partial X}\right)^2 + \frac{1}{2}\left(\frac{\partial v}{\partial X}\right)^2 \simeq \frac{\partial u_0}{\partial X} + \frac{1}{2}\left(\frac{\partial v_0}{\partial X}\right)^2 - Y\frac{\partial^2 v_0}{\partial X^2} \tag{7.11}$$

where $\left(\frac{\partial u}{\partial X}\right)^2$ has been neglected $\left(\left(\frac{\partial u}{\partial X}\right)^2 \ll \frac{\partial u}{\partial X}\right.$ and $\left.\left(\frac{\partial u}{\partial X}\right)^2 \ll \left(\frac{\partial v}{\partial X}\right)^2\right)$.

7.1.2 Nonlinear St. Venant-Kirchhoff model

According to the Euler-Bernoulli theory of bending of straight beams, the normal stress in longitudinal direction $\widetilde{P}_{XX}(\underline{X},t)$ is given by

$$\widetilde{P}_{XX}(\underline{X},t) = F_{XX}(\underline{X},t)\widetilde{S}_{XX}(\underline{X},t) = \left(1+\frac{\partial u}{\partial X}\right) E\varepsilon^{GL}_{XX}(\underline{X},t) \tag{7.12}$$

where E is the Young modulus of the considered material, $P_{XX}(\underline{X},t)$, F_{XX} and $\widetilde{S}_{XX}$ are the $(1,1)$ components of the first Piola-Kirchhoff stress tensor, the deformation gradient and the second Piola-Kirchhoff stress tensor respectively.

The stress resultants $\widetilde{N}(X,t)$ and $\widetilde{M}(X,t)$ are defined as follows

$$\begin{gathered}\widetilde{N}(X,t) = \int_\Omega \widetilde{P}_{XX}(\underline{X},t)d\Omega = \\ E\Omega\left[\frac{\partial u_0}{\partial X} + \frac{1}{2}\left(\frac{\partial v_0}{\partial X}\right)^2 + \left(\frac{\partial u_0}{\partial X}\right)^2 + \frac{1}{2}\frac{\partial u_0}{\partial X}\left(\frac{\partial v_0}{\partial X}\right)^2\right] - EI\left(\frac{\partial^2 v_0}{\partial X^2}\right)^2\end{gathered} \tag{7.13}$$

$$\widetilde{M}(X,t) = -\int_\Omega Y\widetilde{P}_{XX}(\underline{X},t)d\Omega = EI\frac{\partial^2 v_0}{\partial X^2}\left[1+2\frac{\partial u_0}{\partial X}+\frac{1}{2}\left(\frac{\partial v_0}{\partial X}\right)^2\right] \tag{7.14}$$

where $\widetilde{N}(X,t)$ is the normal force, $\widetilde{M}(X,t)$ is the bending moment, Ω is the area of the cross-section and $I_{ZZ} \equiv I$ is the moment of inertia of the cross-section with respect to the Z axis. These are the rigorously developed stress resultants in finite deformations.

According to the von Kármán geometrically nonlinear beam theory, it is additionally assumed that longitudinal strains are small ($\frac{\partial u_0}{\partial X} \ll 1$) meanwhile rotations are moderate ($\frac{\partial u_0}{\partial X}$ and $\left(\frac{\partial v_0}{\partial X}\right)^2$ of the same order), thus leading to von Kármán beam stress resultants [30]

$$\widetilde{N}(X,t) = E\Omega\left[\frac{\partial u_0}{\partial X}+\frac{1}{2}\left(\frac{\partial v_0}{\partial X}\right)^2\right] \tag{7.15}$$

$$\widetilde{M}(X,t) = EI\frac{\partial^2 v_0}{\partial X^2} \tag{7.16}$$

From now on spatial and material time derivatives will be expressed by $(\bullet)'$ and $\dot{(\bullet)}$ respectively.

Applying momentum balance to a differential slice and neglecting rotary inertia, the governing equations of motion are obtained in terms of stress resultants

$$\widetilde{N}' + f_u = \rho_0 \Omega \ddot{u}_0 \tag{7.17}$$

$$-\widetilde{M}'' + \left[\widetilde{N} v_0'\right]' + f_v = \rho_0 \Omega \ddot{v}_0 \tag{7.18}$$

where f_u and f_v are, respectively, the horizontal and vertical components of the external force per unit length.

The nonlinear governing equations of free vibrations ($f_u = f_v = 0$) in terms of the displacements can be obtained by substituting Eqs. (7.15) and (7.16) into Eqs. (7.17) and (7.18) as follows

$$E\Omega \left[u_0' + \frac{1}{2}\left(v_0'\right)^2\right]' = \rho_0 \Omega \ddot{u}_0 \tag{7.19}$$

$$-EIv_0'''' + E\Omega\left(u_0'' v_0' + u_0' v_0'' + \frac{3}{2} v_0'' v_0'^2\right) = \rho_0 \Omega \ddot{v}_0 \tag{7.20}$$

In addition to the governing equation, the initial condition and three boundary conditions at each end of the beam ($X = 0$ and $X = L$) are needed. The boundary conditions may be constrained movement or free movement along the three degrees of freedom in the problem: horizontal movement, vertical movement and rotation.

$$u = 0 \qquad \text{or} \qquad \widetilde{N} = 0 \tag{7.21}$$

$$v = 0 \qquad \text{or} \qquad -\widetilde{M}' + \widetilde{N} v' = 0 \tag{7.22}$$

$$v' = 0 \qquad \text{or} \qquad \widetilde{M} = 0 \tag{7.23}$$

It is important to remark that, in the followed procedure, the constitutive equation of an hyperelastic material has been strictly applied to energy conjugate Green-Lagrange strain and second Piola-Kirchhoff stress tensors. Then, a series of simplifications led to the governing equations of motion (7.19) and (7.20). These equations were directly achieved by other authors without following a meticulous derivation and without clearly stating the required additional simplifications.

7.1.3 Inertia gradient models

All the generalized continuum models presented in the overview (chapter 3) are available to represent the behavior of a microstructured nonlinear beam. In this section, we derive the equation of motion only following the postulated IGN and IGN1 models. Subsequently, both problem formulations are compared between them and with the non-standard continualization of the discrete model. An interesting discussion arises from the comparison in section 7.3.

7.1.3.1 Inertia gradient nonlinear models

According to Eqs. (6.2) and (7.11), the strain energy density of a slice of the presented beam reads

$$W_\Omega = \int_\Omega \frac{1}{2} E \left(\varepsilon^{GL}\right)^2 d\Omega = \int_\Omega \frac{1}{2} E \left(u_0' + \frac{1}{2} v_0'^2 - Y v_0''\right)^2 d\Omega \tag{7.24}$$

From Eqs. (4.26), and (7.7) to (7.9), the kinetic energy density of a slice is

$$\begin{aligned} T = \int_\Omega \frac{1}{2}\rho_0 \Bigg[&\left(\dot{u}_0^2 + \dot{v}_0^2\right) - 2Y\dot{u}_0\dot{v}_0' + \frac{{d_1}^2}{3}\left({k_1}^2 + \frac{{k_2}^2}{2}\right)\dot{u}_0'^2 + \left(Y^2 + \frac{2{d_1}^2}{3}\right)\dot{v}_0'^2 \\ &- 2Y\frac{{d_1}^2}{3}\left({k_1}^2 + \frac{{k_2}^2}{2}\right)\dot{u}_0'\dot{v}_0'' + Y^2\frac{{d_1}^2}{3}\left({k_1}^2 + \frac{{k_2}^2}{2}\right)\dot{v}_0''^2 \Bigg] d\Omega \end{aligned} \tag{7.25}$$

where d_1, k_1 and k_2 are the three different coefficients from the scale parameters tensor l^2_{pkmn}. Additionally, let us use the relation stated in Eq. (6.26) to reduce the number of parameters, $k^2 = \frac{{d_1}^2}{3}\left({k_1}^2 + \frac{{k_2}^2}{2}\right)$. We obtain the following expressions

$$W_\Omega = \frac{E\Omega}{2}\left(u_0'^2 + \frac{v_0'^4}{4} + u_0' v_0'^2\right) + \frac{EI}{2} v_0''^2 \tag{7.26}$$

$$T_\Omega = \frac{1}{2}\Omega\rho_0 \left[\left(\dot{u}_0^2 + \dot{v}_0^2 + \frac{I}{\Omega}\dot{v}_0'^2\right) + k^2\dot{u}_0'^2 + \frac{2}{3}{d_1}^2\dot{v}_0'^2 + 2\frac{I}{\Omega}k^2\dot{v}_0''^2\right] \tag{7.27}$$

As in the continuum classical derivation, the moment of inertia of the cross section is much smaller than the area $\frac{I}{\Omega L^2} \ll 1$. The rotary inertia of the beam may then

be disregarded, leading to

$$T_\Omega = \frac{1}{2}\Omega\rho_0\left[\left(\dot{u}_0^2 + \dot{v}_0^2\right) + k^2\dot{u}_0'^2 + \frac{2{d_1}^2}{3}\dot{v}_0'^2\right] \tag{7.28}$$

The total kinetic and strain energies of the beam are obtained by integration along its axis

$$W = \int_L W_\Omega dX \qquad T = \int_L T_\Omega dX \tag{7.29}$$

In absence of external loads, the Lagrangian reads

$$\mathbb{L} = W - L \tag{7.30}$$

Applying the Hamilton's principle and the fundamental lemma of variational calculus, the following expression in terms of the Lagrangian is reached

$$-\left(\frac{\partial\mathbb{L}}{\partial u_0'}\right)' - \frac{\partial}{\partial t}\left(\frac{\partial\mathbb{L}}{\partial\dot{u}_0}\right) + \frac{\partial}{\partial t}\left(\frac{\partial\mathbb{L}}{\partial\dot{u}_0'}\right)' - \left(\frac{\partial\mathbb{L}}{\partial v_0'}\right)' + \left(\frac{\partial\mathbb{L}}{\partial v_0''}\right)'' - \frac{\partial}{\partial t}\left(\frac{\partial\mathbb{L}}{\partial\dot{v}_0}\right) + \frac{\partial}{\partial t}\left(\frac{\partial\mathbb{L}}{\partial\dot{v}_0'}\right)' = 0 \tag{7.31}$$

Three boundary conditions (at $X = 0$ and $X = L$) must be satisfied [162]

$$u = 0 \qquad \text{or} \qquad \frac{\partial\mathbb{L}}{\partial u'} - \frac{\partial}{\partial t}\left(\frac{\partial\mathbb{L}}{\partial\dot{u}'}\right) = 0 \tag{7.32}$$

$$v = 0 \qquad \text{or} \qquad \frac{\partial\mathbb{L}}{\partial v'} - \frac{\partial}{\partial t}\left(\frac{\partial\mathbb{L}}{\partial\dot{v}'}\right) = 0 \tag{7.33}$$

$$v' = 0 \qquad \text{or} \qquad \frac{\partial^2\mathbb{L}}{\partial v''^2} = 0 \tag{7.34}$$

The governing equation is then expressed by

$$\Omega E u_0'' + \Omega E v_0' v_0'' = \Omega\rho_0\ddot{u}_0 - \Omega\rho_0 k^2\ddot{u}_0'' \tag{7.35}$$

$$-IEv_0'''' + \Omega E\left(u_0''v_0' + u_0'v_0'' + \frac{3}{2}v_0'^2v_0''\right) = \Omega\rho_0\left(\ddot{v}_0 - \frac{2}{3}{d_1}^2\ddot{v}_0''\right) \tag{7.36}$$

and the boundary conditions are

$$u = 0 \qquad \text{or} \qquad \Omega\rho_0 k^2 \ddot{u}_0' + \Omega E \left(u_0' + \frac{v_0'^2}{2} \right) = 0 \tag{7.37}$$

$$v = 0 \qquad \text{or} \qquad \Omega\rho_0 \frac{2}{3} {d_1}^2 \ddot{v}_0' + \Omega E \left(u_0' v_0' + \frac{v_0'^3}{2} \right) - EIv''' = 0 \tag{7.38}$$

$$v' = 0 \qquad \text{or} \qquad EIv_0'' = 0 \tag{7.39}$$

The IGN applied herein contains a fourth order scale parameters tensor, l^2_{pkmn}, see Eq. (3.14), whose values may be expressed by Eq. (3.17). This formulation, which has three independent microstructural parameters, led to the governing Eqs. (7.35) and (7.36) for a 1D element oscillations, in which 2 independent micro-inertia parameters are involved, k and d_1.

7.1.3.2 Inertia gradient model with one microstructure parameter

The special case of IGN1 deserves some attention. It is recalled that, from Mindlin's strain gradient theory in 1965 [25], the kinetic energy may be postulated with only one parameter accounting for the microstructure. This simplification leads to the Form I, II or III of the original theory in the linear case, Eq. (3.23), see [128].

In the axial oscillation problem, there is only one degree of freedom. Therefore, there is no difference whether the problem is formulated with the complete IGN model or with the simplified IGN1 one. On the contrary, using this simplified model may lead to a different equation in this problem.

Recalling the simplified kinetic energy density formulation,

$$T(\underline{X}, t) = \frac{1}{2}\rho_0 \left[\frac{\partial \underline{u}(\underline{X}, t)}{\partial t} \frac{\partial \underline{u}(\underline{X}, t)}{\partial t} + k^2 \frac{\partial \left(\nabla \underline{u}(\underline{X}, t) \right)}{\partial t} : \frac{\partial \left(\nabla \underline{u}(\underline{X}, t) \right)}{\partial t} \right]. \tag{7.40}$$

Applying the kinematic relations from Eqs. (7.7) to (7.8), the kinetic energy density of a slice is

$$T_\Omega = \int_\Omega \frac{1}{2}\rho_0 \left[\left(\dot{u}^2 + \dot{v}^2 \right) + k^2 \left(\dot{u}'^2 + \frac{\partial \dot{u}}{\partial Y}^2 + \dot{v}'^2 \right) \right] d\Omega \tag{7.41}$$

$$T_\Omega = \frac{1}{2}\Omega\rho_0 \left[\left(\dot{u}_0^2 + \frac{I}{\Omega}\dot{v}_0'^2 + \dot{v}_0^2\right) + k^2\left(\dot{u}_0'^2 + \frac{I}{\Omega}\dot{v}_0''^2 + \dot{v}_0'^2 + \dot{v}_0'^2\right)\right] \tag{7.42}$$

The rotary inertia of the beam shall be disregarded again,

$$T_\Omega = \frac{1}{2}\Omega\rho_0 \left[\left(\dot{u}_0^2 + \dot{v}_0^2\right) + k^2\left(\dot{u}_0'^2 + 2\dot{v}_0'^2\right)\right]. \tag{7.43}$$

The last equation is identical to (7.28) if $\left({k_1}^2 + \frac{{k_2}^2}{2}\right) = 1$, that is, if $\frac{{d_1}^2}{3} = k^2$.

Applying the Hamilton's principle to this formulation, the following governing equation is obtained

$$\Omega E\left(u_0'' + v_0' v_0''\right) = \Omega\rho_0\left(\ddot{u}_0 - k^2\ddot{u}_0''\right) \tag{7.44}$$

$$-IEv_0'''' + \Omega E\left(u_0'' v_0' + u_0' v_0'' + \frac{3}{2}v_0'^2 v_0''\right) = \Omega\rho_0\left(\ddot{v}_0 - 2k^2\ddot{v}_0''\right) \tag{7.45}$$

and the boundary conditions are

$$u = 0 \qquad \text{or} \qquad \Omega\rho_0 k^2\ddot{u}_0' + \Omega E\left(u_0' + \frac{v_0'^2}{2}\right) = 0 \tag{7.46}$$

$$v = 0 \qquad \text{or} \qquad \Omega\rho_0 2k^2\ddot{v}_0' + \Omega E\left(u_0' v_0' + \frac{v_0'^3}{2}\right) - EIv''' = 0 \tag{7.47}$$

$$v' = 0 \qquad \text{or} \qquad EIv_0'' = 0 \tag{7.48}$$

The importance of this simplified formulation will be discussed in section 7.5, after comparing the results of the discrete chain with those derived from continuum models.

7.2 Continuous formulation from continualization techniques

There are different procedures to get a continuous equation from the discrete model formulated above. Here we apply the two continualization procedures that were used also in the axial oscillations problem, both the Taylor series and the shift operators method.

7.2.1 Taylor series approach

Following the method presented in section 3.3.1, the axial displacement is continualized using a Taylor series expansion of the displacements of particles $(n+1)$ and $(n-1)$ as a function of the displacement of n^{th} particle and its derivatives

$$u_{n\pm1} = u_n \pm \frac{u'_n d}{1} + \frac{u''_n d^2}{2!} \pm \frac{u'''_n d^3}{3!} + ... \tag{7.49}$$

The same power series expansion is performed for vertical displacement v, longitudinal force N and moment M. Taylor expansion is truncated at third order and introduced in Eqs. (5.33) and (5.35). The continualization of Eq. (5.33) is straightforward. The other equation is continualized as follows

$$N_n\Theta_n - N_{n-1}\Theta_{n-1} - \left(\frac{M_{n+1} - 2M_n + M_{n-1}}{d}\right) + Fv_n = m\ddot{v} \tag{7.50}$$

Developing the first two terms of the equation

$$
\begin{aligned}
&N_n\Theta_n - N_{n-1}\Theta_{n-1} = N_n\frac{v_{n+1}-v_n}{d} - N_{n-1}\frac{v_n - v_{n-1}}{d} = \\
&\frac{N_n\left(2v_{n+1}-2v_n\right) - N_{n-1}\left(2v_n - 2v_{n-1}\right)}{2d} = \\
&\frac{N_n\left(2v_{n+1}-2v_n+v_{n-1}-v_{n-1}\right) - N_{n-1}\left(2v_n - 2v_{n-1}+v_{n+1}-v_{n+1}\right)}{2d} = \\
&\frac{N_n\left(v_{n+1}-v_{n-1}+v_{n+1}-2v_n+v_{n-1}\right) - N_{n-1}\left(v_{n+1}-v_{n-1}-v_{n+1}+2v_n-v_{n-1}\right)}{2d} = \\
&\frac{\left(N_n - N_{n-1}\right)\left(v_{n+1}-v_{n-1}\right) + \left(N_n + N_{n-1}\right)\left(v_{n+1}-2v_n+v_{n-1}\right)}{2d} = \\
&d\left[\left(\frac{N_n - N_{n-1}}{d}\right)\left(\frac{v_{n+1}-v_{n-1}}{2d}\right) + \left(\frac{N_n + N_{n-1}}{2}\right)\left(\frac{v_{n+1}-2v_n+v_{n-1}}{d^2}\right)\right]
\end{aligned}
\tag{7.51}
$$

we reach an expression whose continualization is feasible.

Introducing Taylor series expansion in the last equation,

$$N_n\Theta_n - N_{n-1}\Theta_{n-1} = d\left[N'v' + Nv''\right] = d\left[Nv'\right]' \tag{7.52}$$

and we get the following continuous equations

$$N' + f_u = \frac{m}{d}\ddot{u} \tag{7.53}$$

$$\left[Nv'\right]' - M'' + f_v = \frac{m}{d}\ddot{v} \tag{7.54}$$

where f_u and f_v are horizontal and vertical components of external force per unit length.

$$f_u(X(n)) = \frac{F_{ui}}{d} \tag{7.55}$$

$$f_v(X(n)) = \frac{F_{vi}}{d} \tag{7.56}$$

Continualizing Eqs. (5.36) and (5.37), longitudinal force and couple (N, M) are related to displacements by

$$N = Gd\left(u' + \frac{1}{2}\left(v'\right)^2\right) \tag{7.57}$$

$$M = Cd\left(v''\right) \tag{7.58}$$

Then, in absence of external forces, the governing equations are expressed by

$$Gd^2u'' + Gd^2v'v'' = m\ddot{u} \tag{7.59}$$

$$-Cd^2v'''' + Gd^2v'u'' + Gd^2u'v'' + \frac{3}{2}Gd^2v'^2v'' = m\ddot{v} \tag{7.60}$$

The boundary conditions are, for axial displacements

$$u = 0 \qquad \text{or} \qquad Gdu' + Gd\frac{v'^2}{2} = 0 \tag{7.61}$$

and, for transverse displacements

$$v = 0 \qquad \text{or} \qquad -Cdv''' + Gdu'v' + Gd\frac{v'^3}{2} = 0 \tag{7.62}$$

$$v' = 0 \qquad \text{or} \qquad Cdv'' = 0 \tag{7.63}$$

7.2.2 Shift operators approach

For this model, the Lagrangian of the complete lattice is expressed by

$$\begin{gathered}\mathbb{L}_D = T_D - W_D = \\ \mathbb{L}_D = \sum_n \frac{1}{2} m \left(\dot{u}_n^2 + \dot{v}_n^2\right) - \sum_n \frac{1}{2} C \left(\frac{v_{n+1} - 2v_n + v_{n-1}}{d}\right)^2 \\ - \sum_n \frac{1}{2} G \left(u_{n+1} - u_n + \frac{1}{2}\frac{(v_{n+1} - v_n)^2}{d}\right)^2 .\end{gathered} \tag{7.64}$$

where W_D and T_D are the total strain and kinetic energy in the lattice.

From the previously developed mathematical approach with shift operators, we recall the following applicable relations between the continuous and the discrete definitions of a generic discrete variable ζ_n

$$\zeta_{n+1} = e^{d\partial_x}\zeta_n \tag{7.65}$$

where

$$e^{d\partial_x} = 1 + d\ \partial_x + \frac{d^2}{2}\ \partial_x^2 + O(d^3). \tag{7.66}$$

Defining the continuous variable ζ as

$$\frac{\partial \zeta}{\partial x} = \frac{\zeta_{n+1} - \zeta_n}{d}, \tag{7.67}$$

the following relations are encountered

$$\zeta_n = \mathbb{Q}\zeta = \left(1 - \frac{d}{2}\ \partial_x + \frac{d^2}{12}\ \partial_x^2 + O(d^3)\right)\zeta \tag{7.68}$$

Remember that $\mathbb{Q} = \frac{d\partial_x}{e^{d\partial_x}-1}$. Then,

$$\frac{\zeta_{n+1} - 2\zeta_n + \zeta_{n-1}}{d^2} = \frac{e^{d\partial_x} - 2 + e^{-d\partial_x}}{d^2}\zeta_n = \frac{2}{d^2}\left(\cosh\left(d\partial_x\right) - 1\right)\zeta_n \tag{7.69}$$

$$\frac{\zeta_{n+1} - 2\zeta_n + \zeta_{n-1}}{d^2} = \frac{2}{d^2}\left(\cosh\left(d\partial_x\right) - 1\right)\frac{d\partial_x}{e^{d\partial_x} - 1}\zeta = \left(\partial_x^2 + O(d^3)\right)\zeta \tag{7.70}$$

7.2.2.1 Potential energy

The potential energy in the discrete chain is stated as

$$W_D = \sum_n \frac{1}{2} C \left(\frac{v_{n+1} - 2v_n + v_{n-1}}{d} \right)^2 + \sum_n \frac{1}{2} G \left(u_{n+1} - u_n + \frac{1}{2} \frac{(v_{n+1} - v_n)^2}{d} \right)^2 \tag{7.71}$$

Applying relations (7.67) and (7.69),

$$\sum_n \frac{1}{2} C \left(\frac{v_{n+1} - 2v_n + v_{n-1}}{d} \right)^2 = \sum_n \frac{1}{2} C v''^2 d^2 \tag{7.72}$$

$$\sum_n \frac{1}{2} G \left(u_{n+1} - u_n + \frac{1}{2} \frac{(v_{n+1} - v_n)^2}{d} \right)^2 = \sum_n \frac{1}{2} G \left(u' d + \frac{1}{2} v'^2 d \right)^2 \tag{7.73}$$

Therefore, the potential elastic energy is continualized as

$$\begin{aligned} W = \int_L \left(\frac{1}{2} \frac{C}{d} v''^2 d^2 + \frac{1}{2} \frac{G}{d} \left(u' d + \frac{1}{2} v'^2 d \right)^2 \right) dx = \\ \int_L \frac{1}{2} \left(C d \; v''^2 + G d \left(u'^2 + \frac{1}{4} v'^4 + u' v'^2 \right) \right) dx \end{aligned} \tag{7.74}$$

7.2.2.2 Kinetic energy

The kinetic energy is continualized by making use of relation (7.68).

$$T_D = \sum_n \frac{1}{2} m \left(\dot{u}_n^2 + \dot{v}_n^2 \right) \tag{7.75}$$

Taking advantage of the pseudo-operator $\mathbb{Q}$, the square of the velocities can be transformed into a continuous variable description

$$(\dot{u}_n)^2 = (\mathbb{Q}\dot{u}, \mathbb{Q}\dot{u}) = \dot{u}^2 + \frac{d^2}{12} \dot{u}'^2 + O(d^4) \tag{7.76}$$

$$(\dot{v}_n)^2 = \dot{v}^2 + \frac{d^2}{12} \dot{v}'^2 + O(d^4) \tag{7.77}$$

Therefore,

$$T = \sum_n \frac{1}{2} m \left(\dot{u}^2 + \dot{v}^2 + \frac{d^2}{12} \left(\dot{u}'^2 + \dot{v}'^2 \right) \right) \tag{7.78}$$

The kinetic energy is eventually continualized as

$$T = \int_L \frac{m}{2d}\left(\dot{u}^2 + \dot{v}^2 + \frac{d^2}{12}\left(\dot{u}'^2 + \dot{v}'^2\right)\right) dx \tag{7.79}$$

7.2.2.3 Governing equation

Applying the Hamilton's principle, the following expression in terms of the Lagrangian is reached [162]

$$-\left(\frac{\partial \mathbb{L}}{\partial u'}\right)' - \frac{\partial}{\partial t}\left(\frac{\partial \mathbb{L}}{\partial \dot{u}}\right) + \frac{\partial}{\partial t}\left(\frac{\partial \mathbb{L}}{\partial \dot{u}'}\right)' - \left(\frac{\partial \mathbb{L}}{\partial v'}\right)' + \left(\frac{\partial \mathbb{L}}{\partial v''}\right)'' - \frac{\partial}{\partial t}\left(\frac{\partial \mathbb{L}}{\partial \dot{v}}\right) + \frac{\partial}{\partial t}\left(\frac{\partial \mathbb{L}}{\partial \dot{v}'}\right)' = 0 \tag{7.80}$$

and three boundary conditions (at $X = 0$ and $X = L$) must be satisfied

$$u = 0 \qquad \text{or} \qquad \frac{\partial \mathbb{L}}{\partial u'} - \frac{\partial}{\partial t}\left(\frac{\partial \mathbb{L}}{\partial \dot{u}'}\right) = 0 \tag{7.81}$$

$$v = 0 \qquad \text{or} \qquad \frac{\partial \mathbb{L}}{\partial v'} - \frac{\partial}{\partial t}\left(\frac{\partial \mathbb{L}}{\partial \dot{v}'}\right) = 0 \tag{7.82}$$

$$v' = 0 \qquad \text{or} \qquad \frac{\partial^2 \mathbb{L}}{\partial v''^2} = 0 \tag{7.83}$$

The governing equations in terms of the displacements are expressed by

$$Gd^2u'' + Gd^2v'v'' = m\ddot{u} - \frac{d^2}{12}m\ddot{u}'' \tag{7.84}$$

$$-Cd^2v'''' + Gd^2v'u'' + Gd^2u'v'' + \frac{3}{2}Gd^2v'^2v'' = m\ddot{v} - \frac{d^2}{12}m\ddot{v}'' \tag{7.85}$$

and the boundary conditions are

$$u = 0 \qquad \text{or} \qquad Gdu' + Gd\frac{v'^2}{2} + \frac{d}{12}m\ddot{u}' = 0 \tag{7.86}$$

$$v = 0 \qquad \text{or} \qquad -Cdv''' + Gdu'v' + Gd\frac{v'^3}{2} + \frac{d}{12}m\ddot{v}' = 0 \tag{7.87}$$

$$v' = 0 \qquad \text{or} \qquad Cdv'' = 0 \tag{7.88}$$

Following the method based on shift-operators that was presented in section 3.3.2, a continuum equation that withholds the discrete effects was reached.

7.3 Comparison between models and brief discussion

With the main objective of finding continuous equations for structured solids, we formulated the nonlinear axial-transverse coupled vibrations problem following several approaches.

We used models that are based on two different axioms: matter as a discrete system or matter as a continuum. Then, we achieved six formulations by addressing the problem with three particular strategies:

1. Using the axiomatic discrete model.
2. Formulating the problem using axiomatic continuum models.
   (a) With the classical continuum theory.
   (b) With the postulated inertia gradient nonlinear model (IGN).
   (c) With the postulated one parameter inertia gradient nonlinear model (IGN1).
3. Continualizing the discrete model formulation.
   (a) With a Taylor series approach.
   (b) With pseudo-differential operators.

Table (7.1) summarizes all the formulations and their characteristics.

Model Name	Approach	Governing equation	Eq.	Scale effects?
Reference Discrete	Discrete	$G\left(u_{n+1}-2u_n+u_{n-1}+\frac{1}{2}\left(\frac{v_{n+1}-v_n}{d}\right)^2 d-\frac{1}{2}\left(\frac{v_n-v_{n-1}}{d}\right)^2 d\right)=m\ddot{u}_n$ $G\left(u_{n+1}-u_n+\frac{1}{2}\left(\frac{v_{n+1}-v_n}{d}\right)^2 d\right)\left(\frac{v_{n+1}-v_n}{d}\right)-G\left(u_n-u_{n-1}+\frac{1}{2}\left(\frac{v_n-v_{n-1}}{d}\right)^2 d\right)\left(\frac{v_n-v_{n-1}}{d}\right)$ $-\frac{C}{d^2}\left(v_{n+2}-4v_{n+1}+6v_n-4v_{n-1}+v_{n-2}\right)=m\ddot{v}_n$	(5.33) to (5.37)	Yes
SVK	Classical continuum	$E\Omega\left[u_0'+\frac{1}{2}\left(v_0'\right)^2\right]'=\rho_0\Omega\ddot{u}_0$ $-EIv_0''''+E\Omega\left(u_0''v_0'+u_0'v_0''+\frac{3}{2}v_0''v_0'^2\right)=\rho_0\Omega\ddot{v}_0$	(7.19) (7.20)	No
IGN	Generalized continuum	$\Omega Eu_0''+\Omega Ev_0'v_0''=\Omega\rho_0\ddot{u}_0-\Omega\rho_0k^2\ddot{u}_0''$ $-IEv_0''''+\Omega E\left(u_0''v_0'+u_0'v_0''+\frac{3}{2}v_0'^2v_0''\right)=\Omega\rho_0\left(\ddot{v}_0-\frac{2}{3}{d_1}^2\ddot{v}_0''\right)$	(7.35) (7.36)	Yes
IGN1	Generalized continuum	$\Omega E\left(u_0''+v_0'v_0''\right)=\Omega\rho_0\left(\ddot{u}_0-k^2\ddot{u}_0''\right)$ $-IEv_0''''+\Omega E\left(u_0''v_0'+u_0'v_0''+\frac{3}{2}v_0'^2v_0''\right)=\Omega\rho_0\left(\ddot{v}_0-2k^2\ddot{v}_0''\right)$	(7.44) (7.45)	Yes
Taylor	Taylor continualization	$Gd^2u''+Gd^2v'v''=m\ddot{u}$ $-Cd^2v''''+Gd^2v'u''+Gd^2u'v''+\frac{3}{2}Gd^2v'^2v''=m\ddot{v}$	(7.59) (7.60)	No
Shift ops.	Non-standard continualization	$Gd^2u''+Gd^2v'v''=m\ddot{u}-\frac{d^2}{12}m\ddot{u}''$ $-Cd^2v''''+Gd^2v'u''+Gd^2u'v''+\frac{3}{2}Gd^2v'^2v''=m\ddot{v}-\frac{d^2}{12}m\ddot{v}''$	(7.84) (7.85)	Yes

Table 7.1: Summary of the six formulations used for coupled axial-transverse vibrations problem.

We ended up with a system of second order ODEs for the discrete formulation, and 5 different continuous formulations. These continuous formulations are expressed by a couple of nonlinear PDEs.

Let us compare these 5 continuous formulations. First, it is seen that Eqs. (7.59) and (7.60) from Taylor continualization are formally equivalent to those obtained with the axiomatic nonlinear St. Venant-Kirchhoff continuous model, Eqs. (7.19) and (7.20). In particular, they match term by term if the continuous and discrete material properties are related adequately

$$C = \frac{EI}{d}; \qquad G = \frac{C}{r^2} \tag{7.89}$$

where $r = \frac{I}{\Omega}$ is the radius of gyration of the section. Compatible values of the continuum model constants E and ρ_0 with the last relation are

$$E = \frac{G}{d}; \qquad \rho_0 = \frac{m}{d^3} \tag{7.90}$$

These relations enable to establish the conditions to compare continuum models with an equivalent discrete one, taken as reference.

Now we compare the IGN with the non-standard continualization and IGN1 formulations. By using the last two relations, the equations of the IGN model (7.35,7.36) will completely match the equations of the non-standard continualization (7.84,7.85) if and only if microstructure parameters are set in a proper way

$$k^2 = \frac{{d_1}^2}{3}\left({k_1}^2 + \frac{{k_2}^2}{2}\right) = \frac{d^2}{12} \qquad \text{and} \qquad \frac{2{d_1}^2}{3} = \frac{d^2}{12}. \tag{7.91}$$

The value obtained for k^2 is consistent with the previous reasoning in the nonlinear axial problem.

On the other hand, we also obtained, following the IGN1 model, the governing Eqs. (7.44) and (7.45) in which a single microstructure parameter k is considered (instead of a fourth order tensor of scale parameters). It can be seen that IGN1 formulation is the special case of IGN in which

$$\frac{{d_1}^2}{3} = k^2 \tag{7.92}$$

Therefore, IGN1 governing equations will not match the non-standard continualized discrete for any value of microstructure parameter k^2. It is inferred that the

non-standard continualization is incompatible with the IGN1 generalized continuum model.

In addition, the classic continuum model is recovered if the microstructure is disregarded. When the microstructural length d is much smaller than the total length of the solid L, the microstructure parameters k, d_1 tend to zero, leading to the classical nonlinear model equations.

Moreover, the linear generalized continuum formulation can be also recovered. By considering small displacements and rotations, $v_0' \ll 1$ and $v_0'' \ll 1$, nonlinear terms become much smaller than the others and may be neglected. The Eqs. (7.36) and (7.20) get transformed into the linear nonlocal [123] and linear local governing equations respectively.

In order to identify the minimum number of parameters that influence the nonlinear bending behavior, the different continuum models formulated above are expressed in a non-dimensional form by making use of the following variables

$$\begin{gathered} \bar{u} = \frac{u_0}{L}; \qquad \bar{v} = \frac{v_0}{L}; \qquad s = \frac{X}{L}; \qquad \tau = t\omega_1; \qquad \omega_1 = \frac{1}{\gamma L}\sqrt{\frac{E}{\rho_0}}; \\ \gamma = \frac{L}{r}; \qquad r = \sqrt{\frac{I}{\Omega}}; \qquad h = \frac{k}{L}; \qquad h_2 = \sqrt{\frac{2}{3}}\frac{d_1}{L}; \end{gathered} \tag{7.93}$$

where r is the cross-section's radius of gyration and ω_1 is the characteristic angular frequency of the linear bending problem. Table 7.2 shows a resume of the governing equations for the different models and hypotheses.

Summarizing the comparison of IGN model to the other continuous formulation in non-dimensional terms:

- $h^2 = {h_2}^2 = \frac{d^2}{12L^2} \quad \Rightarrow$ IGN matches Non-standard continualization
- $2h^2 = {h_2}^2 \quad \Rightarrow$ IGN matches IGN1
- $h^2 = {h_2}^2 = 0 \quad \Rightarrow$ IGN matches Classical nonlinear SVK

Now, let us compare the dispersion relation of an infinite discrete chain oscillating under pure bending (linear regime) with the dispersion in an infinite beam formulated with the linearized IGN theory. For the discrete chain, the dispersion was stated in Eq. (5.46)

$$\omega^2 = 16\frac{{c_0}^2 r^2}{d^4}\sin^4\left(\frac{\kappa d}{2}\right)$$

	Non-dimensional Governing Equations	
	Axial direction	Transverse direction
C	$\gamma^2\bar{u}'' = \ddot{\bar{u}}$	$-\bar{v}'''' = \ddot{\bar{v}}$
L-IGN	$\gamma^2\bar{u}'' = \ddot{\bar{u}} - h^2\ddot{\bar{u}}''$	$-\bar{v}'''' = \ddot{\bar{v}} - {h_2}^2\ddot{\bar{v}}''$
SVK	$\gamma^2\left(\bar{u}'' + \bar{v}'\bar{v}''\right) = \ddot{\bar{u}}$	$-\bar{v}'''' + \gamma^2\left(\bar{v}'\bar{u}'' + \bar{u}'\bar{v}'' + \frac{3}{2}\bar{v}'^2\bar{v}''\right) = \ddot{\bar{v}}$
IGN	$\gamma^2\left(\bar{u}'' + \bar{v}'\bar{v}''\right) = \ddot{\bar{u}} - h^2\ddot{\bar{u}}''$	$-\bar{v}'''' + \gamma^2\left(\bar{v}'\bar{u}'' + \bar{u}'\bar{v}'' + \frac{3}{2}\bar{v}'^2\bar{v}''\right) = \ddot{\bar{v}} - {h_2}^2\ddot{\bar{v}}''$
IGN1	$\gamma^2\left(\bar{u}'' + \bar{v}'\bar{v}''\right) = \ddot{\bar{u}} - h^2\ddot{\bar{u}}''$	$-\bar{v}'''' + \gamma^2\left(\bar{v}'\bar{u}'' + \bar{u}'\bar{v}'' + \frac{3}{2}\bar{v}'^2\bar{v}''\right) = \ddot{\bar{v}} - 2h^2\ddot{\bar{v}}''$

Table 7.2: Governing equations for different hypotheses and formulations. C≡classical, L≡linearized.

The dispersion relation of the linearized IGN beam, obtained by imposing a wave solution, reads

$$\omega^2 = c_0^2 r^2 \frac{\kappa^4}{1 + \frac{2}{3}{d_1}^2\kappa^2} \tag{7.94}$$

We develop the Maclaurin series expansion of both dispersion equations and, making the first two terms coincide, we get the following value for the scale parameter, ${h_2}^2 = \frac{d^2}{6L^2}$. Interestingly, this value of ${h_2}^2$ is incompatible with the non-standard continualization, but matches with the IGN1 model, since the optimum value of h^2 is $h^2 = \frac{d^2}{12L^2}$, see Chapter 6.

It is worth to highlight that the dispersion relation in an infinite beam formulated with the original Eringen nonlocal elasticity theory is exactly the same

$$\omega^2 = c_0^2 r^2 \frac{\kappa^4}{1 + {k_e}^2\kappa^2} \tag{7.95}$$

and its adjustment to the discrete chain dispersion leads to the same value of the microstructure parameter ${h_e}^2 = \frac{{k_e}^2}{L^2} = \frac{d^2}{6L^2}$. Note that the coefficient of the term that accounts for size effects is higher in the transverse motion than in the longitudinal one, and that this adjustment conflicts with the calibration of the nonlocal rod dispersion, in which ${k_e}^2 = \frac{d^2}{12}$.

This duality in the calibration of the Eringen nonlocal parameter k_e^2 has been broach by the scientific community prior to this work. The works of Challamel

et al. [123, 166, 167] show an explain this duality from the point of view of different problems. In particular, a specific algorithm is presented in [171] to obtain the optimal value for k_e^2 in an uncoupled axial-bending problem. However, that algorithm requires to know, *a priori*, the ratio between axial and bending deformation.

The dependence of the microstructure parameter value with the character of the addressed problem is unnatural and leads to additional complications in the resolution process. On the contrary, in the simplified Mindlin model (IGN1) the optimal value of the cale parameter is the same for both problems. The inability of the continualization based on the shift operators method to achieve this differentiation between the longitudinal and transverse effects of discreteness may not condition the good performance of the IGN1 model.

An eventual possibility is considering the one parameter IGN1 model and ignoring the non-standard continualization with shift operators. In this case, and in complete concordance with the longitudinal oscillations behavior, the value of k^2 should be suitably adjusted to $\frac{d^2}{12}$. These considerations lead naturally to an adjustment of the microstructural inertia coefficient linked to axial motion as $\frac{d^2}{12}$, and $\frac{d^2}{6}$ for the bending behavior (transverse micro-inertia).

In addition, there could be better or more complete continualization methods that lead to the proper dispersion relation in the bending behavior. There could be also other discrete models that continualize into the proper values of axial and transverse microstructure parameters. This point deserves further research.

Following the discussion herein, the microstructure parameters of the general IGN theory should be adjusted to match the non-standard continualization of the discrete model, $h_2 = h = \frac{k}{L} = \frac{d}{\sqrt{12}L}$, which is also consistent with the value of k found for the axial problem. The one parameter IGN1 theory will consequently lead to different results.

7.3.1 Additional hypotheses leading to uncoupled equations

It is seen that the equations of motion for the nonlinear case are coupled in displacements $\bar{u}$ and $\bar{v}$. In order to get uncoupled governing equations, additional assumptions could be taken into account. It is commonly assumed that the acceleration in the longitudinal direction is negligible compared to the acceleration in the transverse direction [172]. Then, two different additional hypotheses can be applied: to neglect horizontal displacement $\bar{u} = 0$, or to assume constant axial force along the beam $\bar{N}' = 0$. These hypotheses lead to the well-known formulations of the nonlinear beam, see [170, 173] and [31] respectively.

Neglecting horizontal displacement, the following equations are obtained

$$\bar{u} = 0 \tag{7.96}$$

$$\bar{N} = \frac{\bar{v}'^2}{2} \tag{7.97}$$

where the non-dimensional axial force is defined as $\bar{N} = \frac{N}{E\Omega}$.

On the other hand, assuming constant axial force $\bar{N}$, and taking into account fixed-end boundary conditions $u(0,\tau) = u(1,\tau) = 0$, the following expression for the axial force is obtained

$$\bar{N} = \int_0^1 \left[\bar{u}' + \frac{1}{2}\left(\bar{v}'\right)^2\right] ds = \frac{1}{2}\int_0^1 \left(\bar{v}'\right)^2 ds \tag{7.98}$$

as acceleration at boundaries is also zero $\ddot{\bar{u}}(0,\tau) = \ddot{\bar{u}}(1,\tau) = 0$, see Eq.

Note that this hypothesis is a bit controversial in terms of displacements, because constant axial force would imply nil horizontal displacements. The physical meaning behind this hypothesis is very small horizontal displacements compared to vertical ones, and therefore negligible horizontal acceleration. But indeed some small horizontal displacement (compared to the vertical) is needed to get constant axial force $\bar{N}$.

Table 7.3 shows a resume of the governing equations using the classical and the different additional hypotheses, whose suitability will be discussed in subsection 7.5.6.

		Non-dimensional Governing Equations	
Model	Additional hypothesis	Axial direction	Transverse direction
SVK	$\bar{u}=0$	$\bar{u}=0$	$-\bar{v}''''+\frac{3}{2}\gamma^2\bar{v}'^2\bar{v}''=\ddot{\bar{v}}$
SVK	$\bar{N}'=0$	$\ddot{\bar{u}}=0$	$-\bar{v}''''+\frac{\gamma^2}{2}\left(\int_0^1\bar{v}'^2ds\right)\bar{v}''=\ddot{\bar{v}}$
IGN	$\bar{u}=0$	$\bar{u}=0$	$-\bar{v}''''+\frac{3}{2}\gamma^2\bar{v}'^2\bar{v}''=\ddot{\bar{v}}-{h_2}^2\ddot{\bar{v}}''$
IGN	$\bar{N}'=0$	$\ddot{\bar{u}}=0$	$-\bar{v}''''+\frac{\gamma^2}{2}\left(\int_0^1\bar{v}'^2ds\right)\bar{v}''=\ddot{\bar{v}}-{h_2}^2\ddot{\bar{v}}''$
IGN1	$\bar{u}=0$	$\bar{u}=0$	$-\bar{v}''''+\frac{3}{2}\gamma^2\bar{v}'^2\bar{v}''=\ddot{\bar{v}}-2h^2\ddot{\bar{v}}''$
IGN1	$\bar{N}'=0$	$\ddot{\bar{u}}=0$	$-\bar{v}''''+\frac{\gamma^2}{2}\left(\int_0^1\bar{v}'^2ds\right)\bar{v}''=\ddot{\bar{v}}-2h^2\ddot{\bar{v}}''$

Table 7.3: Governing equations for different hypotheses and formulations.

7.4 Solution of the continuous equations

The problem of a simply supported beam is going to be solved for validation purposes. Its behavior is characterized by a system of two coupled nonlinear PDEs. To obtain an accurate solution, the Galerkin method is used. The resulting nonlinear system of ODEs is integrated with a fourth order explicit Runge-Kutta method.

An approximate solution $\bar{V}$, $\bar{U}$ is assumed as

$$\bar{v}(s,\tau)\approx\bar{V}(s,\tau)=\sum_{i=1}^{p}\Phi_i(s)q_i(\tau) \tag{7.99}$$

$$\bar{u}(s,\tau)\approx\bar{U}(s,\tau)=\sum_{i=p+1}^{2p}\Phi_i(s)q_i(\tau) \tag{7.100}$$

where $\Phi_i(s)$ are the shape functions that must satisfy essential boundary conditions and $q_i(\tau)$ are the unknown time-dependent functions to be determined.

Applying the Galerkin method, the system of two coupled nonlinear PDE's is reduced to a system of $2m$ nonlinear second order EDO's

$$\begin{aligned} \int_0^1 \Phi_i \left[\pounds_v(\bar{U}, \bar{V}) \right] ds = 0, \quad i = 1, 2, ..., p \\ \int_0^1 \Phi_i \left[\pounds_h(\bar{U}, \bar{V}) \right] ds = 0, \quad i = p+1, ..., 2p \end{aligned} \tag{7.101}$$

where $\pounds_v, \pounds_h$ are the differential operators associated to the selected nonlinear governing equations of the beam. In the IGN continuum model formulation these operators are

$$\begin{aligned} \pounds_v(\bar{u}, \bar{v}) = -\bar{v}'''' + \gamma^2 \left(\bar{v}'\bar{u}'' + \bar{u}'\bar{v}'' + \frac{3}{2}\bar{v}'^2\bar{v}'' \right) - \ddot{\bar{v}} + {h_2}^2 \ddot{\bar{v}}'' \\ \pounds_h(\bar{u}, \bar{v}) = \gamma^2 \left(\bar{u}'' + \bar{v}'\bar{v}'' \right) - \ddot{\bar{u}} + h^2 \ddot{\bar{u}}'' \end{aligned} \tag{7.102}$$

For the operators $\pounds_v$ and $\pounds_h$ corresponding to other continuum formulations, please refer to Table 7.2. The resulting system of nonlinear ODE's is solved by making use of a numerical fourth order Runge-Kutta method.

To achieve a deeper understanding of the solutions we are seeking for, let us briefly introduce here several concepts of nonlinear oscillations. The explanations herein are applicable to both discrete and continuous systems.

Whenever a problem is governed by a linear equation, the principle of superposition holds. Therefore, every solution can be expressed as a combination of other solutions. There are solutions of motion for which all parts of the system move harmonically with the same frequency and with a fixed phase relation, that is, solutions in separated variables. These spatial solutions are called normal modes. Then, every motion can be expressed as the superposition of normal modes. One interesting characteristic of normal modes is that free motion described by the normal modes takes place at fixed frequencies, independent of the amplitude of the motion, called natural frequencies. Then, in the frequency domain spectrum of any free motion, only the natural frequencies have non nil amplitude.

On the contrary, the principle of superposition does not hold in systems governed by non-linear equations. However, non-linear normal modes may exist, in which all parts of the system move with the same frequency and with a fixed phase relation, although the movement will be no longer sinusoidal and the frequency of motion will depend on its amplitude. Shaw and Pierre [174] demonstrated the existence of normal modes in nonlinear second-order continuous systems.

Likewise, they formulated the normal modes problem, and reached a system of two semi-linear, hyperbolic partial differential equations, which allow for solutions to be obtained in the form of power series [174]. Therefore, the solution procedure restricts to considering nonlinear effects up to some order in an asymptotic sense. Orthogonality holds in nonlinear normal modes, meaning that any initial condition which belongs to a normal mode will excite only that normal mode and no other additional motion.

In the considered beam problem formulations, the nonlinear normal modes are not known a priori, and there is no intention to obtain them. However, it is known that nonlinear normal modes are almost identical to linear modes in the cuasi-linear regime. Therefore, an initial deformation of the m^{th} linear normal mode with finite but small amplitude will excite not only the m^{th} nonlinear normal mode, but also slightly additional modes whose superposition can be asymptotically assumed as linear. So, by imposing an initial deformation close to the the m^{th} nonlinear normal mode, we mainly excite the m^{th} nonlinear normal mode. In addition, the nonlinear normal mode shape can be decompose as a sum of linear normal modes shapes.

After the numerical integration, a Fourier transform is performed over the time-domain numerical solution, allowing to obtain the main oscillation frequency of the considered normal mode.

We focus the attention in the vertical frequencies because we are dealing with a bending problem and, as we will show, the displacements take place mainly in the transverse direction for the initial conditions stated above.

7.5 Results and Discussion

In this section, the performance features of the different continuum models are contrasted by solving the same baseline problem and comparing the predictions with the discrete model solutions.

Several results obtained from the discrete and the continuum models are presented and discussed herein. The discussion is focused in investigating the influence of the dimensionless parameters that control the response of the beam and 1D lattice over the main characteristics of the oscillations. The dimensionless parameters that play a role are:

- the amplitude of oscillations $\bar{A}_0$,
- the microstructure parameter(s) h, h_2,
- the area-inertia ratio γ.

The main aspects investigated in the response are:

- the frequency shift due to the nonlinear behavior,
- the frequency shift due to the discreteness or patterned microstructure,
- the existence of band-gaps and cutoff frequencies.

The organization of contents in the section is the following: first, the discrete model results are presented and discussed. Second, the same is done for the IGN and IGN1 continuum models. In the third part, an exhaustive quantitative comparison is performed to contrast the predictions from generalized continuum models and discover their validity and limitations. The effects of the area-inertia ratio γ on the dynamic response are subsequently studied. Finally, the applicability of the additional hypothesis is investigated.

7.5.1 Definition of a baseline problem

In the study of this problem, simply supported ends are considered as boundary conditions. We intend to excite the nonlinear normal modes and compute their main frequency of oscillation.

As initial condition, the rod is at rest and deformed following a sinusoidal shape, which is compatible with the essential BCs. In the discrete system this means

$$^{\tau=0}\bar{u}_n = \bar{A}_0 \sin\left(m\pi\frac{n-1}{N-1}\right); \quad ^{\tau=0}\dot{\bar{u}}_n = 0 \tag{7.103}$$

where n is the number of the particle, $n = 1, ..., N$. The position of particles in equilibrium is

$$X(n) = (n-1)\, d \tag{7.104}$$

To excite the nonlinear normal mode m, we use the initial condition of the m linear normal mode.

Initial conditions in the continuum model are expressed by

$$\bar{u}(X,0) = \bar{A}_0 \sin\left(m\frac{\pi X}{L}\right); \quad \dot{\bar{u}}(X,0) = 0 \tag{7.105}$$

where $\bar{A}_0$ is a free parameter of the problem that will be used to modulate the amplitude of deformations in the beam, $\bar{A}_0 = \frac{A_0}{r}$.

Since a simply supported beam is considered, essential and natural boundary conditions are

$$\bar{u}(0,\tau) = \bar{u}(1,\tau) = \bar{v}(0,\tau) = \bar{v}(1,\tau) = 0 \tag{7.106}$$

$$\bar{v}''(0,\tau) = \bar{v}''(1,\tau) = 0 \tag{7.107}$$

Therefore, taking into account how the solution of the continuum models is expressed as a combination of shape functions in Eqs. (7.99) and (7.100)

$$\bar{v}(s,\tau) \approx \bar{V}(s,\tau) = \sum_{i=1}^{p} \Phi_i(s) q_i(\tau); \qquad \bar{u}(s,\tau) \approx \bar{U}(s,\tau) = \sum_{i=p+1}^{2p} \Phi_i(s) q_i(\tau) \tag{7.108}$$

and with the objective of meeting BCs, we choose a family of harmonic shape functions $\Phi_i(s)$

$$\Phi_i(s) = \sin\left(i\pi s\right), \; i \subset \mathbb{N} \tag{7.109}$$

As stated above, the initial conditions that we impose are rest and initial amplitude $\bar{A}_0 \neq 0$ only in the vertical time-dependent function $q_i(\tau)$ $(i = 1, ..., p)$ whose associate shape function $\Phi_m(s)$ is intended to be excited

$$\dot{q}_i(0) = 0; \qquad q_i(0) = \bar{A}_0 \delta_{im}; \tag{7.110}$$

where m is the normal mode intended to be excited.

Due to the symmetry of the problem, some of the linear normal modes are, *a priori*, known to be nil (not excited). This phenomena is schematically illustrated in Fig. 7.1.

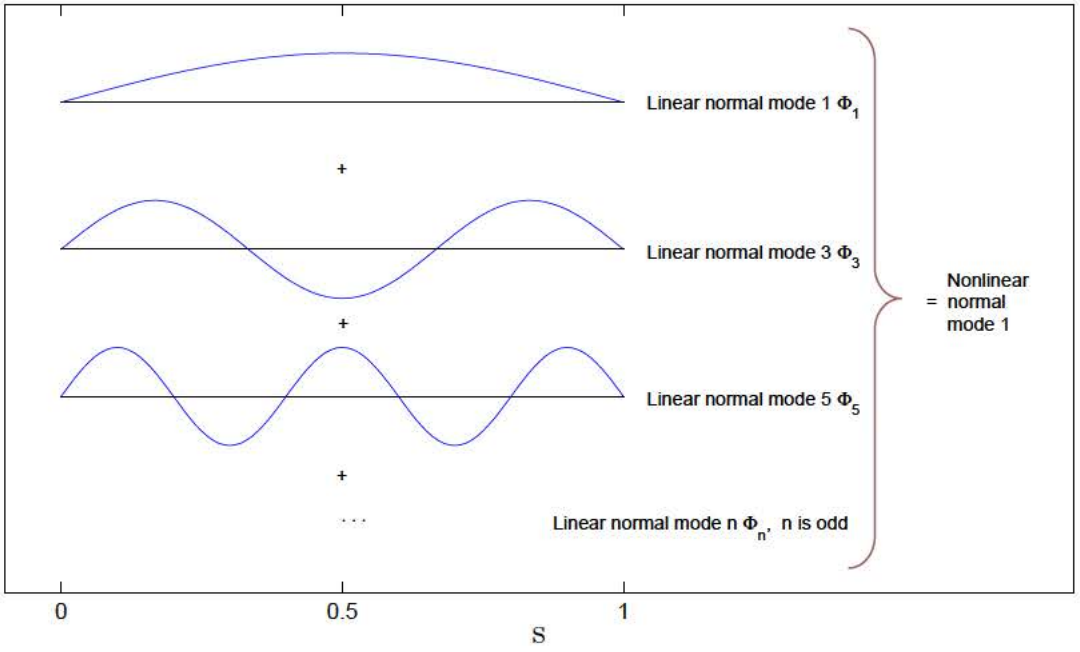

Figure 7.1: Non nil terms in nonlinear normal mode 1 series.

Some of the time dependent functions may remain nil all along the Runge-Kutta algorithm integration time. Therefore, it is computationally more efficient to use, in the series expansion of the solution, only those shape functions whose associated -dependent functions $q_i(\tau)$ are known to be non-nil.

7.5.2 Results from the nonlinear discrete model

Using the procedure developed in section 5.3.2, numerical simulations of the discrete chain oscillation have been calculated. The imposed initial condition is a deformed shape of sine-type with amplitude A_0 and zero velocity. Boundary conditions are no displacements of the first and the last particles in the chain.

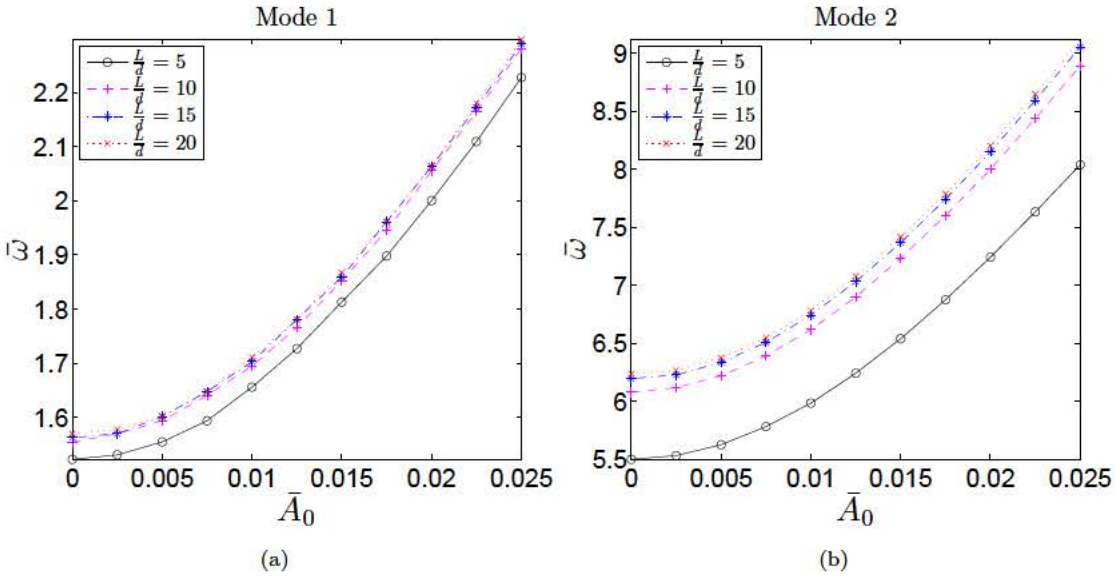

Figure 7.2: Observed oscillation frequency $\bar{\omega}$ vs. initial amplitude $\bar{A}_0$ in the discrete model for different $\frac{d}{L}$ ratios. (a) First nonlinear mode of vibration (b) second nonlinear mode.

Some results from the numerical simulations are shown in Fig. 7.2, where dimensionless oscillation frequencies are presented for different initial amplitudes and number of particles in the chain. Dimensionless area-inertia ratio γ was set to 100. From the results, the following features were revealed:

- Frequencies tend to increase as the initial amplitude $\bar{A}_0$ increases. This effect can be physically explained: distances between particles augment when deflections are big compared to chain length (rotations are big), thus causing longitudinal springs to play a role. Flexural stiffness is therefore strengthened, and the normal oscillation frequency rises.

- Frequencies tend to decrease as the total number of particles n along the chain decreases. Augmenting the ratio $\frac{d}{L}$ results in softening the chain stiffness, as in the linear case [123]. Due to this effect, the dispersion diagram

of the discrete linear 1D chain differs from the dispersion curve of the classical Euler-Bernouilli beam model dispersion curve when the wave number approaches the end of the first Brillouin zone. Size effects become more important for higher modes, since the wavelength becomes comparable to distance between particles d.

- Frequencies are higher for higher modes of vibration, as long as the wave number does not go beyond the first Brillouin zone ($\bar{\kappa} = \pi$). At that point, the frequency reaches its maximum, and no higher frequencies can be excited. That is called a cutoff frequency.

To understand the natural existence of cutoff frequencies, let us use a simple example of a 6 particle chain, see schematics in Fig. 7.3.

Figure 7.3: Discrete model of a pinned-pinned 6 particle chain with $L = 1$, $d = 0.2$ and ratio $\frac{L}{d} = 5$.

The maximum frequency for a given ratio $\frac{d}{L}$ is reached at the end of the first Brillouin zone, showing a band gap from this point on. This phenomenon is illustrated in Fig. 7.4.

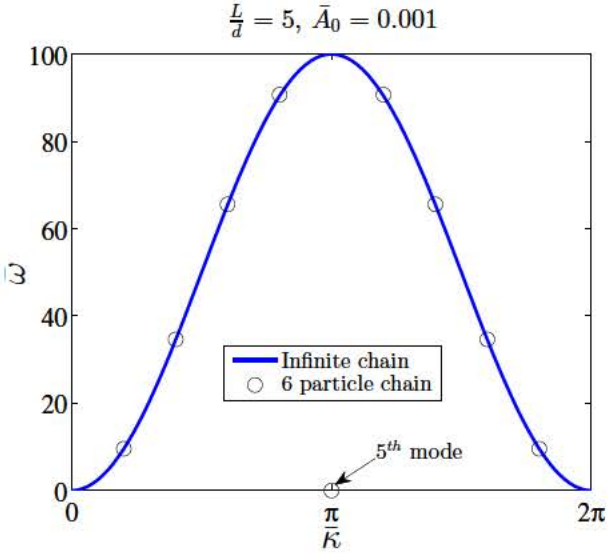

Figure 7.4: Observed frequency in a pinned-pinned 6 particle discrete chain (black dots) when excited with an initial deformation of a normal linear mode, $\bar{A}_0 = 0.001$. Analytical dispersion in an infinite chain (blue line).

Fig. 7.4 requires a deeper explanation to understand why the fifth mode does not belong to the dispersion curve. A pinned-pinned six particle chain has four degrees of freedom in vertical direction, therefore exhibiting only four natural modes of vibration. When the fifth mode (of a continuous chain) is intended to be excited, nothing occurs, as all the particles are placed at the nodes, see Fig. 7.5(a).

Moreover, the initial condition of a higher mode corresponds to a wavenumber beyond the first Brillouin zone, that is, the wave length will be shorter than twice the distance between particles. Then, modes of initial deformation beyond $\bar{\kappa} = \pi$ excite one of the first four natural modes in a reflective way (the 6^{th} excites the 4^{th}, the 7^{th} excites the 3^{rd}, etc.). Figs. 7.5(b) illustrates this phenomenon. This effect, that causes different continuous signals to become indistinguishable when sampled, is called aliasing. In linear lattices, spatial aliasing is the reason for all possible modes to lie within the first Brillouin zone [62].

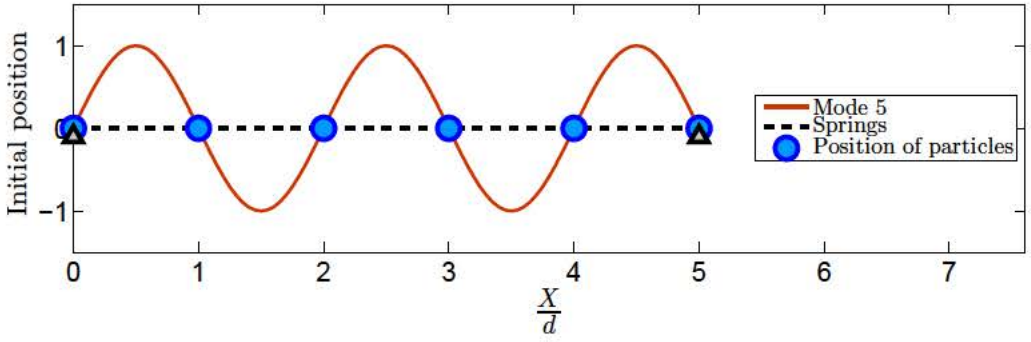

(a)

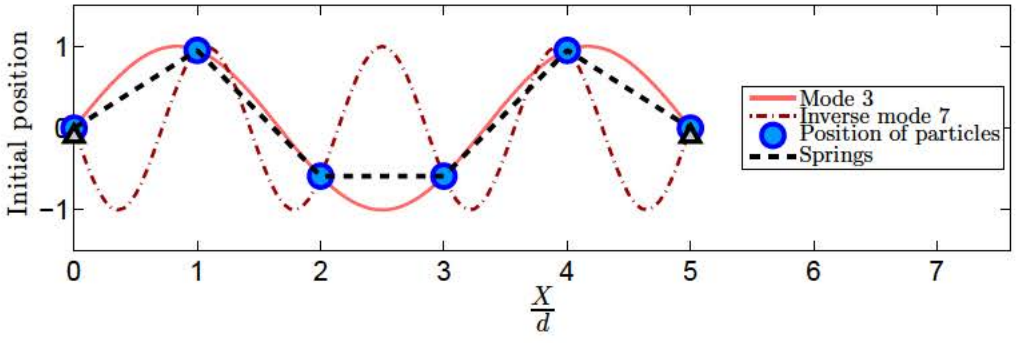

(b)

Figure 7.5: Initial deformation of (a) mode 5 results in no excitation. (b) mode 7 results in the excitation of mode 3. $\bar{A}_0 = 1$.

In an infinite chain, there are no boundary condition requirements, and all wavenumbers can be excited. As a result, the dispersion diagram is continuous. Moreover, the natural frequencies of a finite chain are, from all the possible frequencies of the

infinite one, those whose associated shape function (wavenumber in the dispersion diagram) meet the boundary conditions.

7.5.3 Predictions of the nonlinear generalized continuum models

Oscillation frequencies of the classical and the inertia gradient continuum models are shown in Figs. 7.6 to 7.10. Recall that the angular frequency is normalized with the characteristic linear bending frequency ω_1. From the solutions of the continuum models, the following conclusions arise:

7.5.3.1 Nonlinear classical model

- If the characteristic length d of the microstructured solid is negligible when compared to the beam characteristic length L (ratio $\frac{d}{L} \ll 1$), the microstructure parameters h and h_2 tend to zero. The classical nonlinear model is then recovered. Fig. 7.6 shows the oscillation frequencies predicted by continuum model vs. those observed in the simulations of the discrete model for a high enough number of particles ($\frac{d}{L} = \frac{1}{50}$). Notice that oscillation frequencies are pretty similar even in the 4^{th} mode of vibration. Recall that the effects of microstructured nature arises for higher modes, as the wavelength becomes comparable to microstructure length d.

- Normal frequencies of vibration are higher for increasing initial amplitude $\bar{A}_0$. This is in complete agreement with discrete model results, see Fig. 7.6.

  When amplitudes are small, nonlinear forces can be neglected. It is seen that oscillation frequencies for small initial amplitudes are coincident with those predicted by the linear model: $\bar{\omega} = \frac{{n_j}^2 \pi}{2}$, where n_j is the excited vertical mode.

  As initial amplitudes are increased, it can be observed from the continuum model that the normal oscillation frequencies tend to increase. As stated above, the increase in frequency is due to the stiffening experimented by the beam as the flexural deflection induces not only bending moments, but significant axial forces too. Additionally, their vertical component over the different beam sections rises as slopes are also increased. The combination of

the aforementioned effects make oscillation frequencies to grow as amplitude is increased.

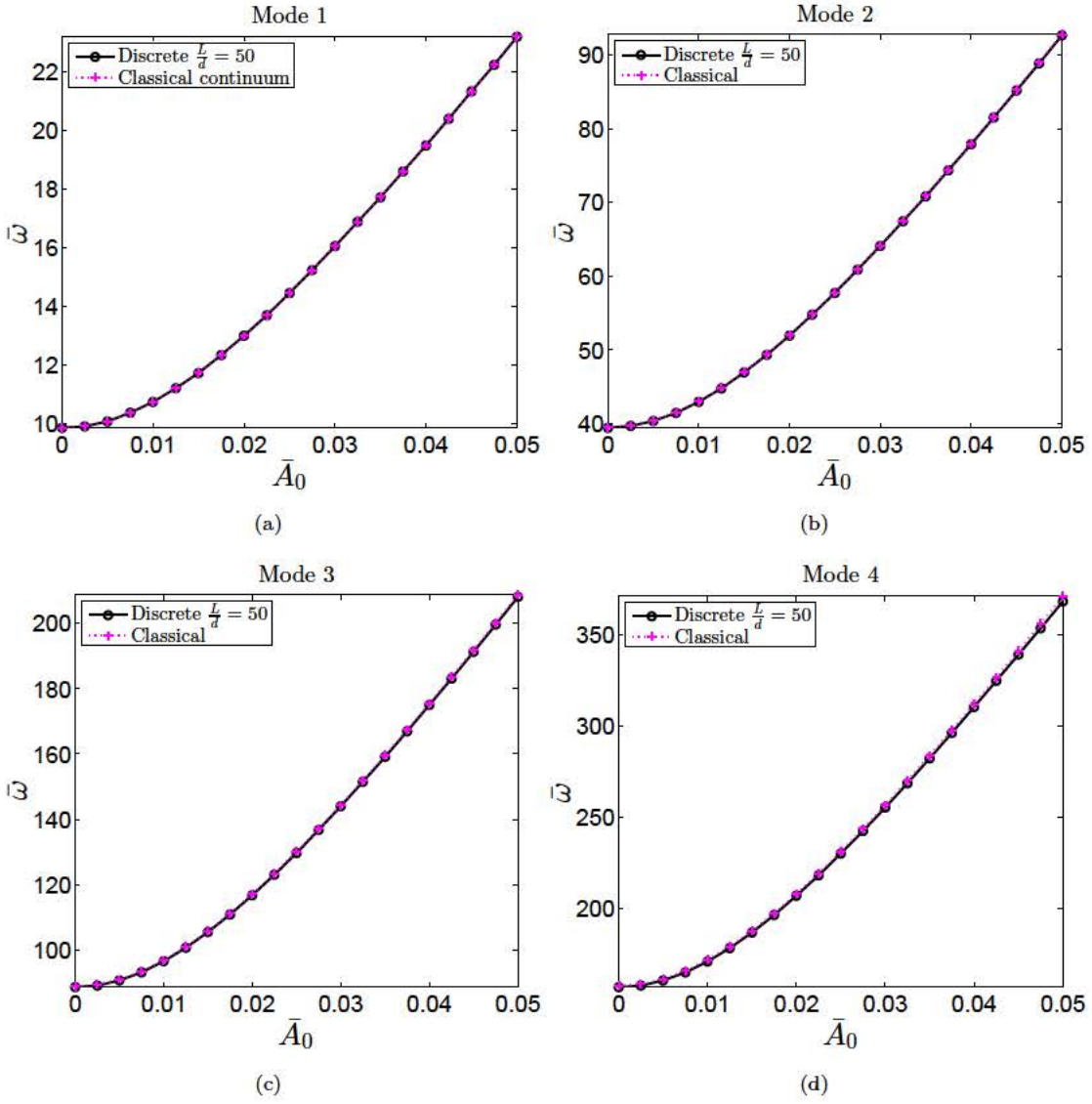

Figure 7.6: Oscillation frequency vs. initial amplitude $\bar{A}_0$ from 51 particle discrete model simulations ($\frac{L}{d} = 50$) and from solutions of the classical model ($h = 0$). First four modes of vibration are shown (a) $m = 1$ (b) $m = 2$ (c) $m = 3$ (d) $m = 4$.

- Frequencies are higher for higher modes of vibration. However, as size effects are not taken into account, this model predicts infinite normal modes of vibration, no band-gaps, and without any dependence on the ratio $\frac{d}{L}$.

7.5.3.2 Nonlinear generalized continuum models

From the results quoted at Figs. 7.7 to 7.10, the following conclusions are extracted:

- The classical local model is not able to capture size effects, so predicted oscillation frequency is independent of microstructure characteristic length d. Nevertheless it is seen from Fig. 7.7 that the developed IGN and IGN1 models take into account the size effects, showing a good agreement with the discrete model frequencies in linear regime. It can be observed from the figure that the main discrete effect is to decrease oscillation frequency as microstructure parameter(s) h, h_2 are augmented. This descent is exacerbated as the mode of vibration is increased. This effect is consistent with observed behavior of the discrete model.

- To adequately capture the size effect that takes place in the discrete model when the ratio $\frac{d}{L}$ is augmented, the value of microstructure parameter h has to be suitably adjusted. It has been seen that a good agreement between frequencies in the IGN1 continuum model and the discrete one is achieved by analytically adjusting the microstructure parameter to $h = \frac{1}{\sqrt{6}}\frac{d}{L}$.

- If initial amplitude is small enough, nonlinear forces can be neglected. The linear oscillation regime is a specific case of the complete model. Fig. 7.7 shows that the linear generalized continuum solution [124] is recovered. In nonlinear regime, normal frequencies of vibration are higher for increasing initial amplitude $\bar{A}_0$, as in the local case.

- Frequencies are higher for higher modes of vibration as in the local model. Moreover, the size effects also increase in higher modes, showing a higher discrepancy in frequency with the local model for the same value of microstructure parameter h.

  However, the generalized continuum model doesn't show a frequency limit nor a band gap for any value of h and/or oscillation mode in flexural elements (beams). Although IGN model predicts a frequency limit in axially oscillating elements (rods), it is not able to show a band gap in the problem under study. This indicates that this generalized continuum elasticity theory in finite deformations has a certainly wide range of application for

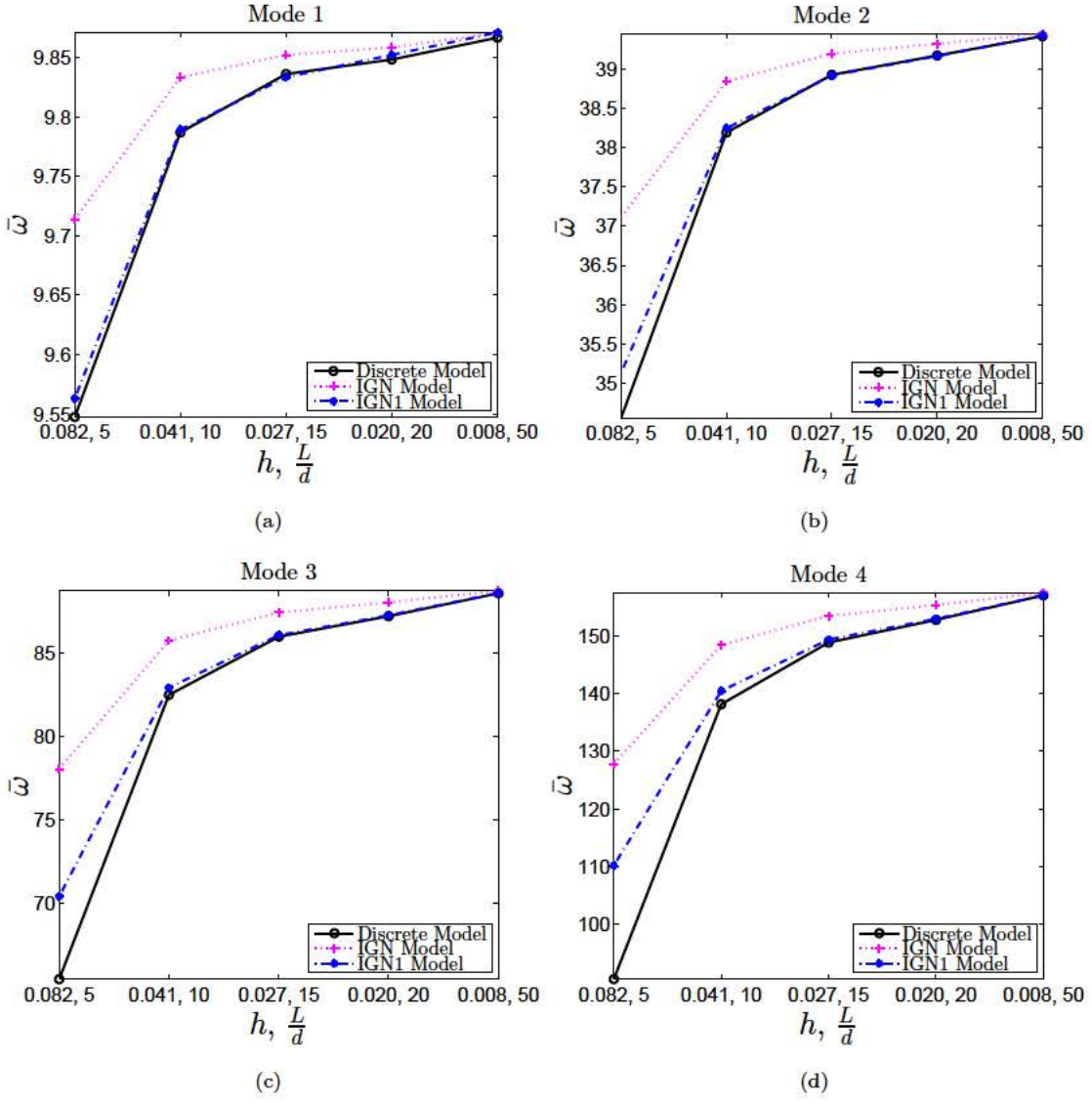

Figure 7.7: Linear case $A_0 \approx 0$. Oscillation frequency vs.: microstructure parameter(s) h, h_2 in IGN and IGN1 generalized continuum models and $\frac{L}{d}$ ratio in discrete model. First four modes of vibration are shown (a) $m = 1$ (b) $m = 2$ (c) $m = 3$ (d) $m = 4$.

flexural problems, but its use is not appropriate to face those which involve wavelengths shorter than twice the microstructural distance d.

7.5.4 Quantitative comparison. Accuracy of the generalized continuum models

The main features of continuum models have been presented and discussed. In Figs. 7.8, 7.9 and 7.10, the oscillation frequencies predicted by the continuum models are compared to those of the discrete chain, where the suitable values of the scale parameters h and h_2 found in section 7.3 are used.

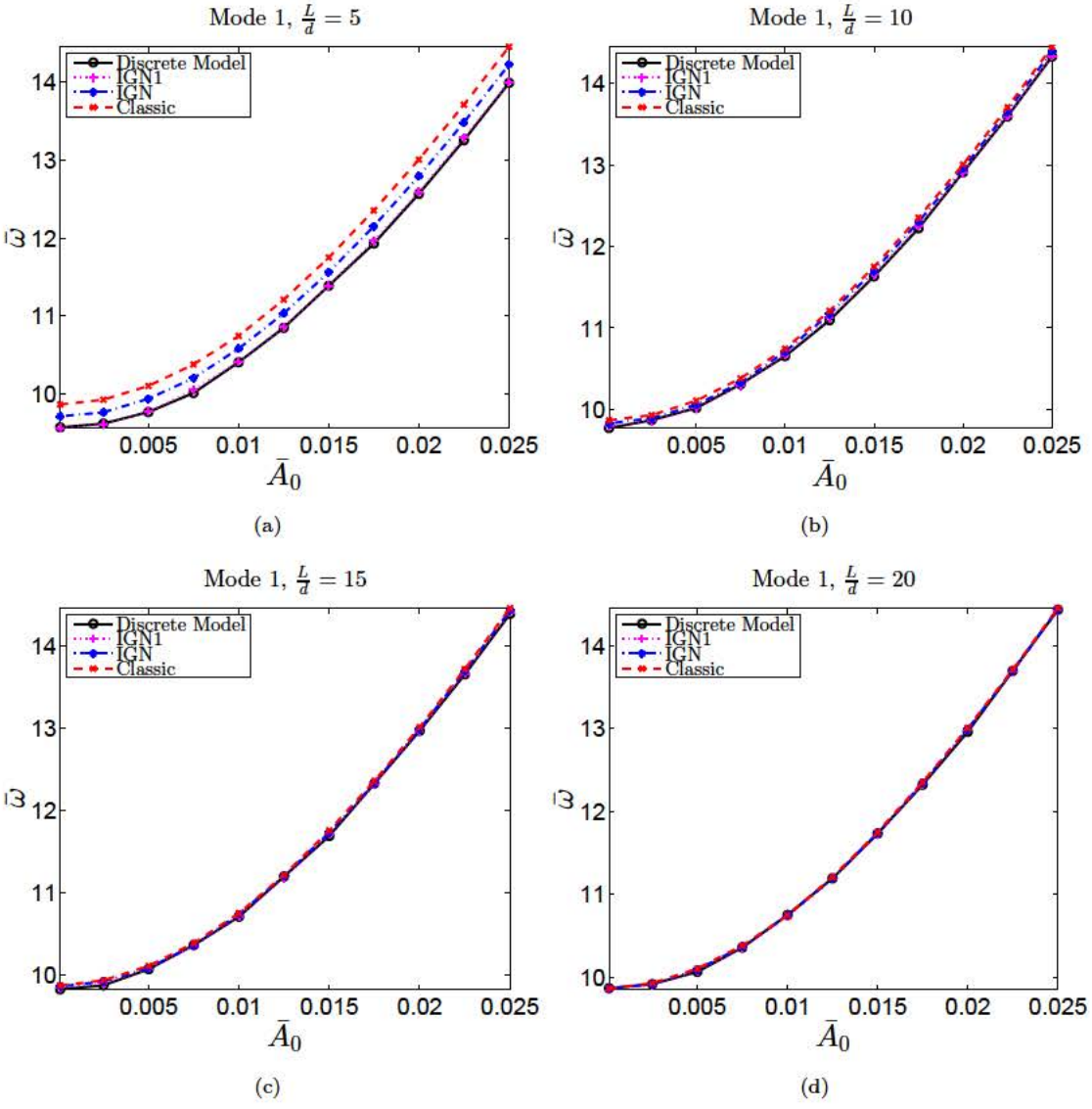

Figure 7.8: Oscillation frequency of mode 1 vs. initial amplitude $\bar{A}_0$ in the discrete model, both IGN and IGN1 models and the classical continuum model with (a) $\frac{L}{d} = 5$ (b) $\frac{L}{d} = 10$ (c) $\frac{L}{d} = 15$ (d) $\frac{L}{d} = 20$.

From the examination of the figures cited above, a good agreement between the one parameter IGN1 model and the discrete one is encountered. Interestingly,

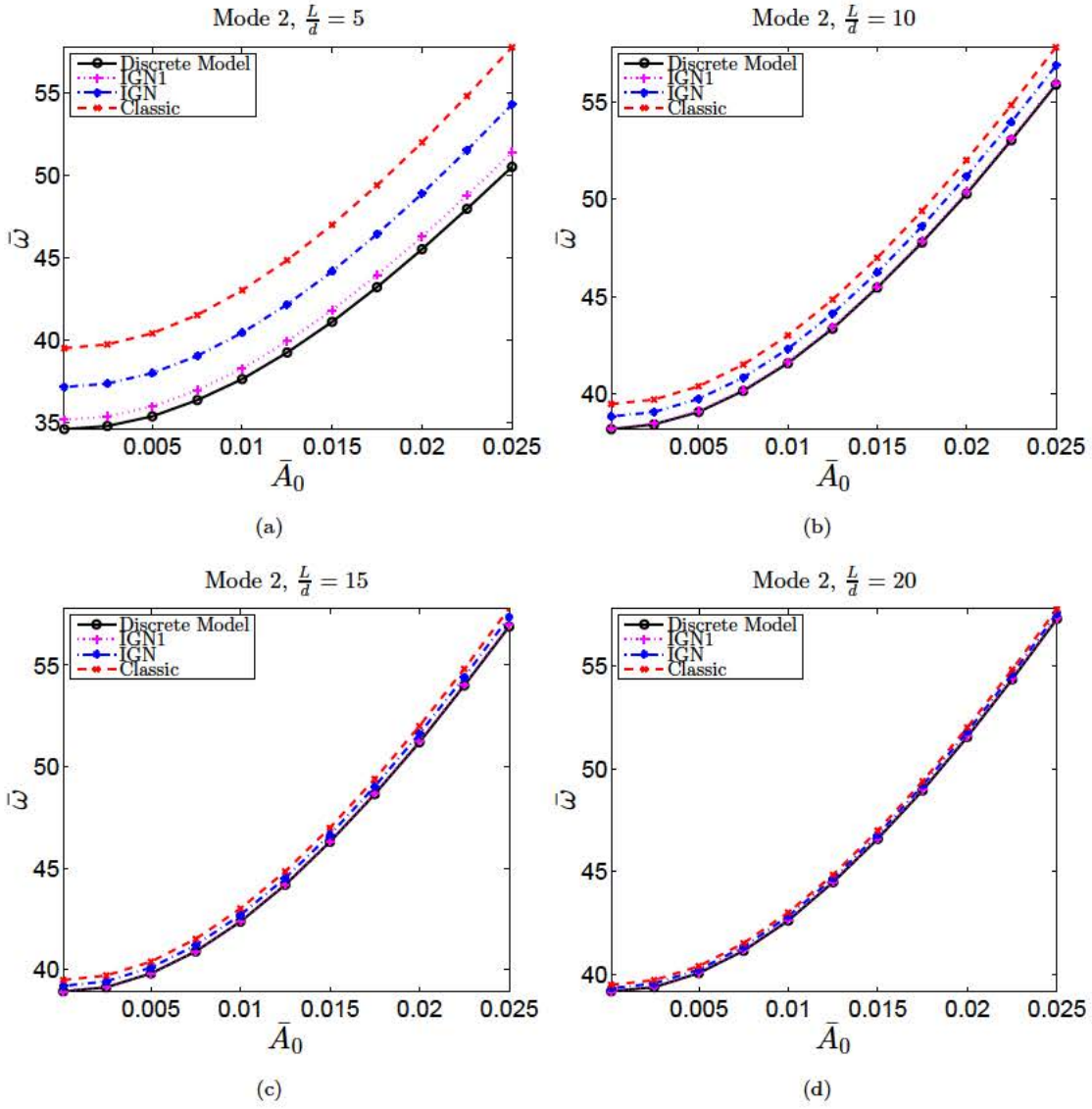

Figure 7.9: Oscillation frequency of mode 2 vs. initial amplitude $\bar{A}_0$ in the discrete model, both IGN and IGN1 models and the classical continuum model with (a) $\frac{L}{d} = 5$ (b) $\frac{L}{d} = 10$ (c) $\frac{L}{d} = 15$ (d) $\frac{L}{d} = 20$.

the full IGN model's prediction, with its parameters h and h_2 adjusted to the non-standard continualization, is less accurate than the IGN1 model.

It is inferred that, despite its simplicity, the IGN1 model is more appropriate for modeling microstructured elements than the complete IGN one. The adjustment of the micro-inertia parameter h is consistent with the study of longitudinal oscillations.

It is also seen that the IGN model proposed herein is able to capture, not only the nonlinear effects present in the von-Kármán beam, but also the coupled effect of nonlinearity and discreteness.

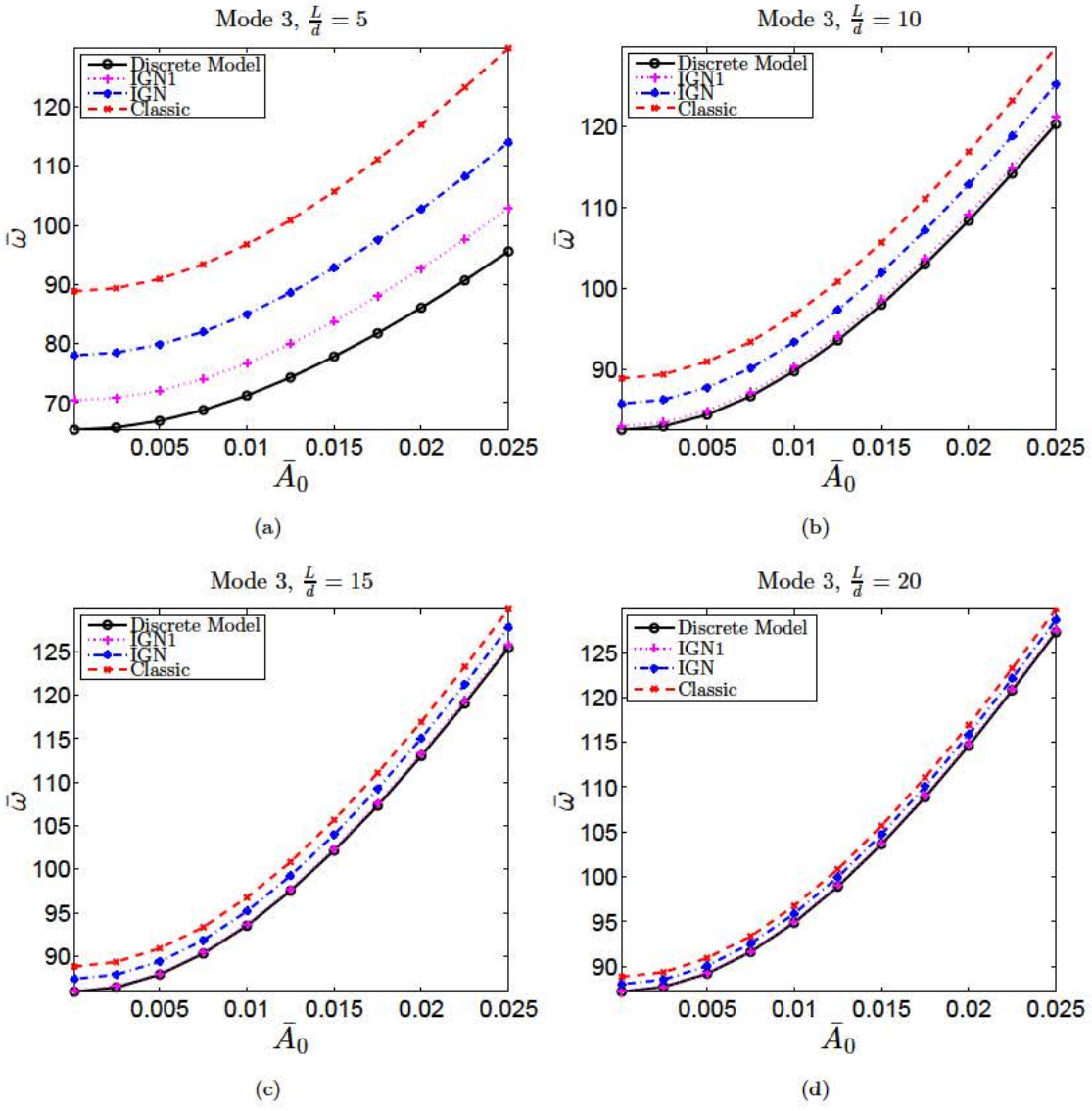

Figure 7.10: Oscillation frequency of mode 3 vs. initial amplitude $\bar{A}_0$ in the discrete model, both IGN and IGN1 models and the classical continuum model with (a) $\frac{L}{d} = 5$ (b) $\frac{L}{d} = 10$ (c) $\frac{L}{d} = 15$ (d) $\frac{L}{d} = 20$.

It can be seen that the accuracy of the generalized continuum diminishes when the wavelength λ approximates twice the characteristic length d. Thus, for a highly discrete beam in which $\frac{L}{d} = 5$, when higher modes are excited, the accuracy of predictions from the IGN model is compromised, see Fig. 7.10(a). Nevertheless, we see that the predictions of this model are in perfect agreement with the simulations of the discrete model for all the other scenarios simulated in this section, exhibiting minimal errors compared with the results of the discrete model.

As expected, all the discrete and the generalized continuum models simulations and predictions coincide with the prediction of the classical continuum model when

the microstructure characteristic length d is much smaller than the wavelength, e. g. the $\frac{L}{d} = 20$ discrete chain oscillating in the first normal mode.

7.5.5 Influence of area-inertia ratio

As it has been defined, the dimensionless area-inertia parameter γ is intimately related to the slenderness of the beam. For the results showed above, the value of $\gamma = 100$ was chosen. To contextualize the order of magnitude of γ, notice that for a square beam with a height to length ratio of $c = \frac{L}{25}$ (c being the height), $\gamma \simeq 86.6$.

Conceptually, the ratio between bending and axial displacements is conditioned by the slenderness. In fact, it is shown in Table 7.2 that the terms related to axial stresses are enlarged by γ^2.

The nonlinear effects in the von Kármán beam are due to the geometric elongation of the neutral fiber when the element is bent. Therefore, the nonlinearity is produced by axial stresses. As the slenderness γ^2 indicates the ratio between axial and bending stiffness, it is also the ratio between nonlinear and linear effects in the bending behavior, see vertical balance Eq. C-NL in Table 7.2, repeated here for convenience

$$-\bar{v}'''' + \gamma^2 \left(\bar{v}'\bar{u}'' + \bar{u}'\bar{v}'' + \frac{3}{2}\bar{v}'^2\bar{v}'' \right) = \ddot{\bar{v}} \tag{7.111}$$

Let us analyze the order of magnitude analysis of the different forces acting in the vertical equation of the IGN1 model.

$$-\bar{v}'''' + \gamma^2 \left(\bar{v}'\bar{u}'' + \bar{u}'\bar{v}'' + \frac{3}{2}\bar{v}'^2\bar{v}'' \right) = \ddot{\bar{v}} - 2h^2\ddot{\bar{v}}'' \tag{7.112}$$

In this equation there are four terms that represent four types of forces:

- $\bar{v}''''$ is the variation of shear force, which is related to the bending stiffness, as it comes from angular momentum equilibrium in the section
- $\gamma^2 \left(\bar{v}'\bar{u}'' + \bar{u}'\bar{v}'' + \frac{3}{2}\bar{v}'^2\bar{v}'' \right)$ is the axial force projected in transverse direction
- $\ddot{\bar{v}}$ are macro-inertia forces
- $2h^2\ddot{\bar{v}}''$ is the non-standard micro-inertia force

Taking into account that displacements in $\bar{v}$ (and its derivatives) are of the order of $\bar{A}_0$, it can be observed in the last Eq. (7.112) that the bending related forces are of the order of $\bar{A}_0$, that the projected axial forces order is $\gamma^2\bar{A}_0^3$ and that horizontal displacements are in the order of $\bar{A}_0^2$. Axial and bending forces will be then of the same order if $\bar{A}_0$ and $\frac{1}{\gamma}$ are too. The value of $\bar{A}_0 = \frac{1}{\gamma}$ constitutes a transition region between linear and nonlinear behavior. Indeed, pure linear bending is encountered for $\bar{A}_0\gamma \ll 1$ and oscillations completely driven by axial forces occur when $\bar{A}_0\gamma \gg 1$. Then, low amplitudes $\bar{A}_0$ may trigger nonlinear effects when the slenderness is high and vice versa.

From the axial direction governing equation in Table 7.2,

$$\gamma^2\left(\bar{u}'' + \bar{v}'\bar{v}''\right) = \ddot{\bar{u}} - h^2\ddot{\bar{u}}'' \tag{7.113}$$

it is found that the axial forces are of the order of $\gamma^2\bar{A}_0^2$.

Let us also analyze the order of magnitude of oscillation frequencies. From the classical linear equations

$$\gamma^2\bar{u}'' = \ddot{\bar{u}} \qquad \text{and} \qquad -\bar{v}'''' = \ddot{\bar{v}}$$

the following frequencies of oscillation of a simply supported beam are derived

$$\bar{\omega}_a = \gamma\pi m \tag{7.114}$$

$$\bar{\omega}_t = \pi^2 m^2 \tag{7.115}$$

where $\bar{\omega}_a$ and $\bar{\omega}_t$ are the dimensionless angular frequencies of oscillation in the axial and transverse motions respectively, and m is the normal mode of vibration.

It is seen that the order of the axial and the transverse motion dimensionless frequencies are in a ratio of $\frac{\gamma}{\pi n}$. In fact, looking at the characteristic frequencies in Eqs. (6.55) and (7.93), the relation $\omega_0 = \gamma\omega_1$ is found (ω_0 is the characteristic frequency of the axial oscillations and ω_1 is the characteristic frequency of bending oscillations). This is sound since the stiffness is in the ratio of γ^2. This phenomenon holds for nonlinear oscillations.

From all this concerns, we want to remark that a high value of slenderness is required for the validity of the hypotheses of the von Kármán beam. We considered that the axial stresses are not negligible even though the displacements are small,

which is only possible for high values of γ. For short beams, the assumptions over the discrete chain and the kinetic derivations of the continuous beam may be revisited, in addition to the Euler-Bernoulli hypotheses in the continuum model.

7.5.6 Applicability of additional hypotheses

The oscillation frequencies predicted by the classical continuum model using different additional hypotheses ($\bar{u} = 0$ or $\bar{N}' = 0$) are shown in Fig. 7.11.

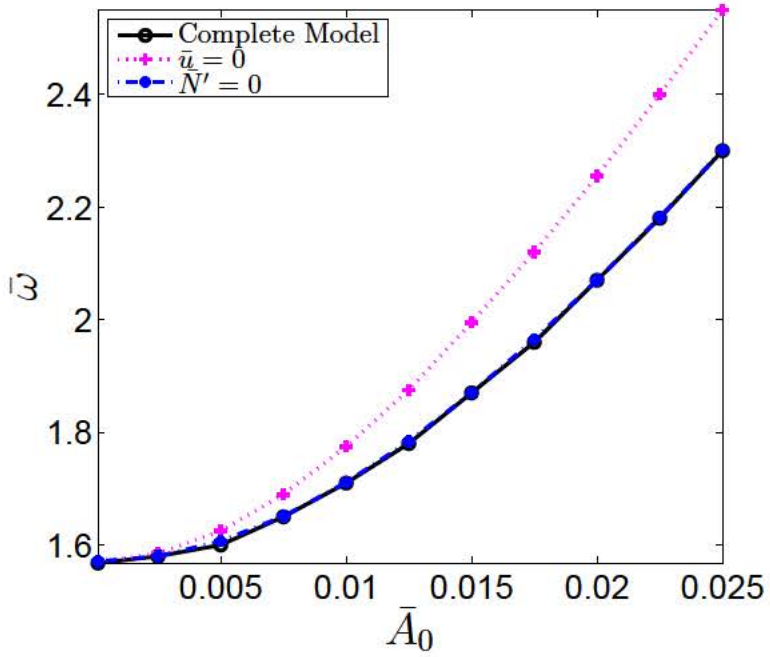

Figure 7.11: Predicted oscillation frequency vs. initial amplitude $\bar{A}_0$ by classical continuum model using different additional hypotheses.

Comparing the results obtained from the different formulations with those of the complete one, it can be seen that, for the same amplitude $\bar{A}_0$, nonlinear oscillation frequencies predicted by the model with $\bar{N}' = 0$ are quite similar to the complete model, meanwhile the model with $\bar{u} = 0$ and $\bar{N}' \neq 0$ predicts higher frequencies. The predicted nonlinear normal shape in these conditions is also slightly different from the other two (complete model and $\bar{N}' = 0$). A more detailed examination of the complete model solution can explain this fact.

When the axial force $\bar{N}$ is not constant along the chain, horizontal forces over a particle are not balanced. As a result, the particle is accelerated towards its horizontal equilibrium position, starting oscillation. Since the slenderness γ is

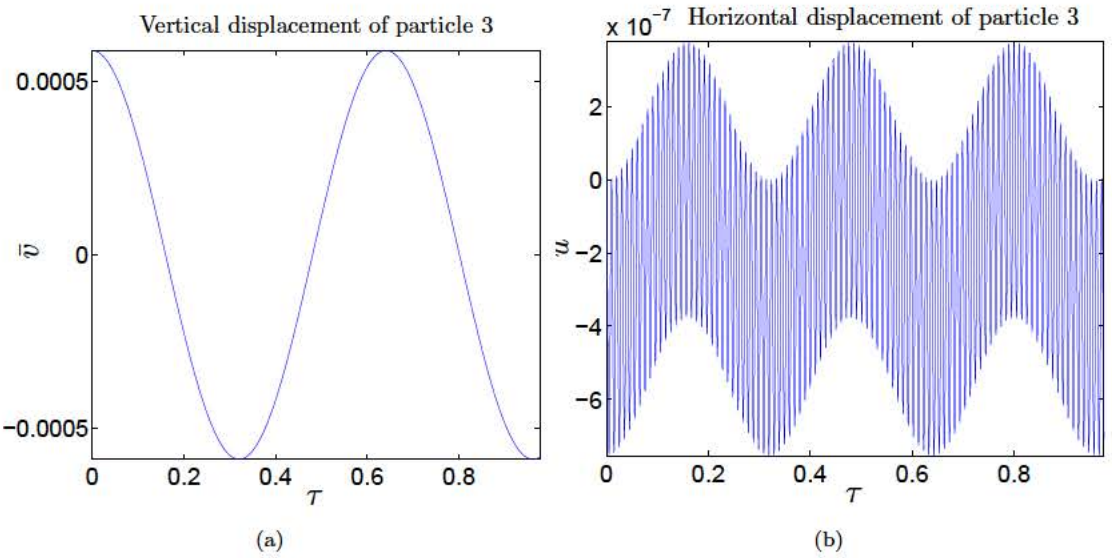

Figure 7.12: Oscillation of particle 3 in a chain with 11 particles ($\frac{L}{d} = 10$) with $\bar{A}_0 = 0.001$, nonlinear regime. The simulation is performed with no additional hypothesis and non-dimensional slenderness $\gamma = 100$ (a) Vertical dimensionless displacement $\bar{v}$. (b) Horizontal dimensionless displacement $\bar{u}$

.

high, the order of magnitude of axial normal frequency of vibration is higher than the order of transverse normal frequency.

The particles are therefore oscillating horizontally a hundred of times for every vertical period. Thus, the axial force $\bar{N}$ is varying a hundred times above and below the horizontal dynamic equilibrium (which is constant $\bar{N}$ along the chain), creating the overall effect for the vertical movement of a constant axial force along the chain. Fig. 7.12 shows this phenomena.

Therefore, it is a good decision to simplify the model by making use of the hypothesis of constant axial force $\bar{N}$ to characterize the transverse oscillations in those problems in which the horizontal movement is free and the non-dimensional slenderness γ is high.

7.6 Remarks

From the above results and their discussion, the following remarks ca be summarized:

- First, it is important to remark that Eqs. (7.57) and (7.58) from Taylor continualization are formally equivalent to those obtained with the axiomatic nonlinear St. Venant-Kirchhoff continuum model, Eqs. (7.19) and (7.20). This model reproduces the nonlinear effects with high accuracy. However, its weakness is the inability to predict scale effects.

- The inertia gradient model may conduces to different governing equations depending whether the additional simplifications of Mindlin [25] are applied or not. While the complete formulation [126] of the enriched kinetic energy leads to a governing equation with 2 scale parameters, the simplified one [25] conduces to a governing equation with one scale parameter.

- Therefore, we derived 2 different governing equations using generalized continuum models (IGN and IGN1).

- The governing equations of the complete IGN model are formally equivalent to the non-standard continualization of the discrete one. From the comparison, the values of the two microstructure parameter are found.

- The governing equations of the simplified IGN1 model are slightly different to the non-standard continualization of the discrete one. Therefore, the value of the one microstructure parameter k cannot be found by this procedure. Instead, we can use the value of the parameter taken from the axial oscillations case.

- From the comparison of the predictions of generalized continuum models with the discrete system simulations, it is found that the IGN1 model is more accurate than the complete one. The predictions of IGN1 model match the behavior of the discrete model, capturing nonlinear and scale effects adequately.

- In the derivation of the nonlinear beam governing equation, we used the hypotheses of small displacements and moderate rotations. In order to appreciate the nonlinear behavior and fulfill these kinematic assumptions, the dimensionless slenderness γ should be high ($\gamma \ll 1$).

- Due to the complexity of the governing equations, some authors apply additional hypotheses so that these equations are simplified. It was found that the hypothesis of constant axial force along the beam $N' = 0$ leads to good results in the vertical motion prediction. On the contrary, the assumption of nil horizontal displacement $u = 0$ leads to results that differ significantly from the behavior observed with the complete formulation.

- The generalized continuum model doesn't show a frequency limit nor a band gap for any value of h and/or oscillation mode in flexural elements (beams). Although IGN model predicts a frequency limit in axially oscillating elements (rods), it is not able to show a band gap in the transverse oscillations problem.

8 Conclusions

In view of the results obtained from the different models, the comparison with the discrete system taken as reference and the outcomes drawn from them, several conclusions arose. They may be synthesized and highlighted for the sake of expressing all the original work and scientific value of the thesis.

In this chapter, the main achievements and conclusions are fist summarized. Once the most important information of this work is expressed, new improvements and implementations may be thought, indicating future lines of investigation.

8.1 Achievements

At the beginning of the document, several objectives were formulated with a common target. Pursuing that goal, we achieved the following:

- Two linear generalized continuum models have been extended for solids subjected **to finite deformations**. Specifically, we formulated a **nonlocal nonlinear model (NNL)** and a gradient velocity nonlinear model here referred to as the **inertia gradient nonlinear model (IGN)**. These are extensions of the linear nonlocal Eringen elasticity theory and of the Form I of the Mindlin strain gradient model, respectively.
- The continuum equations of two dynamic problems of a 1D solid vibrating in nonlinear regime have been obtained by using these models: **the axial vibrations of a rod under finite deformations**, and **the axial-transverse coupled vibrations of a beam under small deformations and moderate rotations**.

- The discrete system solution for the mentioned problems has been obtained. For the **nonlinear axial-transverse coupled oscillation** problem, **we did not found solutions available in the literature**. Instead, researchers normally apply additional hypotheses to get uncoupled equations that can be solved with easier methods. Nevertheless, we solved the complete problem. This allowed us to justify some simplifications of the continuum models and the validity of the additional hypotheses commonly adopted in their application.

- We successfully applied a **non-standard continualization method** to the aforementioned nonlinear 1D discrete systems. Unlike with the postulated generalized continuum models, **this continualization technique permits to derive**, from the characteristics of the solid structure, **the additional parameters** appearing in the model.

- Although different generalized continuum formulations can be found in literature, mainly for linear problems, comparison with experimental results or numerical simulations is not usual. Thus, in those cases the accuracy of the published models cannot be assessed. Here, for validations purposes, the **results obtained from the proposed nonlinear models have been compared to those derived from discrete solution taken as reference**. In this respect, the advantages and shortcomings of the different models have been pointed out.

- We devised the procedure for: i)modeling a discrete system ii) continualizing it following non-standard procedures and iii)comparing the results of novel generalized continuum models with the results of this one. This innovative methodology has proved to be fruitful, becoming a valuable tool that can be used by other researchers whenever experimental results are not available.

- All in all, we derived a generalized continuum model (IGN1) that adequately captures the nonlinear and scale effects in 1D structured solids vibrating in axial and axial-transverse coupled motion subjected to finite deformations.

8.2 Conclusions

In this research two novel generalized continuum models were formulated: the nonlinear nonlocal model (NNL) and the inertia gradient nonlinear one (IGN). The application of the NNL model leads to equations of motion in which an additional scale parameter is present. On the other hand, the IGN model leads to equations of motion in which three scale parameters are present. The latter can be specialized into a one scale parameter model, the so called IGN1 model. In general, these extensions to finite deformations enable to study and predict the behavior of structured solids in nonlinear regime within the general framework of continuum mechanics.

Although the formulations of the aforementioned models have been devised for general three-dimensional solids, in this thesis they have been applied for the study of nonlinear axial and nonlinear axial-transverse coupled vibrations of a kind of 1D structured solids. For validation purposes a nonlinear discrete problem, taken as a reference, has been formulated and solved.

Moreover, a non-standard continualization technique has been applied to the discrete system in order to get appropriate continuous equations of motion, permitting to derive the values of the scale parameters present in the new continuous model.

Regarding the results obtained from **the discrete model**, the following ideas arose:

- In the axial vibrations problem, it is observed that, for the adjustment of the stiffness parameters matching the St. Venant-Kirchhoff constitutive model, higher amplitudes of vibration lead to lower frequencies. However, higher amplitudes led to higher frequencies in the transverse motion.
- In general, for the axial and the axial-transverse coupled vibrations, it is observed that the higher the characteristic size of the underlying structure, the lower the frequencies of oscillation (scale effects).
- Regarding the axial-transverse coupled vibrations problem, researchers usually make additional hypotheses to get uncoupled equations. Here the complete coupled problem has been solved. The deep study of the dynamics in

the coupled problem permitted to understand and justify the validity of the hypothesis of constant longitudinal force along the 1D solid.

Regarding the **continuum models** applied to the **nonlinear axial vibration problem**, the following main ideas could be drawn:

- Both generalized continuum models (NNL and IGN) are sensitive to the scale effects and capture the nonlinear effects.
- The standard Taylor series continualization of the discrete formulation leads to an equation that is formally equivalent to the nonlinear classical model (SVK).
- The continuum equations from IGN and the non-standard continualized one are identical, but the latter permits to obtain the scale parameter from the solid characteristics.
- Although the NNL model is sensitive to nonlinear and scale effects, it does not properly reproduce the results of the discrete model.
- The IGN model, with the scale parameters derived from the non-standard continualization, shows the better performance in capturing both scale and nonlinear effects.

Regarding the **continuum models** applied to the **nonlinear axial-transverse coupled vibration problem**, the following conclusions arose:

- The IGN model, specialized to this problem, contains two scale parameters. These parameters can be reduced to one if specific values are adopted (leading to the IGN1 model).
- The standard Taylor series continualization of the discrete formulation leads to an equation that is formally equivalent to the nonlinear classical model (SVK).
- From the non-standard continualization, equations of motion formally identical to that of the IGN model are obtained.
- Although the IGN model captures the scale effects, the results of the dicrete model are not faithfully reproduced from a quantitative point of view.

- However, the IGN1 model accurately reproduces the discrete results when using the value of the scale parameter that was found in the continualization of the discrete model for the axial vibrations problem.

- Although the IGN model predicts a cutoff frequency in axially oscillating solids, it is not able to show a proper one in the problem under study. This indicates that this generalized continuum elasticity theory in finite deformations has a certainly wide range of application for flexural problems, but its use is not appropriate to model those involving wavelengths shorter than twice the microstructural distance d.

Summarizing, in this thesis we have derived an original inertia gradient continuum model and applied it to predict the dynamic behavior of a kind of nonlinear one-dimensional solids. We compared the predictions with simulations of a reference discrete system, finding satisfactory results. As a final conclusion: the computationally efficient generalized continuum model (IGN1) is able to accurately reproduce the essential features of the dynamical behavior of 1D structured solids undergoing finite deformations.

8.3 Future works

This research about generalized continuum models for structured solids under finite deformations may open the door to further research opportunities and new lines of investigation. In addition, a scientific collaboration with the Wave Propagation Lab (Aerospace Department) at Georgia Institute of Technology was established during the PhD research, and a wide range of possibilities in lattices and structured solids has been opened too. Among all the different directions for future works, the following are the most immediate:

Regarding 1D structured solids

- Extension to nonlinear 1D solid, considering all the possible independent DOFs, other elastic constitutive equations (Mooney-Rivlin, Ogden or Neo-Hookean, among others). This would permit to analyze problems involving torsion and shear deformation, and other kind of material response.
- Experimental validation using appropriate 1D lattice. The validation with the numerical results of discrete models is highly valuable, but experimental testing cannot be disregarded in order to more faithfully capture the real behavior of the structured solid.

Regarding 2D and 3D structured solids

- Extension of the developed generalized continuum models, and non-standard continualization techniques, to both two- and three-dimensional nonlinear lattices and structured solids. These structures exhibit richer and more complex dynamical features: group velocities, band-gaps and cutoff frequencies are highly dependent on directionality, and new effects, such as beaming, are found.
- Experimental validation would be suitable to complete the theoretical analyses. With the help of advanced 3D-printers, lattices of a variety of topologies can be constructed and tested. Figure 8.1 shows examples of 3D-printing possibilities.

Cooperation with Georgia Institute of Technology

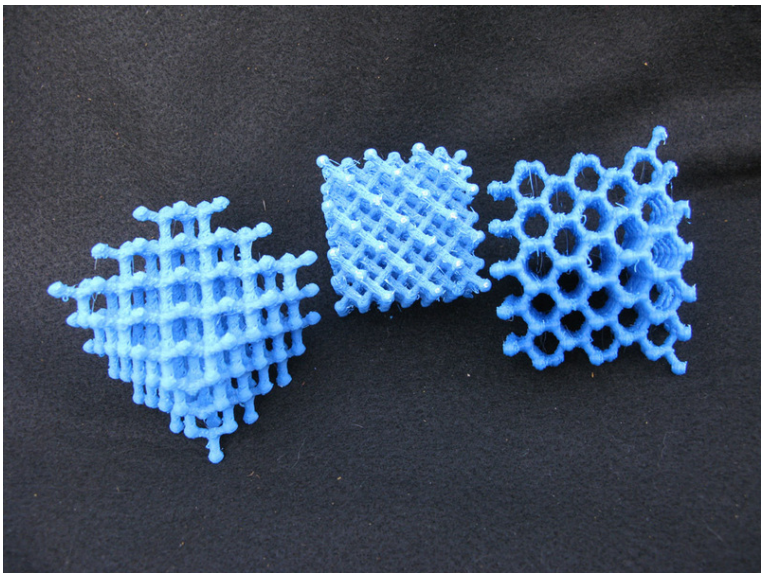

Figure 8.1: 3D lattices printed in PLA.

- In collaboration with the Georgia Institute of Technology, we are working in stiffness tunable lattices that achieve time reversal symmetry. The scientific community is focusing in this field since it would permits to design and manufacture mechanical diodes, selectors, circulators, new generation filters and other mechanical devices which may be critical for new developments in telecommunications industry.

More lines of research are in the mind of the author and directors of this project that could become to a tangible end. Now it is the time to continue exploring.

We hope that this document encouraged the reader to increase the existing knowledge about structured solids behavior and possibilities, and to contribute to the scientific community with novel and high value investigations.

"God does not play dice with the universe."

A. Einstein

8 Conclusiones

En vista de los resultados obtenidos de los diferentes modelos continuos, la comparación con el modelo discreto de referencia y las ideas que se derivan de todo ello, se pueden extraer varias conclusiones. Estas se han sintetizado con el objetivo de poner en valor toda la información científica original de la tesis.

Tras las conclusiones, se han expresado las futuras líneas de investigación que surgen a raíz de los resultados de esta investigación. En este capítulo primero se resumen los principales logros del trabajo realizado, después se presentan las conclusiones más importantes extraídas y finalmente se proponen algunas de las ideas que se pretenden abordar en futuras investigaciones.

8.1 Logros

Al principio del documento, se formularon varios objetivos con una finalidad común. Persiguiendo éstos, se han alcanzado los siguientes logros:

- Se ha extendido la formulación de dos modelos lineales del continuo generalizado para sólidos sometidos **a deformaciones finitas**. En concreto, se ha formulado un **modelo no lineal no local (NNL)** y un modelo no lineal enriquecido con el gradiente de la velocidad, aquí denominado el **modelo no lineal de gradiente de inercia (IGN)**. Éstos son extensiones de la teoría lineal no local de Eringen y de la Forma I del modelo de gradiente de deformación de Mindlin, respectivamente.

- Los modelos desarrollados se han aplicado específicamente a dos problemas relativos a las vibraciones no lineales de un sólido 1D: **las vibraciones longitudinales de una barra bajo deformaciones finitas**, y **las vibraciones axiales-transversales acopladas de una viga sometida a pequeñas deformaciones y rotaciones moderadas**.

- Se ha obtenido la solución del modelo discreto para los problemas mencionados. Para el problema de la oscilación no lineal axial-transversal acoplada, **no se han encontrado soluciones disponibles en la literatura**. En su lugar, los investigadores normalmente aplican hipótesis adicionales para obtener ecuaciones desacopladas, que se pueden resolver con métodos más sencillos. Sin embargo, en esta tesis se ha resuelto el problema completo. Esto nos ha permitido justificar algunas simplificaciones de los modelos continuos y la validez de las hipótesis adicionales comúnmente adoptadas en su aplicación.

- Se aplicó con éxito un **método de continualización no estándar** para los sistemas discretos no lineales 1D antes mencionados. A diferencia de los modelos continuos generalizadas postulados, esta técnica de continualización permitió derivar, a partir de las características estructurales del sólido, el valor de los parámetros adicionales que aparecen en el modelo.

- A pesar de la gran cantidad de diferentes formulaciones del continuo generalizado que se puede encontrar en la literatura, principalmente para problemas lineales, la comparación con resultados experimentales o simulaciones numéricas no es habitual. Por lo tanto, en estos casos no se puede evaluar la exactitud de los modelos publicados. En este caso, para los propósitos de validación, los **resultados obtenidos a partir de los modelos no lineales propuestos han sido comparados con los obtenidos del modelo discreto, los cuales se han tomado como referencia**. A este respecto, las ventajas y las limitaciones de los diferentes modelos han sido señalados.

- Hemos llevado a cabo un procedimiento para: i) modelar un sistema discreto, ii) continualizarlo siguiendo técnicas no estándar y iii) comparar los resultados de nuevos modelos del continuo generalizado con los resultados de éste. Esta metodología ha demostrado ser fructífera, convirtiéndose así en una buena herramienta que puede ser utilizada por otros investigadores para validar modelos novedosos cuando no existan resultados experimentales al efecto.

- En definitiva, se ha derivado un modelo del continuo generalizado (IGN1) que captura adecuadamente los efectos no lineales y de escala en sólidos estructurados 1D vibrando axialmente y en movimiento axial y transversal acoplados sometidos a deformaciones finitas.

8.2 Conclusiones

En esta investigación se han formulado dos nuevos modelos del continuo generalizado: el modelo no lineal no local (NNL) y el modelo no lineal de gradiente de inercia (IGN). La aplicación del modelo NNL conduce a ecuaciones de gobierno integro-diferenciales, en las que está presente un parámetro de escala adicional. Por otro lado, el modelo IGN conduce a una formulación del movimiento en el que están presentes tres parámetros de escala. Estas extensiones a deformaciones finitas permiten estudiar y predecir el comportamiento de los sólidos estructurados en régimen no lineal desde el punto de vista de la mecánica de medios continuos.

Las formulaciones de los modelos antes mencionados se han planteado para sólidos tridimensionales. En esta tesis se han aplicado para el estudio de las vibraciones no lineales axiales y axiales-transversales acopladas en un tipo de sólidos 1D estructurados. Con el fin de validar los modelos, estos problemas se han planteado y resuelto también mediante un modelo discreto no lineal, tomado como referencia.

Por otra parte, se ha aplicado al sistema discreto una técnica de continualización no estándar con el fin de obtener las ecuaciones continuas del movimiento. A diferencia de los modelos del continuo generalizado postulados, esta técnica de continualización permitió derivar, a partir de las características del sólido estructurado, el valor de los parámetros adicionales que aparecen en el modelo.

A partir de los resultados obtenidos a partir de la resolución del **modelo discreto**, se extraen las siguientes conclusiones:

- En el problema de vibraciones longitudinales se observa que, al ajustar las constantes al modelo constitutivo de St. Venant-Kirchhoff, mayores amplitudes de vibración conducen a frecuencias más bajas. Sin embargo, en el movimiento transversal, mayores amplitudes resultan en frecuencias más altas.

- Se ha observado que, por efecto tamaño, cuanto mayor es la longitud característica de la estructura subyacente, menor es la frecuencia de oscilación son en el sólido.
- En cuanto al problema de las vibraciones axiales y transversales acopladas, los investigadores generalmente hacen hipótesis adicionales para obtener las ecuaciones desacopladas. Aquí se ha resuelto el problema acoplado completo. El estudio detallado del comportamiento dinámico del sólido ha permitido entender y justificar la validez de la hipótesis de esfuerzo axil constante a lo largo del sólido 1D.

En cuanto a los resultados correspondientes a los **modelos continuos** aplicados al **problema de vibración axial no lineal**, se extraen las siguientes ideas principales:

- Los dos modelos continuos generalizados son sensibles a los efectos de escala y recogen los efectos no lineales.
- La continualización estándar con el desarrollo en serie de Taylor de la formulación discreta conduce a una ecuación que es formalmente equivalente a la del modelo clásico no lineal (SVK).
- La ecuaciones continuas del modelo IGN y las obtenidos con la técnica de continualización no estándar son idénticas, pero con ésta última se obtiene el valor del parámetro de escala directamente a partir de las características del sólido.
- El modelo NNL, si bien es sensible a los efectos de escala y a los no lineales, no reproduce adecuadamente los resultados del discreto.
- De la comparación con los resultados del discreto se observa que el modelo que mejor se adecúa a estos resultados es el IGN usando el parámetro de escala obtenido de la continualización no estándar.

Del estudio de los resultados de los **modelos continuos** aplicados al problema de **vibración acoplada axial y transversal no lineal** se puede concluir:

- El modelo IGN aplicado a este problema contiene dos parámetros de escala que se pueden reducir a uno (el modelo IGN1) adoptando valores pariculares de estos parámetros.

- La continualización estándar del modelo discreto conduce a una ecuación que es formalmente equivalente a la del modelo clásico no lineal (SVK).
- De la continualización no estándar se obtienen ecuaciones que son formalmente idénticas al modelo IGN.
- De la comparación con los resultados del modelo discreto se observa que el modelo que mejor se adecúa a estos resultados es el IGN.
- Sin embargo, usando el valor del parámetro de escala derivado de la continualización del problema axial, los resultados del modelo IGN1 concuerdan adecuadamente con los del discreto.
- Aunque el modelo IGN predice una frecuencia de corte en los sólidos que oscilan axialmente, no es capaz de capturar este fenómeno en el problema de vibraciones transversales. Por ello, esta teoría del continuo generalizado en deformaciones finitas tiene una ciertamente amplia gama de aplicaciones para los problemas de flexión, pero su uso no es apropiado para modelar los problemas que implican longitudes de onda más cortas que el doble de la distancia estructural d.

En resumen, en esta tesis se ha derivado un modelo original continuo con gradiente de la inercia (IGN) y se ha aplicado para predecir el comportamiento dinámico de un tipo de sólidos unidimensionales no lineales. Se han comparado las predicciones con resultados numéricos de un sistema discreto de referencia encontrándose que el modelo continuo los reproduce satisfactoriamente. Como conclusión final: el modelo del continuo generalizado IGN1 es capaz de reproducir con precisión las características esenciales del comportamiento dinámico de sólidos estructurados 1D sometidos a deformaciones finitas.

8.3 Trabajos futuros

Esta investigación sobre modelos del continuo generalizado para sólidos estructurados bajo deformaciones finitas puede abrir la puerta a nuevas oportunidades y líneas de investigación. Además, se ha establecido, durante la realización de la tesis doctoral, una colaboración científica con el "Vibration and Wave propagation Lab (Aerospace Department)" del Instituto de Tecnología de Georgia (EEUU). De entre las diferentes direcciones para futuros trabajos, las siguientes son las más inmediatas:

Respecto a los sólidos 1D estructurados

- Extensión a sólidos 1D no lineales, teniendo en cuenta todos los posibles grados de libertad independientes, otras ecuaciones constitutivas elásticas (Mooney-Rivlin, Ogden o Neo-Hookean, entre otros). Esto permitiría analizar los problemas relacionados con la torsión y la deformación por cortante, así como otro tipo de respuesta material.
- Validación experimental utilizando redes "*lattice*" 1D apropiadas. La validación con los resultados numéricos de modelos discretos es muy valiosa, pero los ensayos experimentales no pueden ser obviados con el fin de capturar más fielmente el comportamiento real del sólido estructurado.

Respecto a los sólidos estructurados 2D y 3D

- Extensión de los modelos de medios continuos generalizados desarrollados y las técnicas continualization no estándar a sólidos estructurados en dos y tres dimensiones. Estas estructuras presentan características dinámicas más ricas y complejas: velocidades de grupo, bandas de frecuencia prohibida y frecuencias de corte con alta dependencia de la direccionalidad, y nuevos efectos, como el efecto "beaming".
- La validación experimental sería adecuada para completar los análisis teóricos. Con la ayuda de impresoras 3D avanzadas, se pueden fabricar y ensayar sólidos estructurados con una amplia variedad de topologías. En la Fig. 8.1 se muestran varios ejemplos de posibilidades de impresión 3D.

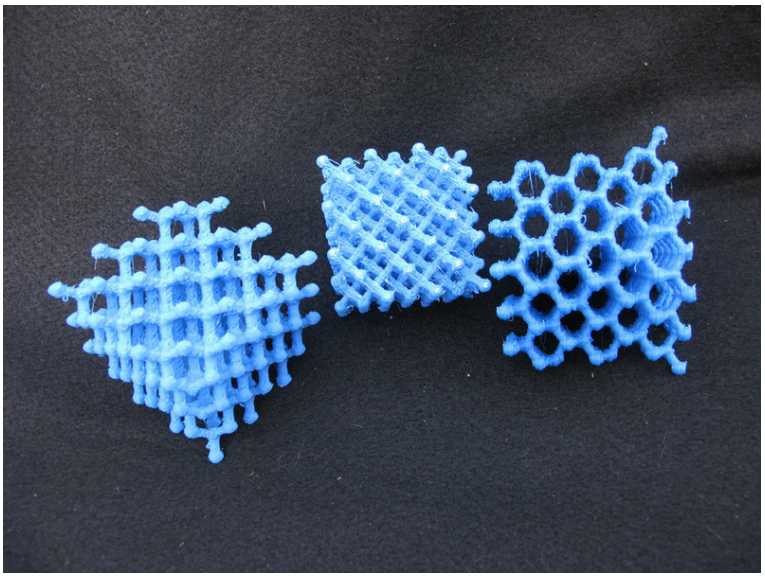

Figure 8.1: Celosías 3D impresas en PLA.

Cooperación con el Instituto de Tecnología de Georgia

- En colaboración con el Instituto de Tecnología de Georgia se está trabajando en estructuras periódicas de rigidez modulable, que logran romper la simetría de inversión del tiempo. La comunidad científica está centrando muchos esfuerzos en este campo, ya que permitiría diseñar y fabricar diodos mecánicos, selectores, circuladores, filtros de nueva generación y otros dispositivos mecánicos que pueden ser críticos para los nuevos desarrollos en la industria de las telecomunicaciones.

Otras líneas de investigación que podrían llegar a buen puerto están en la mente del autor y directores de este proyecto. Ahora es el momento de continuar explorando.

Esperamos que esta tesis anime al lector a trabajar para aumentar el conocimiento existente sobre el comportamiento y las posibilidades de los sólidos estructurados, y a contribuir con investigaciones novedosas y de alto valor.

"El azar no existe; Dios no juega a los dados."

A. Einstein

Bibliography

Bibliography

[1] W. Wang, I. Ruiz, S. Guo, Z. Favors, H. H. Bay, M. Ozkan, and C. S. Ozkan. Hybrid carbon nanotube and graphene nanostructures for lithium ion battery anodes. Nano Energy, 3:113 118, 2014.

[2] A. D. Smith, F. Niklaus, A. Paussa, S. Vaziri, A. C. Fischer, M. Sterner, F. Forsberg, A. Delin, D. Esseni, P. Palestri, M. Ostling, and M. C. Lemme. Electromechanical piezoresistive sensing in suspended graphene membranes. Nano Letters, 13:3237 3242, 2013.

[3] L. Martí Bonmatí, A. Alberich-bayarri, G. García-Martí, R. Sanz Requena, C. Pérez Castillo, J.M. Carot Sierra, and J.V. Manjón Herrera. Imaging biomarkers, quantitative imaging, and bioengineering. Radiología (English Edition), 54:269 278, 2012.

[4] T. C. Gasser, R. W. Ogden, and G. A. Holzapfel. Hyperelastic modelling of arterial layers with distributed collagen fibre orientations. Journal of The Royal Society Interface, 3:15 35, 2006.

[5] S. Gonella and M. Ruzzene. Analysis of in-plane wave propagation in hexagonal and re-entrant lattices. Journal of Sound and Vibration, 312:125 139, 2008.

[6] A. Spadoni, M. Ruzzene, S. Gonella, and F. Scarpa. Phononic properties of hexagonal chiral lattices. Wave Motion, 46:435 450, 2009.

[7] M. Schaeffer and M. Ruzzene. Wave propagation in reconfigurable magneto-elastic kagome lattice structures. Journal of Applied Physics, 117, 2015.

[8] D. Y. Fozdar, P. Soman, J. W. Lee, L. Han, and S. Chen. Three-dimensional polymer constructs exhibiting a tunable negative Poisson's ratio. Advanced Functional Materials, 21:2712 2720, 2011.

[9] S.S. Gupta and R.C. Batra. Continuum structures equivalent in normal mode vibrations to single-walled carbon nanotubes. Computational Materials Science, 43:715 723, 2008.

[10] C. R. Martin. Membrane-based synthesis of nanomaterials. Chemistry of Materials, 8:1739 1746, 1996.

[11] K. E. Drexler. Nanosystems: Molecular Machinery, Manufacturing, and Computation. John Wiley & Sons, New York, 1992.

[12] J. Han, A. Globus, R. Jaffe, and G. Deardorff. Molecular dynamics simulation of carbon nanotubebased gear. Nanotechnology, 8:95 102, 1997.

[13] A. Fennimore, T. D. Yuzvinsky, W. Q. Han, M. S. Fuhrer, J. Cumings, and A. Zettl. Rotational actuators based on carbon nanotubes. Nature, 424: 408 410, 2003.

[14] B. Bourlon, D. C. Glattli, C. Miko, L. Forro, and A. Bachtold. Carbon nanotube based bearing for rotational motions. Nano Letters, 4:709 712, 2004.

[15] V. S. Saji, H. C. Choe, and K. W. K. Young. Nanotechnology in biomedical applications-a review. International Journal of Nano and Biomaterials, 3: 119 139, 2010.

[16] E. M. Miandoab, H. N. Pishkenari, A. Yousefi-Koma, and F. Tajaddodianfar. Chaos prediction in MEMS-NEMS resonators. International Journal of Engineering Science, 82:74 83, 2014.

[17] E. M. Miandoab, A. Yousefi-Koma, H. N. Pishkenari, and F. Tajaddodianfar. Study of nonlinear dynamics and chaos in MEMS/NEMS resonators. Communications in Nonlinear Science and Numerical Simulation, 22:611 622, 2015.

[18] Z. G. Djurić, I. M. Jokić, M. M. Djukić, and M. P. Frantlović. Fluctuations of the adsorbed mass and the resonant frequency of vibrating MEMS/NEMS structures due to multilayer adsorption. Microelectronic Engineering, 87: 1181 1184, 2010.

[19] R. D. Mindlin and H. F. Tiersten. Effects of couple-stresses in linear elasticity. Archive for Rational Mechanics and Analysis, 11:415 448, 1962.

[20] E. Kröner. On the physical reality of torque stresses in continuum mechanics. International Journal of Engineering Science, 1:261 278, 1963.

[21] R. A. Toupin. Elastic materials with couple-stresses. Archive for Rational Mechanics and Analysis, 11:385 414, 1963.

[22] R. A. Toupin. Theories of elasticity with couple-stress. Archive for Rational Mechanics and Analysis, 17:85 112, 1964.

[23] A. E. Green and R. S. Rivlin. Multipolar continuum mechanics. Archive for Rational Mechanics and Analysis, 17:113 147, 1964.

[24] R. D. Mindlin. Micro-structure in linear elasticity. Archive for Rational Mechanics and Analysis, 16:51 78, 1964.

[25] R. D. Mindlin. Second gradient of strain and surface-tension in linear elasticity. International Journal of Solids and Structures, 1:417 438, 1965.

[26] R. D. Mindlin and N. Eshel. On first strain-gradient theories in linear elasticity. International Journal of Solids and Structures, 4:109 124, 1968.

[27] A. C. Eringen. Linear theory of nonlocal elasticity and dispersion of plane-waves. International Journal of Engineering Science, 10:425 435, 1972.

[28] A. C. Eringen. Nonlocal polar elastic continua. International Journal of Engineering Science, 10:1 16, 1972.

[29] A. C. Eringen. On differential-equations of nonlocal elasticity and solutions of screw dislocation and surface-waves. Journal of Applied Physics, 54:4703 4710, 1983.

[30] J. N. Reddy. Nonlocal nonlinear formulations for bending of classical and shear deformation theories of beams and plates. International Journal of Engineering Science, 48:1507 1518, 2010.

[31] M. Şimşek. Large amplitude free vibration of nanobeams with various boundary conditions based on the nonlocal elasticity theory. Composites Part B: Engineering, 56:621 628, 2014.

[32] Y. Zhao and D. G. Truhlar. A prototype for graphene material simulation: Structures and interaction potentials of coronene dimers. The Journal of Physical Chemistry C, 112:4061 4067, 2008.

[33] S. K. Jalali, E. Jomehzadeh, and N. M. Pugno. Influence of out-of-plane defects on vibration analysis of graphene: Molecular dynamics and non-local elasticity approaches. Superlattices and Microstructures, 91:331 344, 2016.

[34] T. Fang, W. Chang, and Y. Feng. Mechanical characteristics of graphene nanoribbons encapsulated in single-walled carbon nanotubes using molecular dynamics simulations. Applied Surface Science, 356:221 225, 2015.

[35] R. E. Roussou and K. Karatasos. Graphene/poly(ethylene glycol) nanocomposites as studied by molecular dynamics simulations. Materials & Design, 97:163 174, 2016.

[36] C. Yu, K. Chen, H. Cheng, and W. Chen. A study of mechanical properties of multi-layered graphene using modified Nosé-Hoover based molecular dynamics. Computational Materials Science, 117:127 138, 2016.

[37] C. Soldano, A. Mahmood, and E. Dujardin. Production, properties and potential of graphene. Carbon, 48:2127 2150, 2010.

[38] S.K. Georgantzinos, G.I. Giannopoulos, D.E. Katsareas, P.A. Kakavas, and N.K. Anifantis. Size-dependent non-linear mechanical properties of graphene nanoribbons. Computational Materials Science, 50:2057 2062, 2011.

[39] S.A. Mikhailov. Electromagnetic response of electrons in graphene: Non-linear effects. Physica E: Low-dimensional Systems and Nanostructures, 40: 2626 2629, 2008.

[40] W. A. Curtin and B. W. Sheldon. CNT-reinforced ceramics and metals. Materials Today, 7:44 49, 2004.

[41] M. Loos. Carbon Nanotube Reinforced Composites. William Andrew Publishing, Oxford, 2015.

[42] A. Peigney, Ch. Laurent, E. Flahaut, R.R. Bacsa, and A. Rousset. Specific surface area of carbon nanotubes and bundles of carbon nanotubes. Carbon, 39:507 514, 2001.

[43] H.W. Zhou, L. Mishnaevsky Jr., H.Y. Yi, Y.Q. Liu, X. Hu, A. Warrier, and G.M. Dai. Carbon fiber/carbon nanotube reinforced hierarchical composites: Effect of CNT distribution on shearing strength. Composites Part B: Engineering, 88:201 211, 2016.

[44] E. Benvenuti. Electromechanical behavior, end enhancements and radial elasticity of single-walled CNTs: A physically-consistent model based on nonlocal charges. International Journal of Solids and Structures, 72:190 205, 2015.

[45] A. G. Arani and M. Sh. Zarei. Nonlocal vibration of y-shaped CNT conveying nano-magnetic viscous fluid under magnetic field. Ain Shams Engineering Journal, 6:565 575, 2015.

[46] M. Rahmanian, M.A. Torkaman-Asadi, R.D. Firouz-Abadi, and M.A. Kouchakzadeh. Free vibrations analysis of carbon nanotubes resting on Winkler foundations based on nonlocal models. Physica B: Condensed Matter, 484:83 94, 2016.

[47] L. Li and Y. Hu. Wave propagation in fluid-conveying viscoelastic carbon nanotubes based on nonlocal strain gradient theory. Computational Materials Science, 112, Part A:282 288, 2016.

[48] B. Akgoz and O. Civalek. Bending analysis of embedded carbon nanotubes resting on an elastic foundation using strain gradient theory. Acta Astronautica, 119:1 12, 2016.

[49] B. Shahriari, M.R. Karamooz Ravari, and H. Zeighampour. Vibration analysis of functionally graded carbon nanotube-reinforced composite nanoplates using Mindlin's strain gradient theory. Composite Structures, 134:1036 1043, 2015.

[50] L. Li, Y. Hu, and L. Ling. Wave propagation in viscoelastic single-walled carbon nanotubes with surface effect under magnetic field based on nonlocal strain gradient theory. Physica E: Low-dimensional Systems and Nanostructures, 75:118 124, 2016.

[51] R. Ansari, F. Sadeghi, and M. Darvizeh. Continuum study on the oscillatory characteristics of carbon nanocones inside single-walled carbon nanotubes. Physica B: Condensed Matter, 482:28 37, 2016.

[52] X. Wang, J. Wang, and X. Guo. Finite deformation of single-walled carbon nanocones under axial compression using a temperature-related multiscale quasi-continuum model. Computational Materials Science, 114:244 253, 2016.

[53] K. Eom, H. S. Park, D. S. Yoon, and T. Kwon. Nanomechanical resonators and their applications in biological/chemical detection: Nanomechanics principles. Physics Reports, 503:115 163, 2011.

[54] E. Thielicke and E. Obermeier. Microactuators and their technologies. Mechatronics, 10:431 455, 2000.

[55] L. Li, X. Li, and Y. Hu. Free vibration analysis of nonlocal strain gradient beams made of functionally graded material. International Journal of Engineering Science, 102:77 92, 2016.

[56] A. Madeo, D. George, T. Lekszycki, M. Nierenberger, and Y. Remond. A second gradient continuum model accounting for some effects of micro-structure on reconstructed bone remodelling. Comptes Rendus Mécanique, 340:575 589, 2012.

[57] I. M. Gitman. Anisotropic gradient elasticity for modelling bone tissue. Computational Materials Science, 52:136 138, 2012.

[58] I. M. Gitman, H. Askes, E. Kuhl, and E. C. Aifantis. Stress concentrations in fractured compact bone simulated with a special class of anisotropic gradient elasticity. International Journal of Solids and Structures, 47:1099 1107, 2010.

[59] H. S. Hosseini, M. Horák, P. K. Zysset, and M. Jirásek. An over-nonlocal implicit gradient-enhanced damage-plastic model for trabecular bone under large compressive strains. International Journal for Numerical Methods in Biomedical Engineering, 31, 2015.

[60] R. Brighenti, A. Spagnoli, M. Lanfranchi, and F. Soncini. Nonlinear deformation behaviour of auxetic cellular materials with re-entrant lattice structure. Fatigue & Fracture of Engineering Materials & Structures, 39:599 610, 2016.

[61] M. Braun and J. Fernández-Sáez. A new 2D discrete model applied to dynamic crack propagation in brittle materials. International Journal of Solids and Structures, 51:3787 3797, 2014.

[62] L. Brillouin. Wave Propagation in Periodic Structures. McGraw-Hill, New York, 1946.

[63] A. C. Eringen and D. G. B. Edelen. Nonlocal elasticity. International Journal of Engineering Science, 10(3):233 248, 1972.

[64] A.C. Eringen. Nonlocal Continuum Field Theories. Springer-Verlag, New York, 2002.

[65] M. Lazar, G. A. Maugin, and E. C. Aifantis. On a theory of nonlocal elasticity of bi-Helmholtz type and some applications. International Journal of Solids and Structures, 43:1404 1421, 2006.

[66] S. Gopalakrishnan and S. Narendar. Wave Propagation in Nanostructures. Nonlocal Continuum Mechanics Formulations. Springer, Switzerland, 2013.

[67] S. Ghosh, V. Sundararaghavan, and A. M. Waas. Construction of multi-dimensional isotropic kernels for nonlocal elasticity based on phonon dispersion data. International Journal of Solids and Structures, 51:392 401, 2014.

[68] A. A. Pisano, A. Sofi, and P. Fuschi. Nonlocal integral elasticity: 2D Finite Element based solutions. International Journal of Solids and Structures, 46: 3836 3849, 2009.

[69] K. G. Eptaimeros, C. C. Koutsoumaris, and G. J. Tsamasphyros. Nonlocal integral approach to the dynamical response of nanobeams. International Journal of Mechanical Sciences, 115-116:68 80, 2016.

[70] S. B. Altan. Uniqueness of initial-boundary value problems in nonlocal elasticity. International Journal of Solids and Structures, 25:1271 1278, 1989.

[71] R. Abdollahi and B. Boroomand. Nonlocal elasticity defined by Eringen's integral model: Introduction of a boundary layer method. International Journal of Solids and Structures, 51:1758 1780, 2014.

[72] C. Polizzotto, P. Fuschi, and A.A. Pisano. A strain-difference-based nonlocal elasticity model. International Journal of Solids and Structures, 41:2383 2401, 2004.

[73] M. Schwartz, N.T. Niane, and R. K. Njiwa. A simple solution method to 3D integral nonlocal elasticity: Isotropic-bem coupled with strong form local radial point interpolation. Engineering Analysis with Boundary Elements, 36:606 612, 2012.

[74] P. Khodabakhshi and J.N. Reddy. A unified integro-differential nonlocal model. International Journal of Engineering Science, 95:60 75, 2015.

[75] A. C. Eringen. Theory of nonlocal elasticity and some applications. Res Mechanica, 21:313 342, 1987.

[76] J. Peddieson, G. R. Buchanan, and R. P. McNitt. Application of nonlocal continuum models to nanotechnology. International Journal of Engineering Science, 41:305 312, 2003.

[77] C. T. Sun and H. T. Zhang. Size-dependent elastic moduli of platelike nanomaterials. Journal of Applied Physics, 93(2):1212 1218, 2003.

[78] T. Murmu and S. C. Pradhan. Small-scale effect on the vibration of nonuniform nanocantilever based on nonlocal elasticity theory. Physica E: Low-dimensional Systems and Nanostructures, 41:1451 1456, 2009.

[79] M. Aydogdu. Axial vibration of the nanorods with the nonlocal continuum rod model. Physica E: Low-dimensional Systems and Nanostructures, 41: 861 864, 2009.

[80] K. Kiani. Free longitudinal vibration of tapered nanowires in the context of nonlocal continuum theory via a perturbation technique. Physica E: Low-dimensional Systems and Nanostructures, 43:387 397, 2010.

[81] S. Narendar and S. Gopalakrishnan. Ultrasonic wave characteristics of nanorods via nonlocal strain gradient models. Journal of Applied Physics, 107:084312, 2010.

[82] T. Murmu and S. Adhikari. Non local effects in the longitudinal vibration of double-nanorod systems. Physica E: Low-dimensional Systems and Nanostructures, 43:415 422, 2010.

[83] S. Narendar. Terahertz wave propagation in uniform nanorods: A nonlocal continuum mechanics formulation including the effect of lateral inertia. Physica E: Low-dimensional Systems and Nanostructures, 43:1015 1020, 2011.

[84] J.A. Loya, J. Aranda-Ruiz, and J. Fernández-Sáez. Torsion of cracked nanorods using a nonlocal elasticity model. Journal of Physics D: Applied Physics, 47:115304, 2014.

[85] M. T. Xu. Free transverse vibrations of nano-to-micron scale beams. Proceedings of the Royal Society A-Mathematical Physical and Engineering Sciences, 462:2977 2995, 2006.

[86] P. Lu. Dynamic analysis of axially prestressed micro/nanobeam structures based on nonlocal beam theory. Journal of Applied Physics, 101:073504, 2007.

[87] C. M. Wang, Y. Y. Zhang, S. S. Ramesh, and S. Kitipornchai. Buckling analysis of micro- and nano-rods/tubes based on nonlocal Timoshenko beam theory. Journal of Physics D-Applied Physics, 39:3904 3909, 2006.

[88] C. M. Wang, Y. Y. Zhang, and X. Q. He. Vibration of nonlocal Timoshenko beams. Nanotechnology, 18(10):105401, 2007.

[89] J. N. Reddy. Nonlocal theories for bending, buckling and vibration of beams. International Journal of Engineering Science, 45:288 307, 2007.

[90] J. Loya, J. Lopez-Puente, R. Zaera, and J. Fernández-Sáez. Free transverse vibrations of cracked nanobeams using a nonlocal elasticity model. Journal of Applied Physics, 105:044309, 2009.

[91] L. L. Ke, Y. S. Wang, and Z. D. Wang. Nonlinear vibration of the piezoelectric nanobeams based on the nonlocal theory. Composite Structures, 94: 2038 2047, 2012.

[92] S. C. Pradhan and T. Murmu. Application of nonlocal elasticity and DQM in the flapwise bending vibration of a rotating nanocantilever. Physica E: Low-dimensional Systems and Nanostructures, 42:1944 1949, 2010.

[93] T. Murmu and S. Adhikari. Scale-dependent vibration analysis of prestressed carbon nanotubes undergoing rotation. Journal of Applied Physics, 108: 123507, 2010.

[94] S. Narendar and S. Gopalakrishnan. Nonlocal wave propagation in rotating nanotube. Results in Physics, 1:17 25, 2011.

[95] J. Aranda-Ruiz, J. Loya, and J. Fernández-Sáez. Bending vibrations of rotating nonuniform nanocantilevers using the Eringen nonlocal elasticity theory. Composite Structures, 95:2990 3001, 2012.

[96] L. Ke, Y. Wang, and Z. Wang. Non-local elastic plate theories. Proceedings of the Royal Society A-Mathematical Physical and Engineering Sciences, 463:3225 3240, 2008.

[97] T. Murmu and S. C. Pradhan. Small-scale effect on the free in-plane vibration of nanoplates by nonlocal continuum model. Physica E: Low-dimensional Systems and Nanostructures, 41:1628 1633, 2009.

[98] S. Hosseini-Hashemi, M. Zare, and R. Nazemnezhad. An exact analytical approach for free vibration of Mindlin rectangular nano-plates via nonlocal elasticity. Composite Structures, 100:290 299, 2013.

[99] Y. Zhang, L.W. Zhang, K.M. Liew, and J.L. Yu. Nonlocal continuum model for large deformation analysis of SLGSs using the kp-Ritz element-free method. International Journal of Non-Linear Mechanics, 79:1 9, 2016.

[100] Q. Wang and V. K. Varadan. Application of nonlocal elastic shell theory in wave propagation analysis of carbon nanotubes. Smart Materials and Structures, 16:178 190, 2007.

[101] Q. Wang and C. M. Wang. The constitutive relation and small scale parameter of nonlocal continuum mechanics for modelling carbon nanotubes. Nanotechnology, 18:075702, 2007.

[102] Y. G. Hua, K. M. Liew, Q. Wang, X. Q. He, and B. I. Yakobson. Nonlocal shell model for elastic wave propagation in single- and double-walled carbon nanotubes. Journal of the Mechanics and Physics of Solids, 56:3475Â 3485, 2008.

[103] E. Ghavanloo and S. A. Fazelzadeh. Nonlocal elasticity theory for radial vibration of nanoscale spherical shells. European Journal of Mechanics - A/Solids, 41:37 42, 2013.

[104] R. Zaera, J. Fernández-Sáez, and J. A. Loya. Axisymmetric free vibration of closed thin spherical nano-shell. Composite Structures, 104:154 161, 2013.

[105] J. Vila, R. Zaera, and J. Fernández-Sáez. Axisymmetric free vibration of closed thin spherical nanoshell with bending effects. Journal of Vibration and Control,, 2015. doi: 10.1177/1077546314565808.

[106] R. D. Firouz-Abadi, M. M. Fotouhi, and H. Haddadpour. Free vibration analysis of nanocones using a nonlocal continuum model. Physics Letters A, 375:3593 3598, 2011.

[107] P. Tsai and T. Fang. A molecular dynamics study of the nucleation, thermal stability and nanomechanics of carbon nanocones. Nanotechnology, 18: 105702, 2007.

[108] K. M. Liew, J. X. Wei, and X. Q. He. Carbon nanocones under compression: Buckling and post-buckling behaviors. Physical Review B- Condensed Matter and Materials Physics, 75:195435, 2007.

[109] C. M. Wang and W. H. Duan. Free vibration of nanorings/arches based on nonlocal elasticity. Journal of Applied Physics, 104:014303, 2008.

[110] H. Moosavi, M. Mohammadi, A. Farajpour, and S. H. Shahidi. Vibration analysis of nanorings using nonlocal continuum mechanics and shear deformable ring theory. Physica E: Low-dimensional Systems and Nanostructures, 44:135 140, 2011.

[111] E. Ghavanloo and S. A. Fazelzadeh. Radial vibration of free anisotropic nanoparticles based on nonlocal continuum mechanics. Nanotechnology, 24: 075702, 2013.

[112] N. A. Fleck and J. W. Hutchinson. Strain gradient plasticity. Advances in Applied Mechanics, 33:295 361, 1997.

[113] S. J. Zhou and Z. Q. Li. Length scales in the static and dynamic torsion of a circular cylindrical micro-bar. Journal of Shandong University of Technology, 31:401 407, 2001.

[114] L. J. Sudak. Column buckling of multiwalled carbon nanotubes using nonlocal continuum mechanics. Journal of Applied Physics, 94:7281 7287, 2003.

[115] Y. Chen, J. D. Lee, and A. Eskandarian. Atomistic viewpoint of the applicability of microcontinuum theories. International Journal of Solids and Structures, 41:2085 2097, 2004.

[116] H. Heireche, A. Tounsi, A. Benzair, M. Maachou, and E. A. Adda Berdia. Sound wave propagation in single-walled carbon nanotubes using nonlocal elasticity. Physica E: Low-dimensional Systems and Nanostructures, 40: 2791 2799, 2008.

[117] T. Murmu and S. C. Pradhan. Thermo-mechanical vibration of a single-walled carbon nanotube embedded in an elastic medium based on nonlocal elasticity theory. Computational Materials Science, 46:854 859, 2009.

[118] S. Narendar and S. Gopalakrishnan. Critical buckling temperature of single-walled carbon nanotubes embedded in a one-parameter elastic medium based on nonlocal continuum mechanics. Physica E: Low-dimensional Systems and Nanostructures, 43:1185 1191, 2011.

[119] R. Ansari, A. Shahabodini, and H. Rouhi. A thickness-independent nonlocal shell model for describing the stability behavior of carbon nanotubes under compression. Composite Structures, 100:323 331, 2013.

[120] Q. Wang and K.M. Liew. Application of nonlocal continuum mechanics to static analysis of micro- and nano-structures. Physics Letters A, 363: 236 242, 2007.

[121] C. M. Wang, S. Kitipornchai, C. W. Lim, and M. Eisenberger. Beam bending solutions based on nonlocal Timoshenko beam theory. Journal of Engineering Mechanics, 134:475 481, 2008.

[122] N. Challamel and C. M. Wang. The small length scale effect for a non-local cantilever beam: a paradox solved. Nanotechnology, 19:345703, 2008.

[123] N. Challamel, Z. Zhang, C.M. Wang, J.N. Reddy, Q. Wang, T. Michelitsch, and B. Collet. On nonconservativeness of Eringen's nonlocal elasticity in beam mechanics: correction from a discrete-based approach. Archive of Applied Mechanics, 84:1275 1292, 2014.

[124] P. Lu, H. P. Lee, C. Lu, and P. Q. Zhang. Dynamic properties of flexural beams using a nonlocal elasticity model. Journal of Applied Physics, 99, 2006.

[125] J. Fernández-Sáez, R. Zaera, J.A. Loya, and J.N. Reddy. Bending of Euler-Bernoulli beams using Eringen's integral formulation: A paradox resolved. International Journal of Engineering Science, 99:107 116, 2016.

[126] R. D. Mindlin. Micro-structure in linear elasticity. Archive for Rational Mechanics and Analysis, 16:51 78, 1964.

[127] R. D. Mindlin. Second gradient of strain and surface-tension in linear elasticity. International Journal of Solids and Structures, 1:417 438, 1965.

[128] H. Askes and E. C. Aifantis. Gradient elasticity in statics and dynamics: An overview of formulations, length scale identification procedures, finite element implementations and new results. International Journal of Solids and Structures, 48(13):1962 1990, 2011.

[129] R. Gholami, A. Darvizeh, R. Ansari, and F. Sadeghi. Vibration and buckling of first-order shear deformable circular cylindrical micro-/nano-shells based on Mindlin's strain gradient elasticity theory. European Journal of Mechanics - A/Solids, 58:76 88, 2016. ISSN 0997-7538.

[130] H. Zeighampour and Y. T. Beni. Cylindrical thin-shell model based on modified strain gradient theory. International Journal of Engineering Science, 78: 27 47, 2014.

[131] M. R. Nami and M. Janghorban. Resonance behavior of {FG} rectangular micro/nano plate based on nonlocal elasticity theory and strain gradient theory with one gradient constant. Composite Structures, 111:349 353, 2014.

[132] A. Li, S. Zhou, S. Zhou, and B. Wang. A size-dependent model for bi-layered kirchhoff micro-plate based on strain gradient elasticity theory. Composite Structures, 113:272 280, 2014.

[133] M. Mohammadimehr, B. R. Navi, and A. G. Arani. Modified strain gradient Reddy rectangular plate model for biaxial buckling and bending analysis of double-coupled piezoelectric polymeric nanocomposite reinforced by FG-SWNT. Composites Part B: Engineering, 87:132 148, 2016.

[134] D. Ieşan. Deformation of thin chiral plates in strain gradient elasticity. European Journal of Mechanics - A/Solids, 44:212 221, 2014.

[135] I. Zibaei, H. Rahnama, F. Taheri-Behrooz, and M.M. Shokrieh. First strain gradient elasticity solution for nanotube-reinforced matrix problem. Composite Structures, 112:273 282, 2014.

[136] X. Xu and Z. Deng. Effects of strain and higher order inertia gradients on wave propagation in single-walled carbon nanotubes. Physica E: Low-dimensional Systems and Nanostructures, 72:101 110, 2015.

[137] S. Kong, S. Zhou, Z. Nie, and K. Wang. Static and dynamic analysis of micro beams based on strain gradient elasticity theory. International Journal of Engineering Science, 47:487 498, 2009.

[138] L. Qi, S. Zhou, and A. Li. Size-dependent bending of an electro-elastic bilayer nanobeam due to flexoelectricity and strain gradient elastic effect. Composite Structures, 135:167 175, 2016.

[139] J. Lei, Y. He, B. Zhang, Z. Gan, and P. Zeng. Bending and vibration of functionally graded sinusoidal microbeams based on the strain gradient elasticity theory. International Journal of Engineering Science, 72:36 52, 2013.

[140] B. Zhang, Y. He, D. Liu, Z. Gan, and L. Shen. A novel size-dependent functionally graded curved mircobeam model based on the strain gradient elasticity theory. Composite Structures, 106:374 392, 2013.

[141] C. Liebold and W. H. Muller. Comparison of gradient elasticity models for the bending of micromaterials. Computational Materials Science, 116:52 61, 2016.

[142] X. Xu and Z. Deng. Closed-form frequency solutions for simplified strain gradient beams with higher-order inertia. European Journal of Mechanics - A/Solids, 56:59 72, 2016.

[143] X. Liang, S. Hu, and S. Shen. A new Bernoulli-Euler beam model based on a simplified strain gradient elasticity theory and its applications. Composite Structures, 111:317 323, 2014.

[144] S. Sahmani, M. Bahrami, and R. Ansari. Nonlinear free vibration analysis of functionally graded third-order shear deformable microbeams based on the modified strain gradient elasticity theory. Composite Structures, 110:219 230, 2014.

[145] M. Donà, A. Palmeri, and M. Lombardo. Dynamic analysis of multi-cracked Euler-Bernoulli beams with gradient elasticity. Computers & Structures, 161:64 76, 2015.

[146] S. M. Mousavi. Dislocation-based fracture mechanics within nonlocal and gradient elasticity of bi-Helmholtz type - part I: Antiplane analysis. International Journal of Solids and Structures, 87:222 235, 2016.

[147] D. Polyzos and D. I. Fotiadis. Derivation of Mindlin's first and second strain gradient elastic theory via simple lattice and continuum models. International Journal of Solids and Structures, 49:470 480, 2012.

[148] P. Rosenau. Dynamics of dense lattices. Physical Review B- Condensed Matter and Materials Physics, 36:5868 5876, 1987.

[149] P. Rosenau. Hamiltonian dynamics of dense chains and lattices: or how to correct the continuum. Physics Letters A, 331:39 42, 2003.

[150] G. A. Holzapfel. Nonlinear Solid Mechanics: A Continuum Approach for Engineering. John Wiley & Sons, New York, 2000.

[151] J. Bonet and R. Wood. Nonlinear Continuum Mechanics for Finite Element Analysis. Cambridge University Press, New York, 2008.

[152] A. P. Boresi and R.J. Schmidt. Advanced Mechanics of Materials. Wiley & Sons, Inc., 2002.

[153] L. Li and Y. Hu. Buckling analysis of size-dependent nonlinear beams based on a nonlocal strain gradient theory. International Journal of Engineering Science, 97:84 94, 2015.

[154] R. Vatankhah, M.H. Kahrobaiyan, A. Alasty, and M.T. Ahmadian. Nonlinear forced vibration of strain gradient microbeams. Applied Mathematical Modelling, 37:8363 8382, 2013.

[155] A.K. Lazopoulos, K.A. Lazopoulos, and G. Palassopoulos. Nonlinear bending and buckling for strain gradient elastic beams. Applied Mathematical Modelling, 38:253 262, 2014.

[156] K. Tamm and A. Salupere. On the propagation of 1D solitary waves in Mindlin-type microstructured solids. Mathematics and Computers in Simulation, 82:1308 1320, 2012.

[157] I. Sertakov, J. Engelbrecht, and J. Janno. Modelling 2D wave motion in microstructured solids. Mechanics Research Communications, 56:42 49, 2014.

[158] A. Salupere, K. Tamm, and J. Engelbrecht. Numerical simulation of interaction of solitary deformation waves in microstructured solids. International Journal of Non-Linear Mechanics, 43:201 208, 2008.

[159] A. Berezovski, J. Engelbrecht, A. Salupere, K. Tamm, T. Peets, and M. Berezovski. Dispersive waves in microstructured solids. International Journal of Solids and Structures, 50:1981 1990, 2013.

[160] L. Verlet. Computer "experiments" on classical fluids. I. thermodynamical properties of Lennard-Jones molecules. Physical Review, 159:98 103, 1967.

[161] A. Bedford. Hamilton's principle in continuum mechanics, volume 139. Pitman Advanced Publishing Program, 1985.

[162] C. Lanczos. The Variational Principles of Mechanics. Dover Publications, Inc., New York, 1970.

[163] C. S. Jog. Continuum mechanics, volume 1. Cambridge University Press, 2015.

[164] M. H. Abedinnasab and M. I. Hussein. Wave dispersion under finite deformation. Wave Motion, 50:374 388, 2013.

[165] L. Zhifang and Z. Shanyuan. Nonlinear waves and periodic solution in finite deformation elastic rod. Acta Mechanica Solida Sinica, 19:1 8, 2006.

[166] N. Challamel, J. Lerbet, C. M. Wang, and Z. Zhang. Analytical length scale calibration of nonlocal continuum from a microstructured buckling model. ZAMM Zeitschrift fur Angewandte Mathematik und Mechanik, 94:402 413, 2014.

[167] N. Challamel, C.M. Wang, and I. Elishakoff. Discrete systems behave as nonlocal structural elements: Bending, buckling and vibration analysis. European Journal of Mechanics - A/Solids, 44:125 135, 2014.

[168] M. Aydogdu. Longitudinal wave propagation in nanorods using a general nonlocal unimodal rod theory and calibration of nonlocal parameter with lattice dynamics. International Journal of Engineering Science, 56:17 28, 2012.

[169] J. G. Eisley. Nonlinear vibration of beams and rectangular plates. Zeitschrift für angewandte Mathematik und Physik ZAMP, 15:167 175, 1964.

[170] K.L. Manktelow, M.J. Leamy, and M. Ruzzene. Analysis and experimental estimation of nonlinear dispersion in a periodic string. Journal of Vibration and Acoustics, Transactions of the ASME, 136:1 8, 2014.

[171] C. M. Wang, Z. Zhang, N. Challamel, and W. H. Duan. Calibration of Eringen's small length scale coefficient for initially stressed vibrating nonlocal Euler beams based on microstructured beam model. Journal of Physics D: Applied Physics, 46:345501, 2013.

[172] S. A. Emam and A. H. Nayfeh. Postbuckling and free vibrations of composite beams. Composite Structures, 88:636 642, 2009.

[173] A. H. Nayfeh and P. F. Pai. Linear and Nonlinear Structural Mechanics. Wiley, 2004.

[174] S.W. Shaw and C. Pierre. Normal modes of vibration for non-linear continuous systems. Journal of Sound and Vibration, 169:319 347, 1994.